JOHANNES GUTENBERG UNIVERSITÄT MAINZ

„Bioactive and Biodegradable PLGA-Biosilica Biomaterial for Bone Regeneration“

Dissertation

zur Erlangung des Grades

''Doktor der Naturwissenschaften''

am Fachbereich Biologie

der Johannes Gutenberg-Universität

in Mainz

Vorgelegt von

Shunfeng WANG

geb. am 03.06.1984 in Hubei (China)

Mainz, 2019

Tag der mündlich Prüfung: 10,07,2019

D77

To my family

Publication:

Some of the results within the thesis have been published in a peer-reviewed journal:

S.F. Wang, X.H. Wang, F.G. Draenert, O. Albert, H.C. Schröder, V. Mailänder, G. Mitov, W.E.G. Müller, Bioactive and biodegradable silica biomaterial for bone regeneration, Bone 67 (2014) 292–304.

INDEX:

ABSTRACT:

For centuries, orthopedic surgery has applied a variety of materials to repair bone defects caused by infection, tumor, trauma, surgery and so on. Due to the limitations and disadvantages of autografts and allografts, the development of bone substitutes has become a significant clinical challenge.

In traditional bone tissue engineering, bone implants include three main elements: seed cells (stem cells), scaffold materials and growth factors. Such implants are difficult to prepare and often very expensive. Therefore, we developed a new "tissue-inducing biomaterial" (without adding live cells and growth factors) based on biosilica, a biocompatible, natural inorganic polymer formed by an enzymatic reaction, which is mediated by silicatein an enzyme present in the siliceous sponges to form their inorganic skeleton. Biosilica has been shown to exhibit morphogenic activity and to induce mineralization of human osteoblast-like cells (SaOS-2) *in vitro*.

In this study, we developed a scaffold material by encapsulating silicatein and its orthosilicate substrate in the PLGA microspheres. Upon degradation of the microspheres, silicatein and orthosilicate released to form biosilica, and to promote bone regeneration and mineralization. *In vitro* studies showed that the biosilica microspheres are not toxic, compared to the gold standard ß-TCP used in clinic. Furthermore, biosilica caused a stronger induction of proliferation and mineralization of SaOS-2 cells. *In vivo* animal experiments were performed in rabbit femurs, by filling biosilica microspheres into artificial bone defects. After an implantation period of 100 days, most of the scaffold material implanted in the defects was found to be degraded and mature bone tissue was formed. These findings indicate that the biosilica microsphere implant material is a novel (no additionion of living cells and growth factors needed) and promising bone substitute material for bone regeneration. It has broad prospects that can be used clinically to benefit the human health in an aging society.

ZUSAMMENFASSUNG:

Seit Jahrhunderten wurde in der orthopädischen Chirurgie eine Vielzahl von Materialien eingesetzt, um Knochendefekte zu reparieren, die durch Infektionen, Tumor, Trauma, Operationen usw. verursacht wurden. Aufgrund der Limitierung und der Nachteile von Auto- und Allotransplantaten ist die Entwicklung von geeigneten Knochenersatzmaterialien zu einer der bedeutendsten klinischen Herausforderung geworden.

Beim traditionellen Tissue Engineering verwendete Knochenimplantate bestehen aus drei Hauptelementen: Stammzellen, Scaffold-Materialien und Wachstumsfaktoren. Solche Implantate sind schwer herzustellen und häufig zu teuer. Daher haben wir ein neues "Gewebe induzierendes Biomaterial" (ohne Notwendigkeit der Zugabe von lebenden Zellen und Wachstumsfaktoren) entwickelt, das auf Biosilica, einem biokompatiblen, natürlich vorkommenden anorganischen Polymer, basiert. Biosilica wird durch eine enzymatische Reaktion gebildet, die durch das Enzym Silicatein vermittelt wird, welches das anorganische Skelett der siliciumhaltigen Kiesleschwämme bildet. Es wurde gezeigt, dass Biosilica morphogene Aktivität aufweist und *in vitro* die Mineralisierung von humanen Osteoblasten-ähnlichen Zellen (SaOS-2) induziert.

In dieser Arbeit wurde von mir ein Scaffold-Material entwickelt, in dem Silicatein und sein Orthosilikat-Substrat in PLGA-Mikrosphären eingekapselt wurde. Beim Abbau der Mikrosphären werden Silicatein und Orthosilicat freigesetzt, um daraus Biosilica zu bilden, das die Regeneration und Mineralisation des Knochens fördert. *In-vitro*-Studien im Vergleich zu dem in der Klinik verwendeten Goldstandard ß-TCP zeigten, dass die Biosilica-Mikrosphären nicht toxisch sind. Darüber hinaus verursachte Biosilica eine stärkere Induktion der Proliferation und Mineralisierung von SaOS-2-Zellen. *In-vivo*-Tierversuche wurden an Kaninchen-Oberschenkelknochen (Femur) durchgeführt, indem Biosilica-Mikrosphären in künstliche Knochendefekte gefüllt wurden. Nach einer Implantationsdauer von 100 Tagen wurde festgestellt, dass der größte Teil des in die Defekte implantierten Scaffold-Materials abgebaut und reifes Knochengewebe gebildet worden war. Diese Ergebnisse zeigten, dass das hier entwickelte neuartige, eine Zugabe lebender Zellen und Wachstumsfaktoren nicht erfordernde Implantatmaterial aus Biosilica-Mikrosphären ein vielversprechendes Knochenersatzmaterial für die Knochenregeneration ist. Es besitzt weitreichende

Anwendungsmöglichkeiten, die klinisch – insbesondere im Hinblick auf unsere alternde Gesellschaft – genutzt werden können.

Chapter I: Introduction

1 INTRODUCTION

1.1 Bone formation and regeneration process

1.1.1 The human body skeleton – Bone

The adult human skeleton is made of 206 individual bones, which account for up to 14 % of body total weight. And they can be divided into bones of the axial skeleton (80 bones) and into bones of the appendicular skeleton (126 bones) [1]. Each bone has individual shape and size, related to its function and location in the body. All bones in the human body can be categorized into five groups (according to their shape): long bone, short bone, flat bone, sesamoid bone and irregular bone. Moreover, bone is a living tissue, composed of different types of bone cells, extracellular matrix, nerves, blood vessels and inorganic phase. It is characterized by strength and rigidity, and the capability of regeneration and remolding. Each bone constantly undergoes growth and remodeling during the life time, controlled by the process of resorption and formation [2]. This process helps bone to adapt to changing mechanical environments, to maintain its strength, as well as to repair micro-damages occurring in bone [3]. Bone remodeling occurs throughout the whole life, the peak bone mass is usually reached in the third decade of our life. Then from 50 years old, bone mass starts to decrease. Bone resorption by osteoclasts is faster than formation of new bone by osteoblasts, resulting in the loss of bone mineral, so called osteoporosis [4].

Bone itself mainly consists of collagen fibers and inorganic mineral phase in the form of small crystals (hydroxyapatite). The living bone is composed of 60-70 % bone mineral, 20-30 % organic matrix, and 5 to 10 % water [5]. Hydroxyapatite (HA), with a chemical formula [$Ca_{10}(PO_4)_6(OH)_2$], is the principal component of the mineral phase of human bone. The Ca/P molar ratio of mature bones ranges from 1.37 to 1.87; the theoretical value for HA crystals is 1.67 [6]. However, biological HA normally contains certain amount of carbonate ions (CO_3^{2-}) (approximately 7 % in human bone HA), together with magnesium (Mg), sodium (Na), potassium (K), and other ions [7]. The CO_3^{2-} ions can be incorporated into the HA structure at two

different sites, with substitution of OH^- site (A-type) or PO_4^{3-} site (B-type) [7–9]. In 2013, Professor WEG Müller (University Mainz) proposed that calcium carbonate deposits act as bioseeds for calcium phosphate deposition [10,11]. Indeed, exposure of SaOS-2 osteoblasts to bicarbonate containing medium (1 to 10 mM) resulted in a marked increase of the mineralization level. The carbonic anhydrase II (CA-II) turned out to be involved in the calcium carbonate bioseed formation [10,11]. In general, carbonate-substituted apatite [$Ca_{10}(PO_4,CO_3)_6(OH)_2$] is more soluble than synthetic HA crystals, allowing it to support mineral metabolism. Besides of carbonate ions, other ions play an important role in bone metabolism and affect the mineralization process and the stability of the apatite crystals. Magnesium (Mg) has been found to inhibit HA crystal growth, but stimulate osteoblast's growth and proliferation [12]. Plenty of researches has been carried out on incorporation of Mg or other metal ions into HA and other types of ceramic for bone implants [12–15].

1.1.2 Bone function and structure

Bone is a heterogeneous material — a mineralized connective tissue, composed of a mineralized phase (hydroxyapatite, HA), an organic phase and water. It performs a number of functions in our body [16]:

1) Mechanical function: supporting our body structure and protecting internal organs from injury, also aiding locomotion.
2) Mineral reservoir: serving as a storage for calcium and phosphorus. 99 % of calcium in the human body is stored in bones and the remaining 1 % in teeth and other soft tissues.
3) Blood cells production: bone marrow is the flexible tissue located in the interior of trabecular bone. The blood cells are produced in the red bone marrow during the process of hematopoiesis.
4) Growth factors storage: Bone also acts as a store for growth factors that regulate bone formation [17].
5) Acid base system: bone buffers against excessive pH changes by absorbing

or releasing the alkaline salts.

Identifying of the relationship between structure and function in bone is quite challenging, due to its complex structure. There are two types of bone tissue: cortical bone (80 % in skeleton) and trabecular bone (20 % in skeleton), as shown in Fig. 1-1 [18]. Cortical bone is dense and solid, consisting of closely packed osteons or Haversian systems, and forms that outer layer of bone. Trabecular bone usually located in the inner part of bone and has a honeycomb-like structure [19]. Due to its sponge-like structure, it has a higher surface area and shows a higher metabolic activity compared to cortical bone.

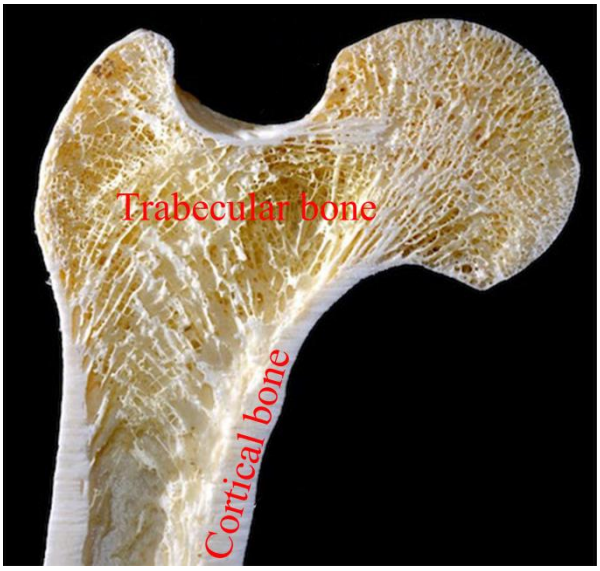

Fig. 1- 1. Two types of bone: Cortical bone (outer layer of bone, thick and dense) and Trabecular bone (soft and porous). Photo was modified and taken from Internet: http://medcell.med.yale.edu/systems_cell_biology/bone_lab.php

Bone is composed of both inorganic components (99 % hydroxyapatite) and an organic phase, mainly consisting of collagen fibers (90 %) and noncollageous proteins (NCPs). The universal elementary building blocks of bone are mineralized collagen fibrils [20]. The initial deposition of bone minerals occurs in the regions between the ends of the collagen fibrils, called “hole” zones. The NCPs regulate both bone mineral deposition and bone cell activity [21].

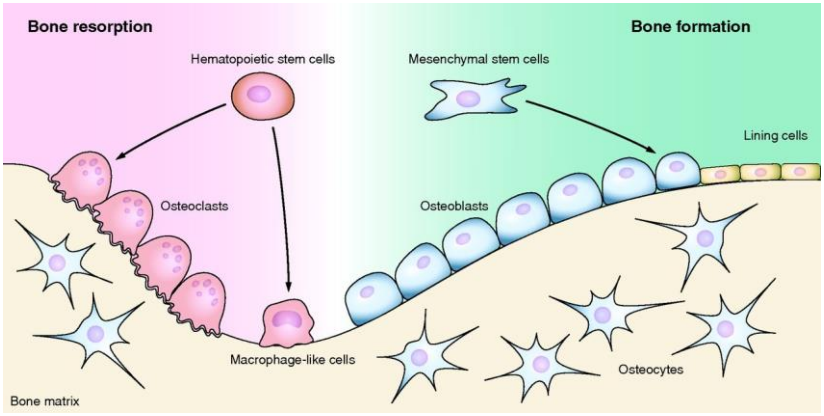

Fig. 1- 2. The main types of bone cells: osteoblasts, osteoclasts, osteocytes and lining cells [22].

Bone growth, modeling and remodeling are driven by the bone cells, which include osteoblasts, osteoclasts, osteocytes and lining cells [22]. The source and relation of the bone cells is presented in the Fig. 1-2 [23]. Osteoblasts are cuboidal mononucleated cells that originate from mesenchymal stem cells. They are responsible for bone formation through regulatiing bone matrix synthesis and mineralization [24]. Two main steps are involved in this process: organic matrix secretion (extracellular matrix) and its subsequent mineralization. In extracellular matrix acts as a framework allowing hydroxyapatite (HA) crystals to deposit and grow on the collagen fibrils. The HA does not spontaneously precipitate, in despite of the fact that the extracellular fluid is supersaturated with calcium and phosphate ions [24]. NCPs can promote HA crystal formation by attracting calcium and phosphate ions through their charged amino acid domains which act as a nucleational core [25]. Osteoclasts are large multinuclear cells, derived from mononuclear hematopoietic stem cells [26]. They bind to the bone surface *via* integrins and are responsible for bone resorption. The bone dissolving process is mainly controlled by secretion of protons by the osteoclasts (dissolution of bone mineral) and of cathepsin K (an enzyme that degrades the organic matrix) [27]. Bone remodeling is a lifelong process to maintain bone strength and repair micro-damages, regulated through the removal of old bone by osteoclasts and new bone formation by osteoblasts. This process consists of three sequential phases: bone resorption, in which osteoclasts digest the old bone; reversal, which mononuclear cells appear on the bone surface; and bone formation, in which osteoblasts lay

down the new bone matrix until the missing bone is completely replaced [2]. During new bone formation, the osteoblasts become entrapped inside the bone tissue, thereby turning into osteocytes. They are the most common cells in bone, amountin to approximately 95 % of bone cells. They are characterized by long branches that connect them with each other. Osteocytes serve as mechanical sensors and orchestrators that regulate bone metabolism [28]. Flattened bone lining cells are quiescent osteoblasts that cover the inactive bone surface and have a thin and flat nuclear profile. They play an important role in regulation of mineral homeostasis, also preventing the direct interaction between bone matrix and osteoclasts [22,29]. All bone cells work together to regulate bone growth, modeling and remodeling during the life time, maintaining bone in healthy condition.

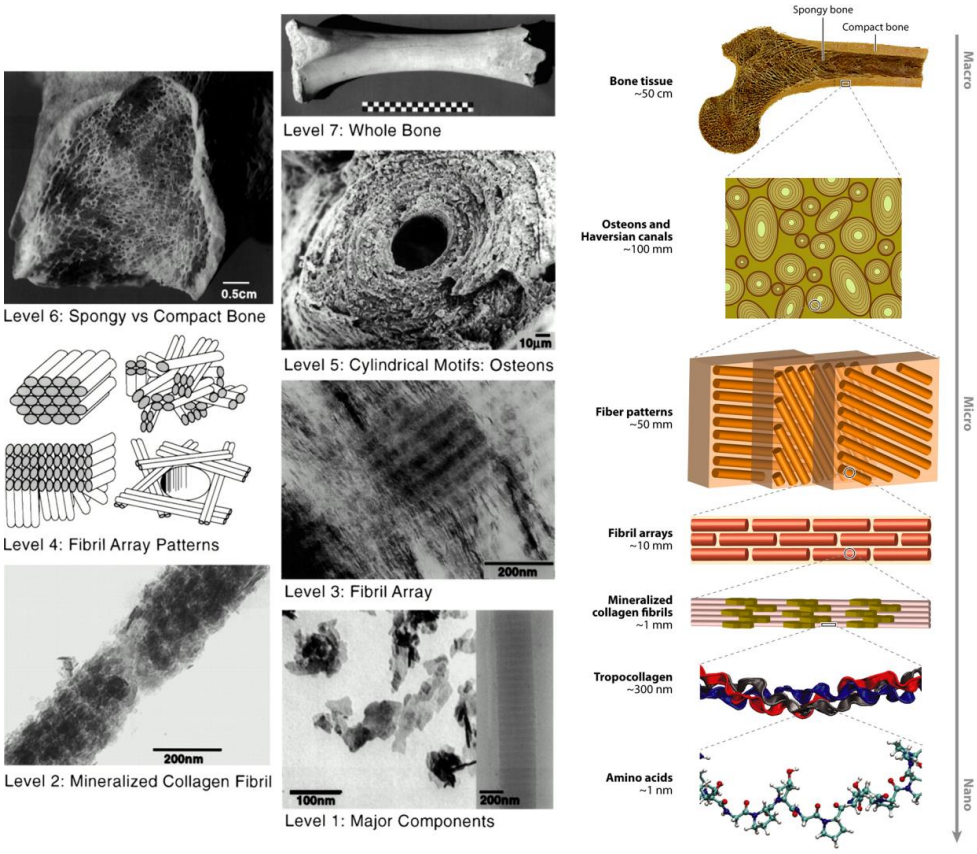

Fig. 1- 3. Seven levels' hierarchical structure in bone from nanoscale to millimeter: Level 1: Sub-nanostructure (< 100 nm) - Mineral nanocrystals and collagen fibril; Level 2: Nanostructure (100 nm - 1 µm) - Mineralized collagen fibril; Level 3: Sub-microstructure (1-10 µm) - Collagen fibril arrays; Level 4: Fiber patterns; Level 5: Microstructure (10-500 µm) - Osteons or Haversian canals; Level 6: Macrostructure - Cortical and spongy bone; Level 7: Whole bone. Photo was modified with permission of ANNUAL REVIEWS [28] and Springer Nature [29]

Bone is a complex hierarchically structured material over many length scales, which fulfills diverse mechanical, biological and chemical functions [19]. The detailed structure of bone has been extensively described in the literature [19,30]. The basic building block of bone is the mineralized collagen fibril [30]. Its various levels of organization and orientation make the (heterogeneous and anisotropic) structure of bone so complicate. The seven levels' hierarchical structure in bone is presented in Fig. 1-3 [30], from the nanometer scale to the millimeter scale [19,31]. In the cross section, cortical bone and trabecular bone can be easily distinguished by their density and porosity. The inner porous trabecular bone is surrounded and protected by the dense cortical bone. Due to its higher surface area, it is metabolically more active. At the microstructural level, the structural arrangement of cortical bone is different from trabecular bone. The osteons or Haversian systems are the fundamental 'building block' of cortical bone. For trabecular bone, the basic architectures are plates (trabeculae) and rods, with a thickness of 100-200 mm. Osteons are cylindrical in shape, with a size of several millimeters in length and 0.2 mm in diameter. They typically run parallel to the long axis of the bone, consisting of different parts: concentric lamellae, Haversian canal, Volkmann canals, osteocytes, and canaliculi. The Haversian canal is located in the centre of osteon, surrounded by concentric lamellae. The blood vessels and nerve fibers are in the centre of canal, supplying blood to osteocytes. The Haversian canals are connected through the Volkmann canals that form transverse canals also containing blood vessels. Osteocytes are located in the small spaces between the lamellae, which are called lacunae. They are also interconnected via tiny channels called canaliculi. Canaliculi are responsible for delivering nutrients to osteocytes and disposing cell waste. However, trabecular bone is made of interconnecting trabeculae, which are lamellae that are arranged as robs or plats. The single trabeculae microstructure includes bone cells, lamellae and canaliculi. Unlike osteons, canals and blood vessel are missing in the trabeculae structure. Three types of bone cells (osteoblasts, osteoclasts and osteocytes) are found in trabeculae, while only osteocytes exist in an individual osteon. All the mature healthy bone consists of lamellar bone, with

various alignment and orientation of the lamellae.

1.2 Nanoindentation technique and its applications on biological samples

1.2.1 Nanoindentation technique

The nanoindentation technique is considered as the most powerful technique for the characterization of mechanical properties (hardness and Young's modulus etc.) at nano scales, in particular for small volume material, thin film/coating [32] and biological samples (bone, teeth and cartilage) [33], even crystals of organic and inorganic materials [34]. The origin of indentation technique can be traced back to the early twentieth century, when Brinell performed a standardized indentation test by using a steel ball. Later in 1953, Grodzinski measured the indentation depth with a low load application, emerging of the micro-indentation instrument [35]. Due to increasing motivation for the characterization of the mechanical properties of thin films, hard coatings and small volume samples, the nanoindentation technique has been well developed in the later twentieth century [36]. After improvement of the technology (reduced tip radius as well as higher resolution of load and displacement) and data analysis [37], nanoindentation has become a reliable tool for measurement of nanomechanical properties, especially in the nanometer range (less than 200 nm) [38]. The radius of the newly manufactured Berkovich diamond tip can reach 100 nm. Presently, the resolution for load and displacement is extremely high, for load < 3 nN and for displacement less than 0.1 nm. The mostly adopted and used data analysis method (Berkovich tip), for extracting hardness and elastic modulus has been introduced by Oliver and Pharr in 1992 [39,40]. This method is one of the most cited work in material sciences, with a citation of over ten thousand times until 2016 (Web of Science). The typical loading and unloading indentation curve is presented in Fig. 1-4, the relationship between applied load and penetration depth (both for loading and unloading process) are recorded during each indentation cycle. Hardness can be estimated by dividing load within contact

area. Indentation can be classified into macro-, micro- and nano-scale indentation, according to the penetration depth and applied load. For indentations at macro or micro scale, the contact area can be measured under the microscope. However, for nanoindentation, it is very hard and difficult to get accurate contact area under optical microscope, due to the very small plastic deformation with hundred nanometers penetration depth [41]. The accurate contact area can be calculated by evaluating the function of this area at calculated contact depth: $A = A(hc)$. Before calculation, the indenter tip geometry should be calibrated by fused silica with a known reduced modulus of 69.9 GPa. In the sub-micro range, the atomic force microscope (AFM) is commonly used for nano-mechanical characterization [42].

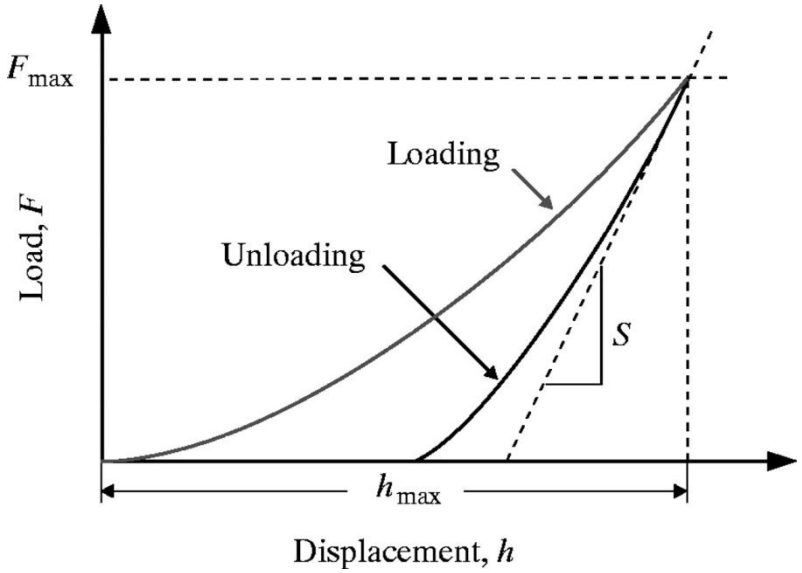

Fig. 1- 4. The typically load-displacement nanoindentation curve (load or depth control). The applied load and penetration depth are recorded during the loading and unloading process [43].

During indentation test, mechanical properties are obtained through forcing an indenter (usually pyramid or spherical diamond tip) into the testing material surface under depth or load control. There are four types of indenter tips with specific geometry used in the commercial nanoindentation instrument for different applications, including three-sided pyramid, four-sided pyramid, conical and spherical shape. The indenter types and their geometry are listed in Table 1.

Normally they are all made of diamond. However, for soft testing materials, they can also consist of steel or glass. Berkovich and Cube Corner tips are three-

sided pyramids with specific face angle. Original Berkovich tip was fabricated by Russian scientist E.S. Berkovich in 1950 with a face angle of 65.03°. It is one of the most frequently used tips in the indentation testing. The advantage of the Berkovich indenter that it is easier to get a sharp point than with the four-sided pyramid indenter [41]. The tip radius of a newly formed Berkovich tip is around 50-100 nm, getting blunt with using. According to the recommendation, the diamond area function calibration should be done by fused silica every three months. Typically, Berkovich indenter has a total angle (plane to edge) of 142.3° with the face angle of 65.27°. With an aspect ratio of 1:8, it has the same projected area as the Vickers indenter ($A_c = 24.5h_c^2$, h_c penetration depth) [43]. Another typical three-sided pyramid tip is the Cube Corner tip, with perpendicular faces like the corner of a cube. It has a total included angle of 90° and a face angle of 35.26°. It is widely used for thin film, scratch testing, fracture and wear testing. Due to the sharp angle of three-sided pyramid tips, it is perfect for *in-situ* images with very high resolution.

Table 1: Types of indenter tips and their geometrical factors [38].

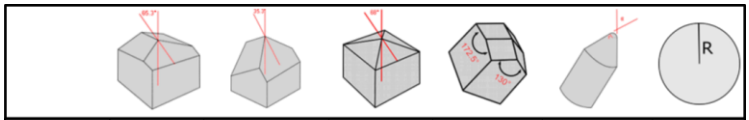

	Berkovich	Cube-Corner	Vickers	Knoop	Cone (angle α)	Sphere (radius R)
Shape	3-sided pyramid		4-sided pyramid		Conical	Spherical
Semi angle	65.27°	35.26°	68°	86.25° 65°	α	/
Effective cone angle	70.3	42.28	70.3	77.64	α	/
Projected area	$A=24.5h_c^2$	$A=2.60h_c^2$	$A=24.504h_c^2$	$A=108.21h_c^2$	$A=\pi hc^2\tan^2\alpha$	$A=2\pi R_i h_c$
Intercept factor ε	0.75	0.75	0.75	0.75	0.727	0.75
Geometry correction factor β	1.034	1.034	1.012	1.012	0.727	1

The Vickers and Knoop indenters have a shape of a four-sided pyramid, widely used in micro-hardness measurements. The Vickers tip is axisymmetric and self-similar, with a face angle of 68°. Its theoretical description is much easier than those of other types of indenters. The Knoop indenter has been developed in 1930s; it was originally designed for testing very hard materials, with two different face angles (172.5° and 130°). Due to its longer diagonal line, the shallow depth of impression could be much more easily measured under the microscope.

The cone tip is characterized by cone angle (from 45° to 120°) and radius of tip curvature. Compared to pyramid tips, it is very hard to manufacture conical shapes with sharp points, normally with the radius over 1 μm. Its attractive part is simplicity of cylindrical symmetry, taking for a modeling standpoint. In general, spherical tips are termed blunt, without a sharp point and mostly employed on soft samples such as biological samples and polymers. At present, for biological samples, spherical tips are desirable. Nanoindentation applied with spherical indenter tips, initially it enables a elastic contact at low load, then has a transition from elastic to plastic deformation at high load [44]. During the indentation process, the contact radius of spherical indenters increases faster than the indentation depth, unlike conical indenters. The limitation of spherical indenters, the indentation depth should be less than one fourth of tip radius [45]. Nanoindetation is widely applied in many areas including aerospace, automotive, biomaterial, micro-electro-mechanical devices, thin-film coating etc.

1.2.2 NanoTest Vantage and Piuma nanoindenter

This moment, we use two types of nanoindentation in the lab, NanoTest Vantage from Micro Materials UK and Piuma nanoindenter from OPTICS11 Amsterdam. The probes for NanoTest and Piuma are typical Berkovich diamond tips and spherical glass probes, respectively. Often, indentations on biological samples (bone), skeleton (spicules and shells) are performed with Berkovich diamond tips. The Piuma indenter is specially designed for soft materials, for example newly formed bone, cartilage, hydrogels, cornea et al. Surprisingly, it can also be used for mechanical scanning of cells.

1.2.2.1 NanoTest Vantage — Micro Material UK

The Micro Micterials company was founded by Dr. Jim Smith in 1988, providing innovative versatile nanomechanical test instruments. It has been a leading international innovator in the area of nanomechanical testing. The NanoTest

Vantage (Fig. 1-5A), released in 2011, is a comprehensive nanomechanical testing platform. It focuses on four key areas: friendly using environment, quickly setting-up, calibration and training, improved performance system and robustness. Up to three mechanical properties (indentation, scanning and impact mechanics) can be determined at the same platform, under environmental options (temperature, humidity and vacuum). This is the only instrument which allows users to perform indentation at extreme conditions, working in the temperature range from -20 ^{o}C up to 750 ^{o}C. With a specially designed wet chamber, it can be used for characterization of mechanical properties under wet condition. The system can be used in conjunction with low load head (0.1-500 mN) or high load head (0.1-20 N), performing nano to micro mechanical testing [46]. In our system, it is conjunction with low load and Berkovich diamond tip, capable of point by point nanoindentation and surface scanning nanoindentation.

The core of NanoTest Vantage, Pendulum in Fig. 1-5B, can rotate on the friction-less pivot, providing full modularity and excellent performance with the highest load and displacement resolution, as high as 3 nN and 0.001 nm, respectively. The most critical parameters during the indentation process are the applied load and penetration depth. The load actuation in NanoTest system is to employ an electromagnetic load coil. The coil is mounted at the top of the pendulum, close to the permanent magnet fixed on granite base frame. With a given current, the coil is attracted to the permanent magnet and force the indenter towards the sample. Theoretically, the applied load is linearly proportional to the current in the coil. The depth is measured by a depth sensor arranged with two parallel plate capacitor systems. Using capacitance bridge unit, the capacitance change is related to the distance between two parallel plates. A plate is attached to indenter holder, the capacitance changes when indenter moves to sample surface. Combination of applied load and depth gives us the load-displacement curve. The hardness and elastic modulus of the sample can be extracted from load-displacement curve using the Oliver-Pharr method [39].

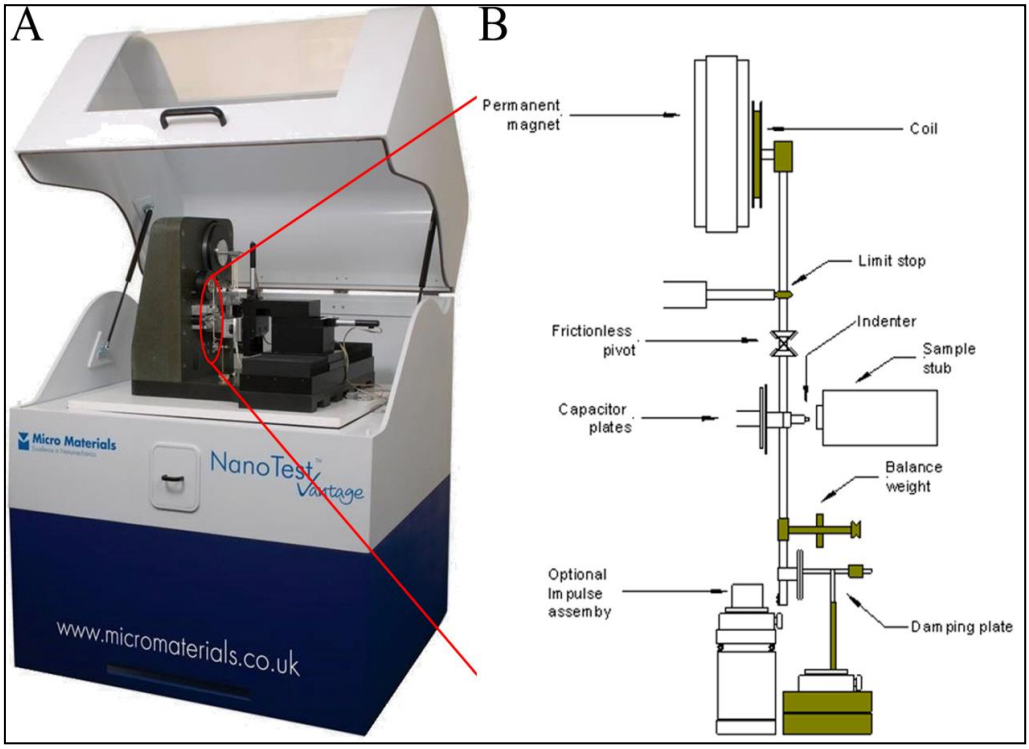

Fig. 1- 5. NanoTest Vantage device from the Micro Material, UK. A: Photo of NanoTest Vantage; B: Pendulum construction. Photos were taken from website: https://www.micromaterials.co.uk/products/nanotest-vantage/

In order to get accurate data and maintain the system in perfect condition, the whole system has to be calibrated manually. All the calibrations required are listed in the Table 2. Calibrations of Pendulum, depth signal and Zero load should be done daily, or before every indent. Pendulum test and Zero load can be done automatically by clicking the calibration button. However, we must be aware of the depth signal, it changes with varying temperatures. The value should be always maintained at 8-9. The pendulum testing indicates if the electronics are functioning correctly. Zero load calibration testing needs to be done more often, it represents the minimum coil voltage which is strong enough to bring pendulum to the limit-stop. Focal plane is taken to determine the distance between microscope and indenter; Crosshair calibration makes sure that indentation areas can be relocated under the microscope. The calibrations mentioned above are used to maintain the system in good condition. The accurate load calibration and diamond area function (DAF) calibration ensure reliable values. Load calibration is performed through hanging three known masses on the setting point. Normally the known masses are

close to 1, 2 and 3 g (1.079 g, 2.062 g and 2.9847 g; supplied in the system). It determines the required coil current which can support pendulum balance at limit stop point [47]. DAF calibration is determined through a series of indentations for fused silica with the recommended indentation depth files. The values of hardness and Young's modulus for fused silica are 8.76 ± 0.06 GPa and 68.9 ± 0.3 GPa, respectively [48]. With accurate DAF calibration, the harness and elastic modulus can be directly calculated through load and penetration depth curve.

Table 2: List of essential calibrations and their frequencies of NanoTest Vantage nanoindenter

Essential calibration	Frequence
Pendulum test (bridge Box Adjustment) Depth signal Zero load calibration	Frequently
Focal Plane calibration Crosshair calibration	Weekly
Load calibration Diamond area functional (DAF) calibration	Every three month

After all these calibrations, the system is ready for indentation testing. NanoTest Vantage allows us to make indentation directly in front of indenter or microscope. For the transparent samples, we have to perform the indentation in front of indenter. The control panel can be depth or load control with the fixed rate. One indentation sequence can be divided into three periods: loading period, dwell period and unloading period. Thermal drift should be collected at post indentation. The system and samples should reach to the thermal balance before indentation. The indentation process will be performed automatically, according to the setting parameters. The hardness and reduced Young's modulus can be extracted from the load to displacement curve, calculated by Oliver-Pharr method [39].

1.2.2.2 Piuma nanoindenter — OPTICS11 Amsterdam

The newly developed nanoindenter Piuma (presented in Fig. 1-6A), based on the ferrule-top technology, was first described by D. Chavan in 2012 [49]. It is a cantilever based nanoindentation, with a glass spherical probe by etching a glass fiber in hydroxy fluoride (HF) (Fig. 1-6B). The glass probe normally used with a radius of over 50 µm is specially designed for soft tissue. The indentation force and depth are measured with an optical interferometer, through cantilever deflection [50]. Then, the reduced Young's modulus (Er) can be extracted from the unloading curve. It should be noted that the indentation depth applied in Piuma is the combination of cantilever deflection and actual penetration depth in the sample. For the NanoTest nanoindenter, the indentation depth is equal to the penetration depth [51].

Fig. 1- 6. Piuma nanoindenter system from OPTICS11 Amsterdam (A: Components of the Piuma system; B: glass probe). The photo in A was taken from website: https://optics11.com/products/piuma/

The Piuma nanoindenter is primarily built of five components: Piuma, computer, OP1550 optical readout interferometer, controller, and probe. The company (OPTICS11) offers probes with different stiffness (0.005 to 200 N/m) and tip radius (3 to 100 µm). The selection of the appropriate probe is critical for correct measurements. Specimens with a high modulus require stiffer probe, while specimen with a very small size require a sharp probe. The recommended stiffness of the cantilever for samples with a different Young's modulus is listed in Table 3

(100 µm tip radius, Piuma guideline). The selected probe must be carefully handled and placed into probe holder without touching the top of the probe (the probe can be easily damaged). It is important to configure the probe correctly in order to get correct results. When we place a new probe or change the measurement condition, the probe geometrical factor must be recalibrated by the stiff material-polished steel or glass.

Table 3: Recommended cantilever stiffness to the samples with different values of Young's modulus.

Young's modulus of sample	Cantilever stiffness (N/m)
100 Pa - 1 Kpa	0.1
1 - 10 Kpa	1
10 - 100 Kpa	10
100 KPa - 10 MPa	50
10 MPa - 500 MPa	150

Besides the probe, one thing which is more important is the configuration of the indentation process. In the indentation panel, indentation depth, loading time and dwell period can be defined individually. The maximum indentation depth should be less than a quarter of probe radius. The maximum depth can be set to 20 µm, but normally 10 µm is taken. The loading and unloading time are set to 2 s. At least ten indents should be performed in each indent area. There are two advantages of Piuma nanoindentation compared to the NanoTest nanoindentation. First, it is not necessary to polish the sample surface. And second, Piuma indentation does not need a special chamber for measurements under wet conditions. The slide with the sample can be simply putted or glued onto the bottom of a petri dish with water or buffer inside.

Approaching to sample surface, two steps are required. First step, bringing the sample directly under the probe and rotating the knob to bring the probe within 1-2 mm above the sample with great caution. Then, bringing the probe to slightly contact the sample surface through an accurate automated finding surface

procedure. By clicking the indentation button, the indentation will be performed and the elastic modulus can be automatically extracted from the load-displacement curve.

1.2.3 Nanoindentation on biological materials

The mechanical properties of biological materials on tissue level are of utmost importance in clinical medicine and tissue regeneration [33,52]. The nanoindentation technique can serve as a powerful tool to determine the mechanical properties of these materials, allowing the measurement and mapping of the mechanical properties at the nano- and micro-scale [53]. The indentation depth of nanoindentation normally ranges from hundred nanometers to a few micrometers, matching the tissue micro-structure. As a typical biological tissue, bone is heterogeneous in composition and structure, and characterized by the presence of multiple structural levels from nano- to macro-scales [54]. The nanoindentation technique has been widely used in the characterization of the mechanical properties of biomineralized samples, such as bone, teeth and shell [55–57]. Meanwhile, application of the nanoindentation technique for the biomechanical characterization of soft tissues is also getting more and more attractive because of the impact of alterations in connecetive tissue on human health and morbidity [58].

The mineralized tissues of primary interest are composed of calcite, aragonite, hydroxyapatite and bio-silica [59]. They are built of organic parts and minerals, formed at ambient condition through biomineralization processes. Biosilica (biogenic silica) is an amorphous metal oxide that is formed by a complex enzyme-mediated biosilicification process. Diatoms and siliceous sponges extract soluble silicate from ocean to build up their species-specific biosilica skeleton, ranging in size from several micrometers to meters [60,61]. The mechanical behavior of the biosilica structures (e.g., from hexactinellid sponges [57-61] and diatoms [62-65] has been intensively investigated through nanoindentation technique because of

the exceptional mechanical properties of these composite materials. Their entire glassy skeleton is hierarchically organized from nanometer to macroscopic length scales: up to seven hierarchical levels are found. This hierarchical structure comprises the silica nano-particles, as well as the spicules, micro-scale beams and macro-scale glassy cylinders formed by them [71,72]. Due to this unique hierarchical structure, the glassy sponges have excellent mechanical performance. It overcomes the brittleness of the mineral, and shows outstanding mechanical rigidity and flexibility [71]. In combination with reverse finite element analysis, the modulus of the laminated architecture within the giant sponge spicules was evaluated *in situ* by nanoindentation. It was found that the organic layer and bio-glass layer have a modulus of 0.7 GPa and 37 GPa, respectively [65]. Diatoms are single-celled algae which have an intricate porous nano-patterned silica frustules [67,69]. The micromechanical properties of the diatom frustules are correlated with their specific nano-patterned structure (pore size, pore distance and porosity), with a Young's modulus of 1.1 - 18.6 GPa and a hardenss of 0.1 - 1.43 GPa [69].

The mechanical properties of bone and teeth, which are hydroxyapatite based biological materials, have been intensively investigated by application of the nanoindentation technique [73–78]. Using nano-scale indenter tips allowing high-depth resolution in the nanometer range, it was possible by applying the nanoindentation technique to measure the elastic modulus and hardness at the tissue level. Bone is a heterogeneous material with a hierarchical structure. The mineral phase (hydroxyapatite) contributes stiffness and collagen contributes elastic and viscoelastic behavior [75]. The mechanical properties of bone vary depending on its structures (microstructure, porosity and donors etc.) and can also be influenced by the method used for sample preparation and preservation and the hydration conditions [33]. Due to the difference in its microstructural organisation, cortical bone is much stiffer and has a higher Young's modulus and hardness compared to trabecular bone [73,79]. The elastic modulus of bone was investigated both under wet and dehydrated conditions, and increases from 11.7±1.7 GPa (hydrated) to 15.0±2.2 GPa (dehydrated) [75]. Teeth enamel are the hardest tissue

in the body, but it has no regeneration potential [78]. With the improvement of the nanoindentation technique, the mechanical behavior of enamel rods and interrods, as well as of peritubular and intertubular dentin can be measured more accurately [52].

With the exception of mineralized tissue such as bone and teeth, the nanonindentation technique is increasingly applied to study the biomechanical properties of soft tissues such as cartilage [80,81], newly formed bone [82–85] and vascular tissue [82,86]. For that purpose, for soft material indentation, a spherical indenter tip is often chosen instead of the Berkovich tip. Up to now, nanoindentation is frequently combined with histological methods to evaluate the repair of cartilage [81] and bone tissue [85]. Using the nanoindentation technology, the mechanical properties of regenerated cartilage and bone tissue are often found to be weaker compared to the control tissue, similar to the histological results [80,81]. Mapping the elastic properties of soft tissue, nanoindentaion was used to distinguish and spatially resolve differences in micromechanical properties of large arteries and veins [87]. Recently, nanoindentation is emerging as an important tool to monitor bone regeneration and osteointegration process [82,83]. The stiffness of newly formed bone tissue is directly correlated to degree of calcification of collagen [88]. Nanoindentation has been proven to be a powerful technique for charactering mechanical behavior of hard coatings, thin film, biological materials at micro- and even at nano-scale. Even so, nanoindentation is still a young technique for the characterization of biological materials and will gain more and more attention in the fields of biomedicine and biomaterial [89].

1.3 Silica in human and its relation to bone health

1.3.1 Silica

Silicon (Si) is the second most abundant element in the earth crust with 28 wt %, just after oxygen, mainly existing in the form of silica or silicate. It is characterized by its wide distribution, found in all natural waters, in the atmosphere

(as dust), in plants and in animals [90]. Even more, the whole skeleton of the siliceous sponges (e.g. the Hexactinellid sponges) is made of pure silica, which is enzymatically formed by the enzyme silicatein which is located in the centre of spicules [61]. The longest silica spicules are found in deep-sea sponges, reaching a length of 3 m. The human body contains approximately 7 g of silica. High concentrations of silica are found in bone, connective tissue and tendons [91]. The main silicon resources for humans are food and drinks. Normally, plant food (particularly cereal grains and roots) are much richer in silicon than meat products. The soluble silica in soil and soil solution is taken up and accumulated in plants, ranging up to 10 % of dry weight [92]. Silica is also present in all kinds of beverages, coming from water and fruits. In the soluble form of $Si(OH)_4$ in drinks, silicon is easier taken up than the solid form of (SiO_2) present in food. By the way, beer contains 19 mg/l silicon and is recommended as a good resource for dietary silicon. Its silicon mainly comes from hops and barley and has been proven as a directly bioavailable silicon source [93,94]. The distribution of silicon in human tissues has been intensively investigated. The highest silicon concentration is generally found in connective tissue and bone, with varying levels [95]. In contrast, in total body fluid and serum, the range of silicon concentration is very narrow, with an average value of 0.5 µg/ml. However, the silicon concentration level remains relatively constant, even with extra intakes. Once silicon enters into the bloodstream, it will be rapidly excreted out of the body in the urine [96]. Silicon is strongly related to human health, playing an important role in many body functions and particularly directing bone formation. Besides of bone, silicon is also responsible for cross-linking of collagen strands, contributing to the strength, integrity and flexibility of connective tissue. All these functions have been proven in animals and humans since mid-1970s. In summary, silicon is an essential nutrient for the human body and has an important function in the development and maintenance of the structural and functional integrity of the connective tissue and the skeletal system. Interesting, the silicon concentration in serum of newborns is much higher than in adults [97].

1.3.2 Silica uptake and excretion

Solid food and drinks are the main sources of silicon in the human body. Up to now, the mechanism for silicon uptake is still not clear. Silicon is mainly taken up in the soluble form in the gastrointestinal tract. Soluble silica (orthosilicic acid) is released from food when digested in the stomach under weak acid condition, and then enters into the tissue fluid in the gastrointestinal tract. The bioavailability of silica differs depending on the type of food and is considered to be low [98]. Orthosilicic acid is the major silica species in drinks. So, silica in drinks is much easier absorbed than silica in solid food. Beer is a dietary source of silica, rich in bioactive silicon derived from cereals. The silica uptake occurs predominately in the proximal small intestine. Two pathways are probably involved in the absorption process, paracellular pathway and small-pore transcellular pathway [99]. Moreover, its absorption and excretion are independent on the gender and the age of adults [100]. Once silicon enters into blood circulation, it rapidly diffuses into tissue fluids and is then excreted out of body in the urine. Despite the wide range of silica intake, the serum silica level can be kept in a narrow range, because of an efficient renal clearance system [101]. After infusion of soluble silica into the bloodstream by continues intravenous injection, most of the silica is eliminated within 4-8 h after ingestion. It is present in the form of free orthosilicic acid in blood and do not interact with proteins. So, the diffusion of total body fluid depends on the silicon concentration gradient and may involve no energy. The absorbed silica is mostly excreted in the urine as orthosilicic acid. A small part is concentrated into connective tissues. The main way for excretion of absorbed silicon is to enter into urine *via* kidney, and the level in urine is influenced by the silica uptake [102].

1.3.3 Silica and bone health

Silicon is an essential element for formation and development of bone and connective tissue. Since the 1970s, its biological function in bone formation has been proven in chicken [103] and rats [104]. In chicken, silica deficiency causes

slower growth rate, pale comb, smaller and less flexible leg bone and abnormal skull deformation. Similar results were observed in rats (fed with low silicon diet) with retarded skeletal development and skull deformation. In the human body, a higher silicon uptake is positively correlated with bone density [94]. The effect of silicon on bone health is shown in Fig. 1-7. Silicon is involved in the regulation of collagen synthesis and calcification. *In vitro*, orthosilicic acid (< 50 µM), under physiological conditions, can stimulate collagen synthesis and enhance the differentiation of osteoblasts [105]. Silicon-substituted hydroxyapatite (Si-HA) affects the attachment of human osteoblast-like cells, metabolic activity and proliferation, and even extensive extracellular matrix synthesis [106]. It also has a dual role on bone formation: stimulating osteoblasts (bone mineralization) and inhibiting osteoclasts (bone resorption). Silica inhibits significantly the activity of osteoclasts, gene expression, and bone resorption *in vitro* [107]. In a co-culture system, osteoblasts (SaOS-2, bottom chamber) and osteoclasts (RAW.264.7, upper chamber) were co-cultured in 24-well culture plates separated by a microporous membrane filter. It turns out that silicate can regulate the cross-talk between osteoblasts and osteoclasts. It causes an increased expression ratio of OPG (osteoprotegerin) / RANKL (NF-kB ligand) and a significant reduction in osteoclasts differentiation [108].

In bone, silica promotes the calcification of organic bone matrix. Collagen, 90 % of organic matrix, is the major constituent of bone matrix. The expression level and stability of collagen have a direct positive effect on bone metabolism. Silica has been shown to enhance collagen expression by the differentiated osteoblast phenotype, by increasing the activity of alkaline phosphatase (ALP), the synthesis of osteocalcin and mineralization [109]. As mentioned above, human osteoblast-like cells increase the expression of collagen type 1 mRNA after supplementation of the culture medium with orthosilicic acid in. The suggested mechanism of the function of silicon or silicate in collagen biosysthesis involves a modulation of the activity of prolyl hydroxylase, which is required for collagen synthesis. This enzyme is responsible for the conversion of hydroxylated proline to hydroxyproline [110].

Hydroxyproline is the major component of collagen and plays the key role in collagen stability together with proline. High silicon contents are found in connective tissue, where it is present as an integral component of glycosaminoglycans and polyuronides [111]. It is firmly bond to the polysacchairide matrix, only released under strong alkaline and acidic conditions. It may function as a cross-linking agent and contributes to the structural framework of connective tissues [112].

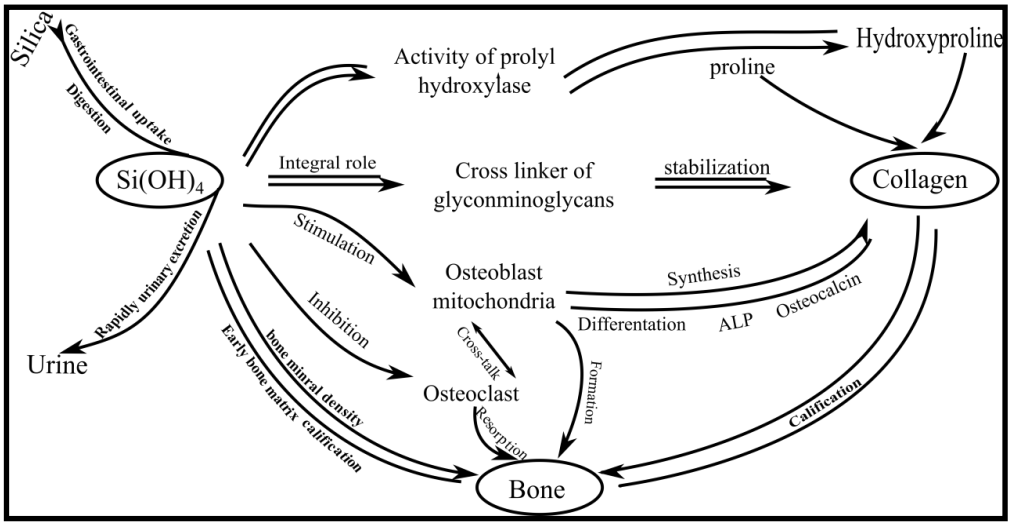

Fig. 1- 7. Diagram of functional mechanism of silicon in bone formation

Numerous studies have confirmed that silicon actively participates in the process of bone calcification and accelerates the rate of bone mineralization. It has also been found that bone growth can be activated in the presence of silica, indicating that silicon is involved in the early calcification of the bone matrix. In newly formed bone, high concentrations of silica occur, but it becomes below the detectable level at the end of the calcification process [113,114]. By an electron microscopic analysis, it has been found that high silica concentrations exist in the mitochondria of active osteoblasts, if rats has been given silica gel by intraperitoneal injection [115]. During the investigation of dietary silicon intake in Belgium, they found that pregnant women have very low concentrations of serum silicon (38 ± 10.3 µg/l, n = 28, 19-39 years), compared with age-matched non-pregnant women (126 ± 73 µg/l, n = 34), while the infant group had an extremely

high silicon level (516 ± 258 µg/l, n = 11), especially babies who were less than one year old [116]. The explanation may be that pregnant mothers provide silicon to the fetuses for the development of bone and connective tissues. So far, there is no direct evidence found that silicon deprivation is related to the health of fetus. In order to take advantage of the positive effect of silicon on bone formation, silicon or silica is used as a component of bone implant materials, such as bioglass [117], biosilica-based biomaterial [118], Si-substituted hydroxyapatite [119] and silica-ceramics [120]. Silicon or silica is leading an evolution in the biomaterials area [121]. Besides of the effects on bone and connective tissue, additional beneficial effects of silicon have been proposed for modulating immune responses and mental health [122].

1.4 Biosilica basic aspects and application in biomedicine

1.4.1 Siliceous sponge skeleton element – Spicules

The skeleton of the siliceous sponges is built up by discrete elements called spicules, providing them a distinct body shape and plan. Spicules are varying in size and shape from species to species, summarized by Van Soest in 2012 [123]. There exists a hollow canal in the center of spicules, with different diameters from 0.3 to 1.6 µm, surrounded by concentric silica layers. The hollow canal hosts an organic filament called axial filament, which consists of silicatein, the enzyme which regulates biosilica formation. In our group, the formation and morphology of the spicules from the marine sponge *Suberites domuncula*, collected in the Northern Adriatic near Rovinj (Croatia), has been intensively investigated [124–126]. The advantage of taking *S. domuncula* as a siliceous sponge model is that it only contains megasclere spiclues which can reach a final size of 300 µm (5-7 µm in diameter) [61]. The spicules are obtained when the sponge tissue is first treated with sulfuric acid/nitric acid, then treated with n-butanol/water/SDS [127]. There are two types of megascleres in the *S. domuncula* skeleton, the monactinal tylostyles and a smaller portion of diactinal oxeas. Oxeas have two identical sharp

tips, while tylostyles have sharp points on one side and swollen knobs on the other side. But both have an axial canal in the centre of spicules, harboring the axial filament. The megascale spicules can reach up to 300 µm in length and 5-7 µm in diameter, containing 6-13 % water with an approximate molecular formula of $(SiO_2)_{2\text{-}5}{\cdot}H_2O$ [125]. They are intercellularlly synthesized by special sponge cells named sclerocytes, and their surface is covered by a silicalemma membrane. The longest spicules can reach 3 m and a diameter of 8 mm. The morphology of the hexactinellid spicules (Fig. 1-8) can be clearly visualized by high resolution scanning electron microscopy (HR-SEM) [126]. The SEM image shows clearly that there are three parts through the cross section of the spicule: *i)* the axial canal located in the center, *ii)* an axially dense and homogeneous silica cylinder surrounding the central axial canal, and *iii)* the outer part, consisting of concentric silica lamellae (up to 800 layers for a 8.5 mm thick spicule) [128]. The image with a larger magnification shows that a small gap exists between the silica lamellae, harboring a proteinaceous material [126].

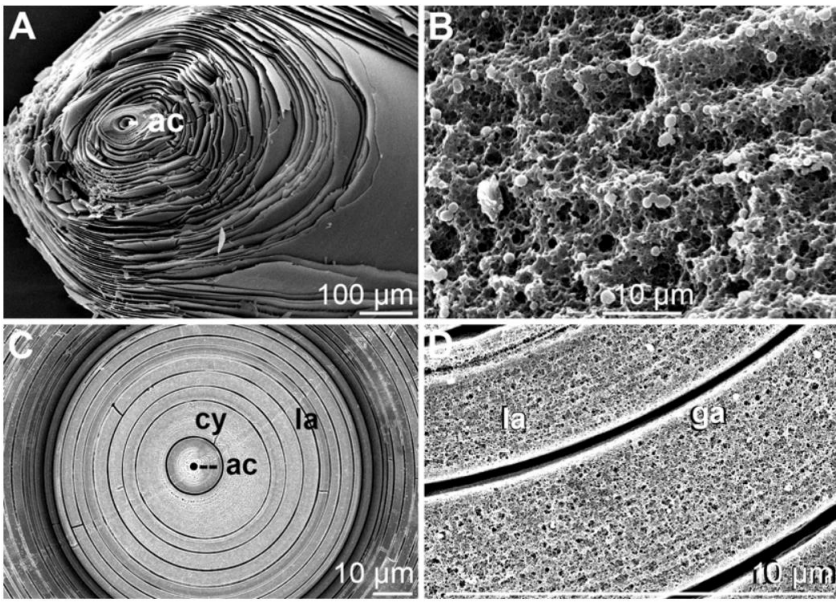

Fig. 1- 8. SEM images of the cross section of a giant spicule. A: Cross section of a spicule with lamellalar structure; B: Biosilica nanoparticles in silica lamellae; C: Polished cross section of spicule; D: Small gap between silica lamellae [116].

1.4.2 Biosilica formation – enzymatically formed by silicatein

In nature, biosilica is enzymatically formed by specific enzymes at neutral pH condition and room temperature. In contrast, in industry silica is produced at extreme pH, high temperature (over several hundred degrees), and high pressure conditions. In siliceous sponges, the specific enzyme which is responsible for biosilica formation is termed silicatein. It can be harvested from the axial filament which harbors in the axial canal located in the centre of spicule. After the siliceous shell of the spicules is dissolved by HF, the organic filament is released. Silicatein is the predominant protein of the axial filament and is expressed by sponge's sclerocytes. Its biological ability (silica formation) has been proven *in vitro* by incubation of this organic filament together with the silicon alkoxide substrate [129]. The mature silicatein comprises 213 amino acids (aa) with a size of 24-25 kDa and belongs to the cathepsin L family; the latter enzymes cannot form silica. Interestingly, the catalytic center of silicatein is formed by His (histidine), Asn (asparagine) and Ser (serine). However, it is different from that of the cathepsins which carry a catalytic triad of the three amino acids Cys (cysteine), His and Asn [130,131]. A new model of the catalytic mechanism of biosilica formation by silicatein has been proposed by Müller and Schröder in 2012, as shown in Fig.1-9 [132]. The highlight is the formation of reactive cyclic silicic acid species (trisiloxane rings and higher-membered silioxane rings), using orthosilicic acid as silicon alkoxide substrate. The formed cyclic trisilicic acid is proposed as the initiator of biosilica particles through a fusion and sintering process, which is modulated by silicatein and other related proteins (silintaphin and silicase), to form the spicule [61,132].

The proposed mechanism consist of six steps and can be summarized as follows [132]:

- Step 1: Nucleophilic attack (S_N2 type) of the (electronegative) oxygen atom of the hydroxyl group of the serine residue at the (electropositive) silicon atom of a silicic acid molecule;
- Step 2: Release of one molecule water, resulting in a silicic acid bound to serine;

- Step 3: Nucleophilic attack of the oxygen from the OH ligand of the bound silicic acid at the silicon atom of a second orthosilicic acid molecule in the catalytic pocket;
- Step 4: Release of one molecule water, resulting in a silicic acid dimer bound to serine;
- Step 5: Nucleophilic attack of the oxygen atom of a further OH ligand of the first silicic acid molecule, after rotation of the Si-O-C bond between this molecule and the enzyme Ser residue, at the silicon atom of a third orthosilicic acid species, again facilitated by hydrogen bridge formation to the imidazole nitrogen;
- Step 6: Cyclization reaction of the siloxane trimer.

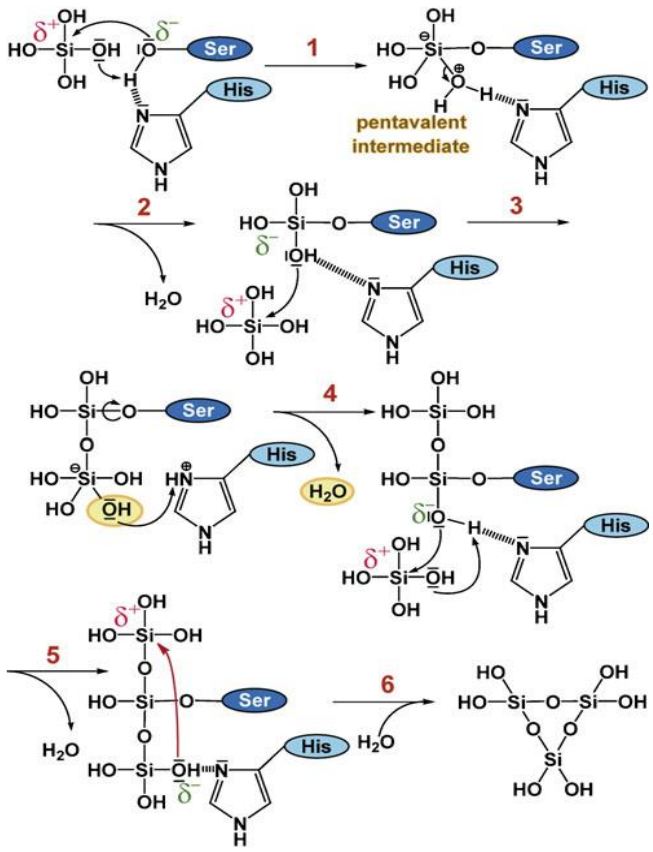

Fig. 1- 9. Proposed mechanism of biosilica formation catalyzed by silicatein in six steps, taking orthosilicic acid as silicon alkoxide substrate [122].

1.4.3 Biosilica application in bone regeneration

Silicon is an essential element for bone formation, where it is involved in the

early stages of organic matrix mineralization [133]. Biosilica, enzymatically formed at ambient condition, has been proposed as a new functionally active natural inorganic polymer in biomedicine and tissue engineering [118,134,135]. For biomedical application, biosilica can be enzymatically formed through polycondensition of silica substrates mediated by recombinant silicatein, or it can be purified from biosilica skeletons (siliceous sponge spicules) [136,137]. Studies on biosilica (enzymatically formed) as a bone regeneration material have been extensively conducted by our group, and are now listed below:

- Year 2004:

Prof. Müller et al. proposed for the first time that biosilica can be used as a blueprint for the fabrication of new biomaterials, in particular for bone replacement, to stabilize tissue. Furthermore, biosilica can also be used as an bioactive coating for bone implants to increase their capability of bone healing [138].

- Year 2005:

The bioactivity of biosilica modified surface (stimulation of osteoblasts mineralization function) was proved by incubation of osteoblasts on biosilica modified culture plates. The culture plates were coated at room temperature overnight with collagen/silicatein/TEOS. Plates coated with collagen or collagen/silicatein were used as control. The biosilica coated plates showed a marked increasing in hydroxyapatite nodules formation, as revealed by Alizarin red staining and SEM [139].

- Year 2010:

The potential of biosilica as a bone substitution material has been successfully demonstrated by *in vivo* studies. Rabbit femur defects were treated by biosilica-based implants and after 3 months, new bone had been completely regenerated in the defects. In this work, silicatein and silicate substrate were encapsulated together in PLA (poly(lactide acid) microspheres. The microspheres were embedded

in a poly(vinyl pyrrolidone)/starch-based matrix at varying ratios. The blend implant material has been proven to be biocompatible and biodegradable in *in vitro* studies: it even shows moldable and self-harding properties at a controlled rate within 30 min to 6 h [140].

To investigate the osteogenic potential of biosilica, osteoblasts were grown on different substrates (bone slices and Ca-P-coated coverslips) modified with biosilica. In these experiments, the expression of bone morphogenetic protein-2 (BMP-2; a key inducer of osteoblast differentiation) was found to be upregulated, while the expression level of TRAP (tartrate-resistant acid phosphatase; a modulator of bone resorption) remained unaffected [141].

Inspired by the highly binding affinity of Glu-rich protein to Ca, Glu-tagged silicatein was developed for immobilization of biological materials on HA (bone and tooth). After incubation with silicate substrate, the silicatein-immobilized material became coated with a layer of biosilica. Synthesized HA nanofibrils were modified with a biosilica coating *via* biosynthesis by immobilized Glu-tagged silicatein. Hence, this provides a novel biological method to supply a morphogenetically active layer on HA or Ca-rich biomaterials, and finally contributes to bone regeneration [142].

Further, we found that incubation of SaOS-2 with biosilica resulted in an unregulation of the expression of BMP-2 and HA formation. Moreover, biosilica was capable of stimulating the expression of osteoprotegrin (OPG) gene. In contrast, the expression of RANKL remained unchanged. OPG, through binding to RANKL, inhibits the differentiation of osteoclasts and protects bone from excessive resorption [143].

- Year 2013:

In order to investigate the response of osteoblasts to morphogenetically active silica, silica supplements were added to the alginate hydrogels, then osteoblasts were seeded onto it and cultured in osteogentic medium. The biomineralization was determined by staining with osteoimage fluorescence. The quantitative real-time PCR (qRT-PCR) data showed an upregulation of expression of BMP-2 (bone morphogenetic protein), COL-I (collagen-I), COL-V (collagen-V), OPN (osteopontin)

and ON (osteonectin), while the steady-state levels of RUNX2 [Runt-related transcription factor 2], OC (osteocalcin) and BSP (bone sialoprotein) remained constant. Based on the qRT-PCR data, it was concluded that silica causes its morphogenetic effect with respect to some bone-related genes [144].

- Year 2014:

For the 3D bioprinting, biosilica and osteoblasts were encapsulated into a printable and degradable hydrogel. The effect of biosilica on the growth and biomineralization of the encapsulated cells was investigated. The results showed an increased proliferation and mineralization rate compared with the control without biosilica. In addition, after blending with biosilica particles the mechanical properties and stability of the alginate/gelatin hydrogel were found to be improved [145].

The fabrication of biopolymer nanofiber containing biosilica was carried out through electrospinning of biopolymer [poly(ε-caprolactone)] together with tetraethyl orthosilicate [TEOS]; subsequently the nanofibre mats were incubated with silicatein to form biosilica [146].

The surface of biopolymers (chitosan-graft-polycaprolactone) was further modified with biosilica *via* immobilized silicatein and incubation with hydrolyzed TEOS. After the modification, contact angle measurements showed that the surface hydrophilicity of the bipolymer graft was dramatically changed (total wetting). In addition, the mineralization and ALP activity of the cells were enhanced. These results indicated that the biosilica-coated bipolymer is an alternative bone replacement material [147].

Furthermore, a bioactive silica-based PLGA microsphere material was developed for bone regeneration. Silicatein and silicate substance were encapsulated separately into large and uniform PLGA microsphere with a diameter of 800 μm. These two kinds of microspheres were mixed together at a weight ratio of 1:1 and then injected into a defect drilled in rabbit femur with a diameter of 5 mm and depth of 7-8 mm. After 100 days, part of the microspheres was degraded

and new bone was grown surrounding the microspheres. The stiffness of regenerated bone area was determined and the value of biosilica-based group is much higher than that of the control group. In conclusion, biosilica is a promising material for bone repair and regeneration [84].

- Reviews

The biomedical applications of biosilica, together with another natural inorganic polymer (polyphosphate) and biocalcite, were highlighted in several review papers [61, 118, 135, 136, 148].

Chapter II:
Fabrication of microspheres and microsphere-based scaffolds

2 Fabrication of microspheres and microsphere-based scaffolds

2.1 Materials and equipment

2.1.1 Materials

Poly(D,L-lactide-*co*-glycolide) (PLGA; lactide : glycolide [75 : 25]; mol wt 66,000 - 107,000	SIGMA*P1941
ß-tri-calcium phosphate, ß-TCP, $Ca_3(PO_4)_2$	SIGMA*16843
N-Methyl-2-pyrrolidinone(NMP), ⩾ 99.8 %	Roth*4306
Poly(vinyl alcohol) 87-90 % hydrolyzed (PVA), average mol wt 30,000-70,000	SIGMA* P8136
Dichloromethane (DCM), CH_2Cl_2; ⩾ 99.8 %	Roth*T162
Filter paper (Whatman™ Grad 595 1/2)	Fisherscientific*10311645
Sodium silicate solution, ~27 % SiO_2 in 14 % NaOH	SIGMA*S1773

2.1.2 Equipment

KDS Single-syringe pump	SIGMA*Z401366
X360 High Speed Homogenizer Drive	CAT Scientific
Freeze dryer (BenchTop Pro with Omnitronics)	SP Industries
Magnetic stirring	Roth
Digital microscope - VHX-1000	Keyence

2.2 Fabrication of PLGA microspheres with active ingredients

2.2.1 PLGA selection

Poly(lactic-*co*-glycolic acid (PLGA), a synthetic aliphatic polymer, a copolymer of poly(lactic acid) and poly(glycolic acid) with different ratios. It has been intensively investigated as a drug delivery system [149] and bone repair material [150]. It is characterized with biocompatible and biodegradable properties. It exhibits a wide range of erosion times, has tunable mechanical properties, and most importantly, is a FDA-approved polymer. The degradation properties of PLGA are related to the ratio between lactide and glycolide, two monomers for the polymerization. Common

forms of PLGA are PLGA (85:15), PLGA (75:25), PLGA (70:30) and PLGA (50:50). PLGA (85:15) is a copolymer whose composition is 85 % lactic acid and 15 % glycolic acid. Its degradation involves the hydrolysis of its ester linkages in presence of water. Its ultimate degradation products are monomeric lactic acid and glycolic acid, which can be metabolized in the tricarboxylic acid cycle and eliminated *via* CO_2 and H_2O. The presence of methyl side group in lactic acid makes this molecule more hydrophobic than glycolic acid. In general, the higher the glycolic acid content is, the shorter the time required for degradation. With one exception, PLGA (50:50) exhibits rapid degradation (about two months). In addition to the monomer ratio, other parameters normally influence the degradation of PLGA such as glass transition temperature, moisture and molecular weight. In 1997, Holy et al conducted an experiment to indentify the optimal ratio between lactide and glycolide for the application of PLGA in bone tissue engineering [151]. They cultured rat bone marrow cell (RBMC) on different types of PLGA membranes (85:15，75:25，50:50, and 100:0). After two weeks of incubation, the bone matrix/formation was present at varying degrees dependent on the substrate composition: PLGA (75:25) > PLGA (85.15) >> PLA. So following the achievements of previous studies, PLGA, at a ratio of 75:25, was taken as the substance in our studies to prepare PLGA-biosilica microspheres for application of bone repair.

2.2.2 Preparation of PLGA/ß-TCP microspheres, termed ß-TCP-micro

In order to prepare large and uniform microspheres for bone repair, a modified double-emulsion solvent extraction/evaporation method (Fig. 2-1) was employed. Solutions with various concentrations (10 %, 15 % and 20 %) of PLGA were prepared in glass vials by dissolving PLGA in DCM. PLGA, a co-polymer of lactide and glycolide with various ratios, is biodegradable and biocompatible, and has been approved by US Food and Drug Administration (FDA). ß-TCP (10 % of PLGA) was added to the PLGA solution and intensively mixed to get a homogeneous PLGA/ß-TCP mixture. Then, using a high speed homogenizer (10,000 rpm), 0.8 ml of distilled water (as the first aqueous phase, w1) was mixed with the PLGA/ß-TCP mixture described above for 3 min at room temperature to obtain a uniform viscous emulsion. Subsequently, the

received emulsion was immediately injected dropwisely into 300 ml of 1 % PVA solution (as the second aqueous phase, w2) *via* a syringe needle (blunt, with different diameters to control the size of the microspheres), controlled by a syringe pump at a speed of 12 ml/h. During the dropping process, the needle tip was kept below the water surface. Thereby, the uniform microspheres can be fabricated under proper and constant water shear force. Finally, the microspheres formed were stirred with a magnetic stirrer at 650 rpm for 4 h to evaporate the organic phase and to harden the microspheres. The solidified microspheres were washed several times with distilled water to remove the residual PVA and collected on the filter paper. They were frozen at -80 ^{o}C overnight, then lyophilized for 24 h and stored at 4 ^{o}C for further studies.

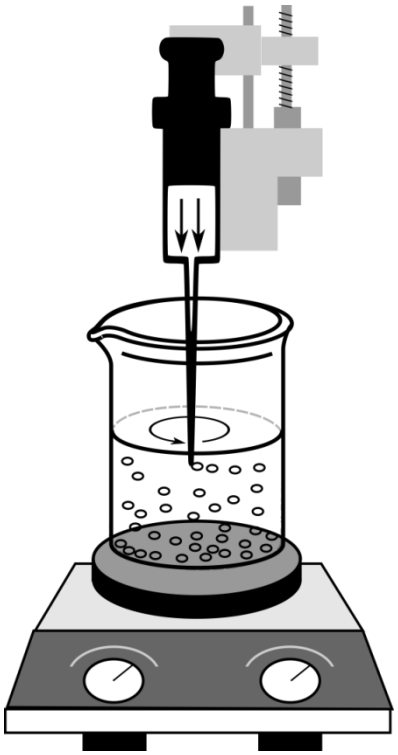

Fig. 2- 1. Schematic diagram of the modified solvent extraction/evaporation method for the PLGA microsphere preparation. (It is important to keep the needle under the water surface)

2.2.3 Preparation of PLGA/ß-TCP/Silica microspheres, termed ß-TCP/Silica-micro

The preparation for ß-TCP/Silica-micro is similar to the preparation of ß-TCP-micro. However, the first aqueous phase consist of 0.8 ml of silicate solution instead of water. Then, 600 mg PLGA was dissolved in 3 ml DCM to get a 20 % PLGA solution.

Subsequently, 60 mg ß-TCP powder and 0.8 ml of silicate solution were mixed with the PLGA solution using a high-speed homogenizer (10000 rpm, 2 min). Then the suspension was injected into 300 ml of 1 % PVA solution with a syringe pump at a speed of 12 ml/h. After stirring for 4 h, the hardened microspheres were washed five times with water, then collected on filter paper and frozen overnight at -80 ^{o}C. The lyophilized microspheres were kept at 4 ^{o}C for further characterization and scaffold preparation.

2.2.4 Preparation of PLGA/ß-TCP/Silicatein microspheres, termed ß-TCP/Silicatein-micro

600 mg of PLGA was dissolved in 3 ml DCM in a coved glass vial to avoid the evaporation of DCM, containing 60 mg ß-TCP. Then, the recombinant silicatein (0.8 ml, 1 mg/ml) was mixed with the PLGA-ß-TCP suspension through vigorous stirring to form a homogeneous emulsion. After that, the emulsion was dropped into 300 ml of 1 % PVA solution through a syringe. The dropping speed was controlled by a syringe pump to form uniform microspheres (with a diameter of 0.8 mm). The received microspheres were stirred at 650 rpm for additional 4 h to evaporate DCM from microspheres. After complete evaporation of the DCM, the solid microspheres were washed five times with water and freeze-dried for 24 h. Finally, the dried microspheres were stored in a glass vial at 4 ^{o}C until further use.

2.3 Biolinker selection and microsphere-based scaffold preparation

2.3.1 Bio-linker selection

In this work, the solvent/non-solvent sintering method was selected for the preparation of microsphere-based scaffolds. This technique involves two miscible solvents; one is a solvent and other one is not a solvent for the polymer used for preparing the microspheres. For PLGA, NMP (N-methyl-2-pyrrolidone) was selected as solvent and water was used as non-solvent. The solvent was mixed with water at different ratios from 50 % to 90 % and the mixture was named as a biolinker for the

preparation of scaffold based on PLGA microspheres. To prepare the scaffolds, 50 mg of PLGA microspheres were placed into the cylindrical steel mold, then 200 µl of biolinker solution (different mixtures) was pipetted over the microspheres until they were completely wet. The submersion time was set from 1min to 30min. After submersion, the wet microspheres were strongly pressed with a steel punch to force the microspheres to connect tightly and to remove most of the biolinker solution from the mould to form the scaffolds. Then, the scaffolds were carefully taken out from the mould and placed onto a Petri dish containing a large amount of water. The remaining NMP solvent was dispersed into water and the scaffolds were solidified. Finally, the hardened scaffolds were lyophilized for 24h before characterization.

2.3.2 Fabrication of microsphere-based scaffolds

After the optimal mixing ratio of the biolinker and and the optimal submersion time were determined, the PLGA microsphere scaffolds were prepared by the solvent/non-solvent sintering method. The preparation procedures are illustrated in Fig. 2-2. 50-55 mg of microspheres (for a scaffold with a diameter of 10 mm and a thickness of 2 mm) were weighted by an electronic balance and poured into the mould. Then 200 µl of bio-linker (75 % NMP/H_2O) was pipetted into the mould. In order to make the surface of the microspheres completely wet, the bio-linker was gently pipetted up and down several times. The mould was left at room temperature for 5 min to conduct a close contact among the adjacent microspheres. Afterwards, the wet microspheres were slightly pressed with a steel pillar to remove the solvent and to strengthen the bonding between the adjacent microspheres. Finally, the microsphere-based scaffolds formed were pushed out of the mould, and placed in the distilled water for several hours. During this process, the residual solvent (NMP) in the scaffolds can be diffused into water, and at the same time, the scaffolds are hardened. The diffusion process can be shortened to 1 hour under ultrasonication. After all, the microsphere-based scaffolds were frozen at -20 ^oC overnight, then lyophilized for 24 h and stored in a refrigerator for further experiments.

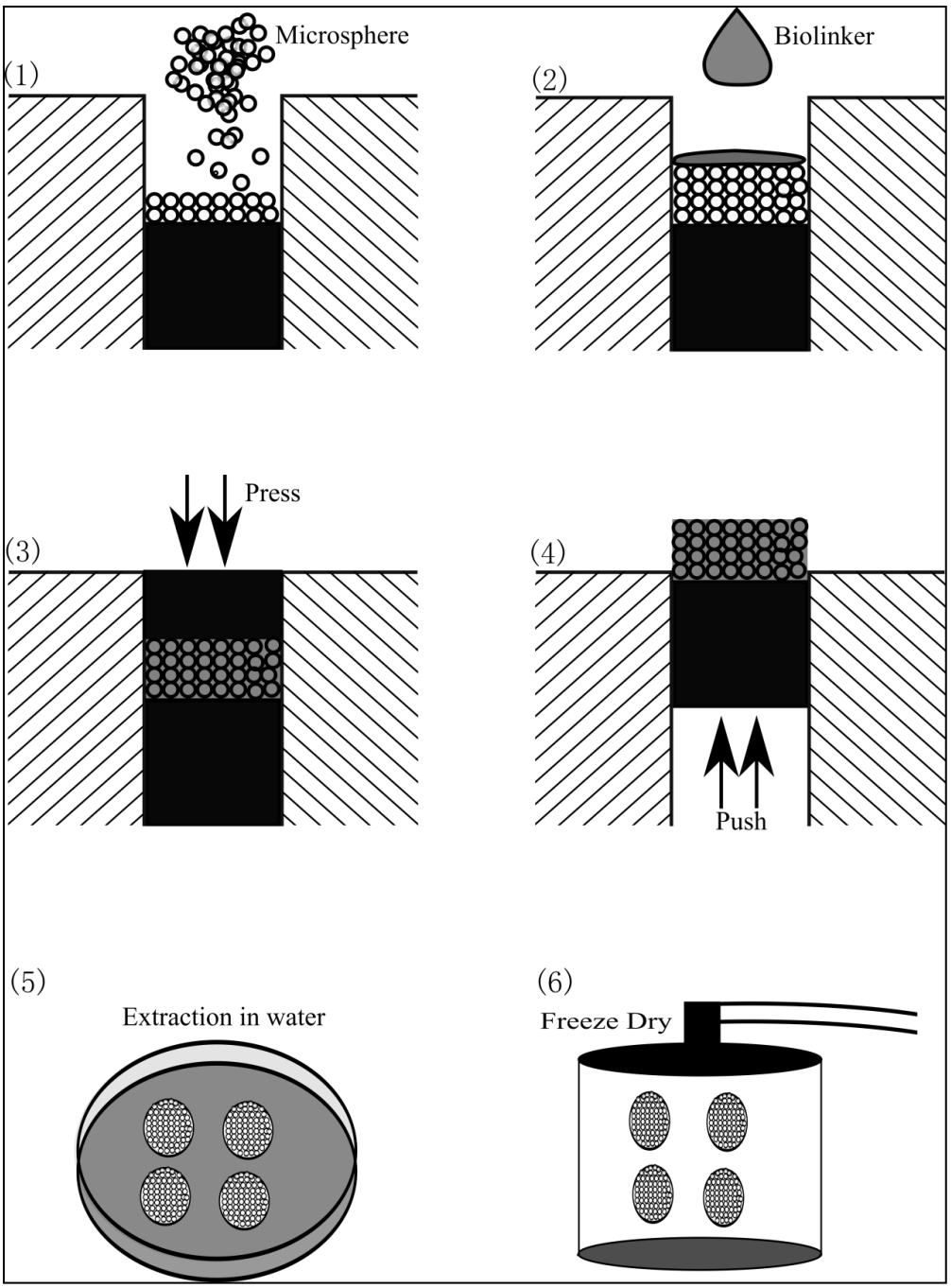

Fig. 2- 2. Schematic diagram for preparation procedures of PLGA microsphere-based scaffolds by solvent/non-solvent sintering. Step 1: Place microspheres into a mould; Step 2: Mixing biolinker with microspheres; Step 3: Press the wet microspheres; Step 4: Recovery scaffolds from mould; Step 5: Cleaning and hardening in water; Step 6: lyophilization.

2.4 Results

2.4.1 Preparation of large and uniform microspheres (800 µm) with a modified double emulsion method

Large and uniform microspheres with the active ingredients (ß-TCP, silicate

substrate and silicatein) were produced by a modified double emulsion method (water-in-oil-in-water emulsions; W/O/W) which was introduced by Freitas et al in 2005 [152]. The critical modification (Fig. 2-1) is that the tip of the needle is kept under water around 2-5 mm. Only with this modification, uniform microspheres can be produced at a constant shear force during stirring.

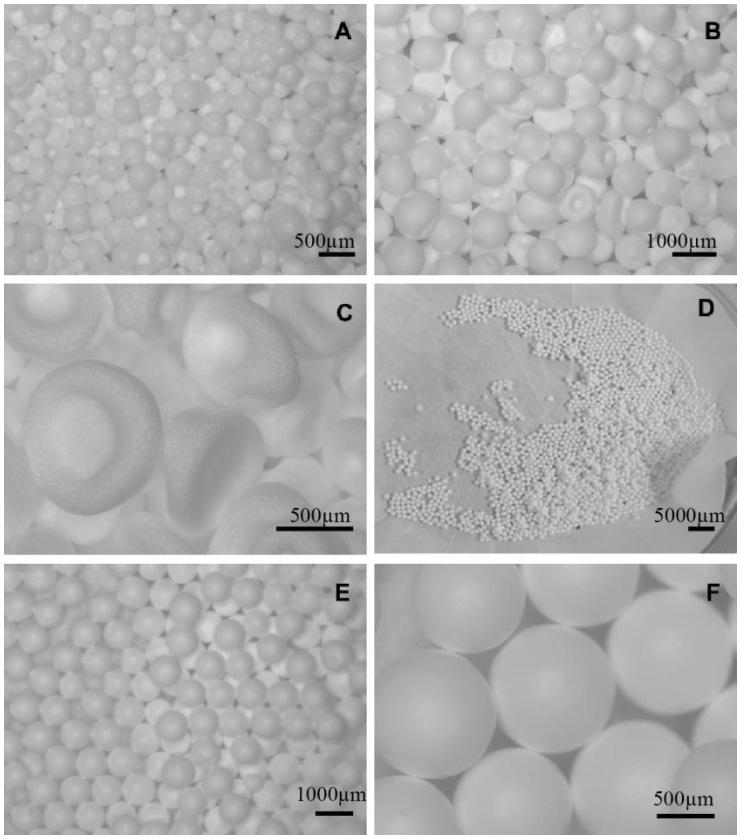

Fig. 2-3. Preparation of uniformly sized PLGA microspheres with a modified solvent extraction/evaporation method. A. PLGA: 15%, needle: 0.8 mm; B. PLGA: 25%, needle: 0.8 mm; C. PLGA: 30%, needle: 1.2mm; D, E and F. PLGA: 20%, needle: 0.8 mm. In D, a photo taken with a digital camera is shown. The other photos were taken with a VHX-2000 Digital Microscope from KEYENCE. Different magnifications.

In order to get the optimal parameters for the preparation of large and uniform microspheres, different batches of microspheres were prepared with different concentrations of PLGA solution (10 %, 15 % and 20 %) and using with needles with different diameters (0.6 mm, 0.8 mm and 1.2 mm), together with the other parameters. If the concentration of the PLGA solution is 15 % or 10 %, along with a needle diameter of 0.8 mm or 0.6 mm, microspheres with a diameter of less than 300 µm and with a large size distribution are obtained (Fig. 2-3A). However, with a PLGA concentration of 20 % and a needle diameter of 0.8 mm, uniform and large

microspheres wuth diameters from 700 µm to 800 µm were prepared (Fig. 2-3D, E and F). When the concentration of the PLGA solution is increased to 25 %, the PLGA solution has a higher viscosity and cannot pass through the needle (diameter of 0.8 mm) fluently. The diameter of microspheres was around 800 µm, but with a slight deformation (Fig. 2-3B). When the needle diameter is 1.2 mm, the PLGA solution can fluently pass the needle and the microspheres can reach a diameter of 1 mm, but with a blood plate-like morphology (Fig. 2-3C). The other parameters (speed of syringe pump: 12 ml/H; stirring speed: 600 rpm) were fixed for all microsphere preparation. The details of the parameters for all microsphere groups are summarized in Table 4. The PLGA microspheres, containing ß-TCP (ß-tricalcium phosphate) and Na-silicate, were named "ß-TCP/Silica-micro". The microspheres with ß-TCP and recombinant silicatein were termed "ß-TCP/Silicatein-micro". Control microspheres with and without ß-TCP were termed as "ß-TCP-micro" and "micro", repectively.

Table 4: Summary of experimental parameters for all microsphere groups

Microsphere	PLGA/DCM	ß-TCP (mg)	Water (ml)	Silicate (ml)	Silicatein (ml)
Group 1	600 mg/3 ml		0.8		
Group 2	600 mg/3 ml	60	0.8		
Group 3	600 mg/3 ml	60		0.8	
Group 4	600 mg/3 ml	60			0.8

Notes: Group 1: micro; Group 2: ß-TCP-micro; Group 3: ß-TCP/Silica-micro; Group 4: ß-TCP/Silicatein-micro.

2.4.2 Fabrication of microsphere-based scaffold

Microsphere-based scaffolds were prepared with pore sizes of 200-600 µm. These pores are interconnected and constitute a 3D porous structure. This open porous structure has the function of transporting oxygen, nutrients and metabolites, and allows the differentiation, proliferation and ingrowth of the cells, finally promoting vascularization and new bone formation in the scaffold material. For the preparation of the PLGA microsphere-based scaffold, the novel solvent/non-solvent sintering method was selected. NMP (different concentrations; 60 % to 90 % mixed

with distilled water) was used as the bio-linker agent. Different amount of microspheres, depending on the diameter and thickness of the scaffold required, were mixed with the bio-linker solution for a few minutes. During this process, the surface of the microspheres was partly dissolved by the solvent. With a slight pressing, the microspheres closely contact the adjacent microspheres and fuse together. After removal of the bio-linker agent, the hardened scaffolds were formed with 3D interconnected porous structure. The effect of the bio-linkers from different ratios of the solvent and non-solvent was studied and the results are shown in Fig. 2-4. Fig. 2-4A shows a piece of scaffold, which was prepared with 60 % bio-linker agent. The connection between the microspheres is very weak and the mechanical properties are very poor. As a consequence, the scaffolds can easily fall apart under a weak external force. Therefore, the 60 % bio-linker agent is not strong enough to fuse the microspheres together to form a scaffold. When the concentration of bio-linker is increased to 80 %, the microspheres start to shrink. They partly dissolve with time (Fig. 2-4B). When the concentration of bio-linker reaches to 90 %, the microspheres are completely dissolved even in a short contacting time (Fig. 2-4C). Under this condition, the formed scaffolds turn out to be a polymer disc; the microsphere morphology and the porous structure are destroyed. If we choose the concentration of 70 %, the microsphere-based scaffold was successfully prepared (Fig. 2-4D and 5E). The morphology of microsphere in the scaffold was perfectly persevered and the adjacent microspheres were fused tightly (Fig. 2-4E). The scaffolds show a porous structure, and the pores are interconnected. Even more, they possess the proper mechanical properties needed for the implantation.

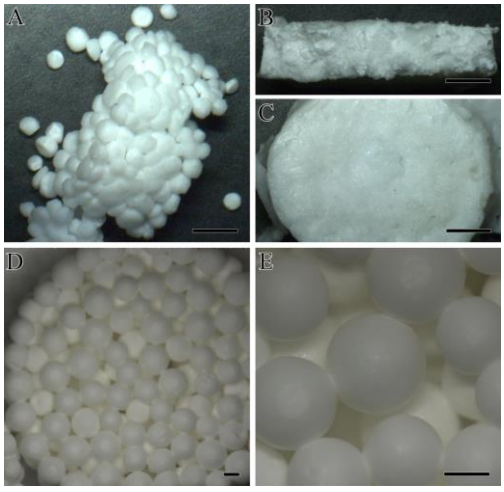

Fig. 2- 4: Optical images of microsphere-based scaffolds prepared by different concentrations (% of NMP) of bio-linker agent. A. Prepared with 60 % bio-linker; B. Prepared by 80 % bio-linker; C. Polymer disc, treated by 90 % bio-linker. D and E: Prepared with 70 % bio-linker. Scale bar (A, B and C): 2 mm; scale bar (D and E): 500 µm.

2.5 Discussion

2.5.1 Uniform microsphere (Ø > 500 µm) preparation by modified classical emulsion method

In 1988, Ogawa Y [153] first described an emulsion/evaporation method to develop injectable microspheres containing leuprolide acetate. The principle of this method is to add an aqueous solution of drug or protein to a polymer solution (oil phase, normally dichloromethane is the suitable non-solvent for PLGA) and mix vigorously to form a primary water-in-oil emulsion. The received emulsion is then poured into a large volume of a second water phase (normally a PVA or PVP water solution) to form microspheres or nanospheres. The spheres are stirred for several hours to evaporate the organic solvent and to solidify. In this conventional stirring method, the microsphere formation is mainly caused by mechanical agitation. Controlling the size of the microspheres is quite difficult; they usually have a broad size distribution [154]. In order to get uniform microspheres, the sphere formation step must be more controllable. The size of the microspheres are affected by the molecular weight and concentration of the polymer, the solubility of the polymer, the ratio between the aqueous phase and the oil phase, the concentration and volume of dispersed phase, the volatility of organic solvent, and the miscibility of aqueous phase. Among them, the polymer concentration plays a decisive role in controlling the size of the microspheres. The higher the concentration of the polymer, the higher the viscosity that the emulsion solution can reach. Therefore, in this study, we fabricated microspheres at three different concentrations of PLGA (25 %, 20 % and 15 %) and selected the optimal concentration of the polymer (20 %) for the large microspheres preparation.

The production of uniform microspheres as drug delivery vehicle has been intensively studied [155]. To obtain uniform microspheres, several improvements have been done for the formation of droplet, such as the technique of direct membrane emulsification and the steam-carrying system [156]. With all those improvements, it is only possible to produce microspheres with a small size (diameter smaller than 100 µm). Small uniform microspheres are perhaps perfect for drug delivery; however, they are not suitable for preparing porous bone scaffolds. So

far, in bone tissue engineering, the large microspheres have been selected through sieving to remove the small microspheres [157].

Emulsion/evaporation is one of the most common methods for encapsulating water-soluble drugs or proteins into polymer microspheres, and is particularly suitable for laboratory-scale academic research. For a drug delivery system, microspheres typically range in size from 1 µm to 100 µm and have a narrow size distribution. In tissue engineering, the pore size of the bone implant plays a very important role in tissue regeneration. It should be large enough to allow the cells to immigrate into the scaffold, and even nutrients and fluids can pass freely. It has been found that the speed of cell migration is linearly correlated to the pore size. The optimal pore size for bone ingrowths is claimed to be larger than 100 µm. The advanced scaffold should have a proper pore size for cell ingrowths; simultaneously it should show reasonable mechanical properties that matche those needed in the regenerative area.

In this study, we tried to produce large microspheres (> 500 µm) for bone regeneration. These scaffolds, based on large microspheres, have a porous structure with a pore size between 100 µm to 300 µm, reaching a similar structure like trabecular bone. By thermal sintering, the scaffolds were fabricated from microspheres (diameter of 600-710 µm) and have an average pore size of 200 µm [158]. In our study, the large and uniform microspheres were prepared through the conventional emulsion solvent evaporation method with a slight modification (Fig. 2-1). Compared to the conventional method, we used a syringe pump system to deliver the emulsion into the second water phase (1 % PVA) instead of directly pouring it. The size of the microspheres is mainly controlled by the pump speed and the stirring speed. It does not require an additional acoustically excited or non-solvent carrier stream system [159]. With the combination of the acoustic excitation and the non-solvent carrier stream technique, uniform microspheres with a size from 5 µm to 500 µm were successfully fabricated. Several parameters were considered to control the size of the microspheres: polymer concentration, volume ratio of water phase and organic phase, pumping speed, stirring speed, diameter of needle, and active ingredients loaded.

In this work, the large and uniform microspheres (Fig. 2-3D, 3E and 3F) were successfully fabricated at a constant pumping rate and water shear force, without additional device. When the PLGA emulsion came out of the blunt needle, the emulsion drops were immediately carried away from the needle tip by the water shear force. After stirring for several hours, the residual solvent (DCM) was diffused into water and air. Then, solidified microspheres were obtained. The formation of the PLGA droplets is a critical step in controlling the size and size distribution of the microspheres [152]. It depends mainly on the viscosity of polymer solution and the water shear force. The increase in the size of the microsphere is caused by an increase in the viscosity of the emulsion [160]. Mechanical stirring causes water shear force to remove droplets (microspheres) from the syringe needle. When the stirring speed increases, the microspheres become smaller and the size distribution becomes narrower [161]. Thus, the polymer concentration and the stirring speed are the key parameters to obtain uniform microspheres with the desired size (> 500 µm). Attention must be paid because of the low boiling point of 39.8 ^{o}C of dichloromethane (DCM). It trends to evaporate during the emulsification process, resulting in a higher viscosity [162]. So, in order to improve the reproduction, we should have a constant emulsion viscosity every time. Therefore, we need to try to prevent the evaporation of large amounts of DCM during the emulsification process, to minimize the evaporation.

There are three active ingredients, which are planned to be encapsulated into the PLGA microspheres: ß-tricalcium phosphate (ß-TCP), silicate and silicatein. ß-TCP is known as a member of calcium phosphate bio-ceramics; it has a Ca/P ratio of 1.5. Its biodegradability is higher than that of the stable phase of hydroxyapatite (HA; Ca/P: 1.67), and it is widely used in the field of bone regeneration [163,164]. When blended with calcium phosphate ceramic, it will improve the biocompatibility of biopolymers and enhance the mechanical properties of polymer scaffolds [165]. Furthermore, bioactive ß-TCP can be used as a pH compensator to buffer the acidic effects of by-products from the acidic degradation of PLGA, thereby reducing the inflammatory response *in vivo* [166]. Blending large amounts of ß-TCP with PLGA, on the one hand, it will improve the potential for bone regeneration. On the other hand,

a large amount of ß-TCP will easily coagulate during emulsification and pumping, thereby blocking the needle. In this study, 20 % PLGA in dichloromethane has been selected, so a maximum of 10 % (w/w) ß-TCP can be encapsulated into the PLGA microspheres without any problem during the fabrication process. Similar problems happen for the encapsulation of silicate, so the highest concentration of silicate in the PLGA microspheres is also around 10 %. Those encapsulated silicate can be released from the PLGA microspheres during PLGA degradation to form biosilica, modulated by silicatein, which is encapsulated separately into PLGA microspheres. The biosilica formation can initiate and enhance the bone formation.

2.5.2 PLGA microsphere-based scaffolds sintered by NMP/H_2O bio-linker

Scaffolds, packed only from microspheres, have recently received increasing attention due to their interconnected porous structure. The microsphere-based scaffolds are normally prepared by thermal sintering and solvent/non-solvent sintering to fuse the microspheres together [167,168]. For thermal sintering, after the polymer microspheres are placed into a mould, the mould is heated to a temperature slightly beyond the polymer glass transition temperature. For PLGA microsphere-based scaffolds, the sintering can be done at 62 ^{o}C since the glass transition temperature of PLGA is 40-60 ^{o}C. At this temperature, the polymer microspheres will become soft and fuse together after cooling. Thermal sintering is the most effective way to create an interconnected porous structure. One of the disadvantages of this method is that heating destroys bioactive components (proteins and thermal sensitive drugs) that are encapsulated in the microspheres. Another disadvantage is that the heating process can last more than 10 hours, which is quite time-consuming. The solvent/non-solvent method fuses the polymer microspheres together at ambient temperature by partially dissolving the microsphere surfaces by the selected bio-linker, [169]. So this method is excellent for the fabrication of tissue engineering scaffolds and drug delivery vehicles. The bio-linker, a combination of a polymer solvent and a miscible non-solvent, sets up a balance between dissolution and precipitation at the polymer surfaces [168]. Using

solvent/non-solvent sintering method, scaffolds can be prepared in a few minutes to be directly used for the implantation of patients. One of the most successful applications by this sintering method is the “Easy Graft” produced by SUNSTAR GUIDOR. This graft is composed of two components: *i)* ß-TCP granules coated with PLGA; and *ii)* a bio-linker solution (a mixture of NMP/H_2O). After the PLGA coated ß-TCP granules are mixed with the bio-linker, it can be directly introduced via a syringe into the bone defect. The injected mixture hardens in a few minutes to form a stable and porous graft, by flushing away the biolinker with body fluid.

PLGA is synthesized by means of ring-opening co-polymerization of two different monomers, the cyclic dimers (1,4-dioxane-2,5-diones) of glycolic acid and lactic acid. It is characterized as biodegradable and biocompatible. Since the body effectively deals with the two monomers, there is minimal systemic toxicity associated with the use of PLGA for drug delivery or biomaterial applications [170]. PLGA can be dissolved in many common solvents, such as tetrahydrofuran, acetone, ethyl acetate, dimethyl sulfoxide (DMSO), *N*-methyl-2-pyrrolidone (NMP) and chlorinated solvents. For biomedical applications, biocompatible solvents, such as DMSO and NMP, are primarily considered. Both of them are water-miscible solvents and are widely used in commercialized injectable products [171]. DMSO has been reported to have potential dose-related toxic effects on vascular and brain tissue [172]. In medicine, NMP has a long-term record as a constituent of medical devices and it is approved by FDA to be safe below a certain concentration. It is a bioactive drug which can enhance the expression of bone morphogenetic protein *in vitro* and bone regeneration *in vivo* [173]. NMP also inhibits the differentiation of osteoclasts and attenuates the resorption of bone by regulating RANKL-induced osteoclastogenesis [174]. Besides of its function on osteoclasts and osteoblasts, it shows anti-inflammatory potential and can be used to prevent loss of bone tissue g due to inflammation [175]. Based on the above mentioned findings, we have chosen NMP as solvent of PLGA in our study. It has a dual function, first as a cross-linker for the microspheres and second as an enhancer for bone regeneration. Since NMP is miscible with water, water has been chosen as non-solvent for PLGA. In order to fuse the PLGA microspheres together in a short time period (less than 30 min) without

destroying the microspheres, 75 % NMP solution (NMP : H_2O = 3 : 1) was selected as bio-linker for the preparation of scaffolds. Fabricated by this bio-linker, the morphology of the microspheres is perfectly preserved and the scaffolds have suitable mechanical properties for implantation and bone regeneration.

Chapter III:

Physicochemical characterization of microspheres and their scaffolds

3 Physicochemical characterization of microspheres and related scaffolds

3.1 Characterization methods

3.1.1 Morphology of microspheres and their scaffolds

3.1.1.1 Optical microscopy

The diameter and morphology of PLGA microspheres with active ingredients were analyzed using a VHX-1000 digital microscopy from KEYENCE (Neu-Isenburg; Germany), equipped with an Ultra-small compact high-performance zoom lens (VH-Z20R/VH-Z20w, 20× to 200× magnification) or a VH-Z100 long-distance high-performance zoom lens (up to 1000× magnification). The diameter was determined by the measurement software supplied for the microscopy. For each microsphere group, at least 100 individual microspheres were measured and the diameter was presented as an average value with standard deviation.

3.1.1.2 Scanning electron microscopy (SEM) and Energy Dispersive X-Ray Spectroscopy (EDX)

For detailed inspection, PLGA microspheres were analyzed by SEM and EDX. The microspheres were mounted on an aluminum specimen stub covered with a diameter of 12 mm standard Leit Adhesive Carbon Tab (G3347, PLano, Wetzlar, Germany). Prior to visualization, the samples were coated with gold, then visualized by the HITACHI SU 8000 electron microscope (Hitachi High-Technologies Europe GmbH, Krefeld, Germany) at a low voltage (less than 1KV). Additionally, element distribution analyses were performed by energy dispersive spectroscopy with an X Flash 5010 detector coupled at a voltage of 4 KV. The data was collected and analyzed by the supplied software.

3.1.2 Determination of active components in the microspheres

3.1.2.1 Determination of ß-TCP content in the microspheres

Fot quantification, the PLGA microspheres (20-50 mg; n = 3 for each group) were weighted with an electric balance and placed in a 2 ml Eppendorf tube. The PLGA

shell was removed by mixing with 1 ml of DCM and shaking for 30 min. The inorganic components released from the microspheres were collected from the pellet after a centrifugation at 10000 rpm for 10 min. Afterwards, the sediment was washed twice more with DCM to remove the PLGA completely. Subsequently, the sediment was kept in a hood to let the DCM evaporate for 2 h. Then, the residual part was mixed with 1M HCl to dissolve ß-TCP at room temperature for 1 h to ensure complete dissolution of ß-TCP. Finally, the mixture was centrifuged at 10000 rpm for 10 min. The supernatant was carefully collected and the concentration of Ca in the supernatant was quantitatively determined using ICP-AES (Inductively Coupled Plasma Atomic Emission Spectrometer; Optima 8300 ICP-OES Spectrometer, PerkinElmer, Waltham, USA). The ß-TCP content was calculated as a percentage and expressed as mean with standard deviation.

3.1.2.2 Determination of silica content in ß-TCP/Silica-micro

In order to determine the silica content in ß-TCP/Silica-micro, 30 to 50 mg of ß-TCP/Silica-micro (n = 3) was accurately weighted with an electronic balance. The PLGA polymer shell was dissolved three times treatment with DCM (1 ml). After centrifugation, the inorganic components (including ß-TCP and silica) were left at the bottom. After the supernatant (PLGA in DCM) was discarded, the remaining material was washed again with DCM and left in a hood for 2h to evaporate the organic solvent (DCM). Afterwards, the substance was mixed with 1 ml of 1 M sodium hydroxide (NaOH). After incubation for 2 h, the mixture was centrifuged and the supernatant collected for measurement of the concentration of silica using the Silica-Test kit (#1.14794, Merck, Darmstadt, Germany), a molybdenum blue colorimetric method described by Ramachandran et al. [176]. Briefly, the pH of the supernatant was adjusted to 7 with 1 N sulfuric acid. Then, 1 ml supernatant was pipetted into a 2 ml Eppendorf tube and mixed with one drop of Si-1 reagent (0.5 M sulfuric acid). The mixture was left to stand for 3 min; the pH should be within 1.2 - 1.6. After 3 min, one drop of reagent Si-2 (1 %, $(NH_4)_6Mo_7O_{24}\cdot 4H_2O$ in 0.1 N sulfuric acid) was added to the mixture and mixed well. Under acidic conditions, silicate reacts with the molybdate reagent to form a yellow silicomolybdate complex. With additional three

drops of reagent Si-3 (0.1 N ascorbic acid solution), this yellow complex can be reduced under formation of the molybdate blue color. The color intensity is proportional to the silica concentration. The absorbance was determined at 795 nm with a spectrophotometer (Varioskan, Thermo Fisher). Firstly, a calibration curve was set up between the absorbance value obtained and the concentrations of silicate standards (#1.09947, Merck, Darmstadt, Germany). Then, the silica concentration in the microsphere was calculated according to the absorbance values. The value of the silica content was presented in percentage, as mean value with standard deviation.

3.1.3 Chemical and immunochemical properties of encapsulated silicatein

3.1.3.1 Encapsulation efficiency

Approximately 30-80 mg of freeze-dried ß-TCP/Silicatein-micro was accurately weighted and transferred into a 15 ml falcon tube, then mixed with 2 ml of dichloromethane (DCM) and kept under stirring (180 rpm) at room temperature for 1 h. Subquently, 3 ml of PBS (phosphate buffered saline) containing 3 % SDS (sodium dodecyl sulfate, #L3711 SIGMA, Germany) was added into the tube and vortex-mixed thoroughly overnight. The mixture was centrifuged (5000 rpm for 10 min) and the supernatant was carefully collected. The bicinchoninic acid (BCA) microassay (QuantiPro^{TM}BCA, #QPBCA, SIGMA) was applied to determine the silicatein concentration in the supernatant, following the description of the manufacturer. Briefly, by mixing of reagent QA, QB and QC ($CuSO_4$) in a ratio of 25: 25: 1, the required amount of working reagent (dependent on the number of samples) was prepared. 100 µl of silicatein extraction solution (n = 5) were placed in a 96-well plate. The BSA (Quick start Bovine Serum Albumin standard, #5000206, 2 mg/ml, BIO-RAD) standard curve had a protein concentration range from 0.5 to 30 µg/ml. Then, the plate was sealed with paraffin film and covered with aluminum foil to prevent light. After mixing with the BCA working solution, the plate was routinely processed at 60 ^{o}C for 1 h. Finally, the absorbance at 562 nm was recorded with a spectrophotometer (Varioskan, Thermo Fisher) and the protein concentration was calculated according to the BSA standard curve. Based on the silicatien concentration, the encapsulation

efficiency of silicatein in the microspheres could be calculated according to the following formula:

$$\text{Silicatein entrapment efficiency}=\frac{\text{the actual silicatein trapment}(\%)}{\text{the theoretical silicatein trapment}(\%)}\times 100\%$$

3.1.3.2 Stability and integrity

The stability and integrity of silicatein in ß-TCP/Silicatein-micro microspheres were analyzed by SDS-polyacrylamide gel electrophoresis (SDS-PAGE) and immunochemistry. SDS-PAGE was performed using a BioRad-Mini Protean gel device (BIO-RAD, Germany). The siliciatein was extracted from ß-TCP/Silicatein-micro with PBS containing 3 % SDS as described in section 3.1.3.1. The extracted silicatein and the positive control (recombinant silicatein-α) were mixed with loading buffer (Roti®-Load 1, 4x conc., Roth) containing DTT (dithiothreitol) and maintained at at 95 °C for 5 min. After that, 25 µl of sample was carefully loaded into 12 % SDS-PAGE duplicate. Meanwhile, 5 µl of protein marker (Prestained Protein Standards, Dual Color, 10-250 kD, BIO-RAD) and 10 µl of recombinant silicatein-α were loaded next to the sample. Electrophoresis was performed at a constant voltage of 180 V for 30 min to 1 h. The determination of silicatein was performed by staining the gel with Coomassie Brilliant Blue R-250 staining solution (#1610436, BIO-RAD) under shaking for 30 min. The destaining was carried out by washing the sample with distilled water three times. After washing, the stained gel was scanned with an Odyssey Infrared Image System (Li-COR, Biosciences), and the images were recorded for further analysis.

Western blot assay for extracted silicatein was carried out as described by Müller et al. [127]. After the electrophoresis, size-separated proteins were transferred to a PVDF (polyvinylidene fluoride) membrane, using a device iblot (iBlot®2 Dry Blotting system, ThermoFisher Scientific) following the instructions of the manufacturer. The membrane was immersed into the blocking solution (1 % in TBS buffer) overnight at 4 °C, to prevent non-specific binding. Afterwards, the membrane was rinsed with TBST buffer (TBS buffer with 0.1 % Tween-20) and treated firstly with primary antibody anti-silicatein-α (1: 2000 in 0.5 % blocking solution), which was produced in rabbit by our group, for 30 min at room temperature with gently shaking. Before the secondary antibody (anti-rabbit IgG,

SIGMA, Germany), the membrane was washed three times with TBST buffer, then incubated with the secondary antibody (1: 2000 in 0.5 % blocking solution) for again 30 min at room temperature with shaking. The immunocomplex was visualized with a color development system NBT/BCIP (alkaline phosphates substrate, NBT-BCIP solution, #72091, SIGMA), this reaction was stopped by washing the membrane with distilled water to reduce the background. Then, the membrane was dried and photographed to provide a permanent record of the experiment.

3.1.4 *In vitro* silicatein and silicate release profile

3.1.4.1 Silicate release profile *in vitro*

The *in vitro* silicate release profile was performed in triplicate at 37 ^{o}C and sterilized 0.9 % saline containing 0.02 % NaN_3 was taken as the release buffer. Approximately 50 mg of ß-TCP/Silica-micro microspheres (n = 3) were suspended in 1 ml of saline, and placed in a shaking incubator which was kept at 37 ^{o}C and stirred at 100 rpm. At the pre-set time points (1, 3, 5, …, and 24 day), 1 ml of the release medium was completely collected after centrifugation. The microspheres were then washed once with saline and refreshed with 1 ml of fresh saline. The collected release medium was stored at -20 ^{o}C for the measurement of silica concentration using the Merck's Silica Kit, as described in section 3.1.2.2. The release profile was plotted based on the cumulative percentage of release of silicate at different time points during 24 days incubation.

3.1.4.2 Silicatein release profile *in vitro*

In vitro silicatein release was also performed in triplicate at 37 ^{o}C, and sterilized PBS buffer was selected as the release buffer. Briefly, approximately 50 mg of ß-TCP/Silicatein-micro microspheres (n = 3) was weighed accurately and dispersed in 1 ml of PBS. These samples were incubated at 37 ^{o}C under shaking of 100 rpm. At defined time intervals (1, 3, 5, ..., and 24 d), the supernatant was discarded after centrifugation. Then 1 ml of fresh PBS was added and the samples were put back into the incubator. The collected supernatants were stored at -20 ^{o}C for further assay. The silicatein concentration in the supernatant was determined using the micro-BCA

assay, as described in chapter 3.1.3.1. The cumulative release percentages were calculated and the release profile was plotted according to time points.

3.1.5 Scaffold water uptake rate and swelling rate

The microsphere-based scaffolds were cylindrical, 10 mm in diameter and 5 mm in thickness, which were prepared by the solvent/non-solvent sintering method described in the section 2.3.2. The water uptake rate and the swelling rate were quantified by measuring the volume and weight changes during the immersion time. Briefly, six scaffolds (n = 6) were placed in the six wells of a 6-well plate separately. Each well contains 10 ml of PBS buffer (10 mM, pH = 7.4). Then the plate was incubated at 37 °C under shaking of 60 rpm. The initial dimension and weight of the scaffolds were measured using a Digital Caliper and electronic balance, respectively. At defined intervals, the scaffolds were taken out, and extra water on the surface of the scaffolds was removed carefully by a filter paper. Afterwards, the weight and dimension were immediately.measured Then, immediately, the scaffolds were put back for the next measurement. The water uptake rate and the swelling rate were calculated using Equations (1) and (2), respectively.

$$\text{Water uptake } E\% = \frac{We - Wi}{Wi} \times 100 \qquad (1)$$

where E is the water uptake rate. *We* is the wet weight of the scaffold which is saturated in buffer and *Wi* is the initial weight of the scaffold before it is placed into the buffer.

$$\text{Swelling percentage } S\% = \frac{Vs}{Vi} \times 100 \qquad (2)$$

where S is the swelling rate. *Vs* is the volume of the scaffold which is saturated in buffer, and *Vi* is the initial volume of the scaffold.

3.1.6 Mechanical properties of microspheres during the enzymatic degradation *in vitro*

The internal mechanical properties of various PLGA microspheres degraded in serum and medium were assessed using the ferrule top nano-indentation method.

This technique is capable of locally determining the mechanical properties of a sample in air and in liquid. A probe having a spherical tip with a stiffness of 156 N/m and a radius of 45 µm was used in this study. The indentation depth was set to 10 µm, which is half of the depth of the full indentation. The indentation procedures were carefully optimized to minimize the viscoelastic effect of the measurements. A 2-second loading period, a 1-second hold period and a 2-second unloading period were applied for all measurements. Before experiments, all microspheres (three groups: ß-TCP-micro, ß-TCP/Silica-micro and ß-TCP/Silicatein-micro) were sterilized under UV light for 1 h in a laminar hood. After sterilization, the microspheres were transferred to a 24-well plate and incubated with 2 ml of fetal bovine serum (Gibco, Germany) for 100 d at 37 ^{o}C. The FBS was refreshed twice a week. At defined time intervals, five microspheres were collected from each group and washed three times with distilled water to remove adsorbed proteins from the surface. Whatman paper was used to dry the microspheres. Finally, the microspheres were fixed on a glass slide with superglue for measurement. Immediately after indentation, the data was analyzed. The load and displacement curves can be seen directly on the relevant tab and the reduced Young's modulus was automatically calculated using the Oliver-Pharr method.

3.2 Results

3.2.1 Morphological evaluation of microspheres and related scaffolds with optical microscopy and scanning electron microscopy

The morphology and size of the microspheres were determined by optical digital microscopy as described in the method section. The surface morphology of the microspheres having various ingredients is shown in Fig. 3-1. The size of the microspheres (n = 100) was evaluated under an optical microscopy and the result was shown as average value with standard deviation. The diameters were found to be 787 ± 75 µm for micro (Fig. 3-1A and B), 830 ± 57 µm for ß-TCP-micro (Fig. 3-1C and D), 843 ± 72 µm for ß-TCP/Silica-micro (Fig. 3-1E and F) and 771 ± 34 µm for ß-TCP/Silicatein-micro (Fig. 3-1G and H), respectively.

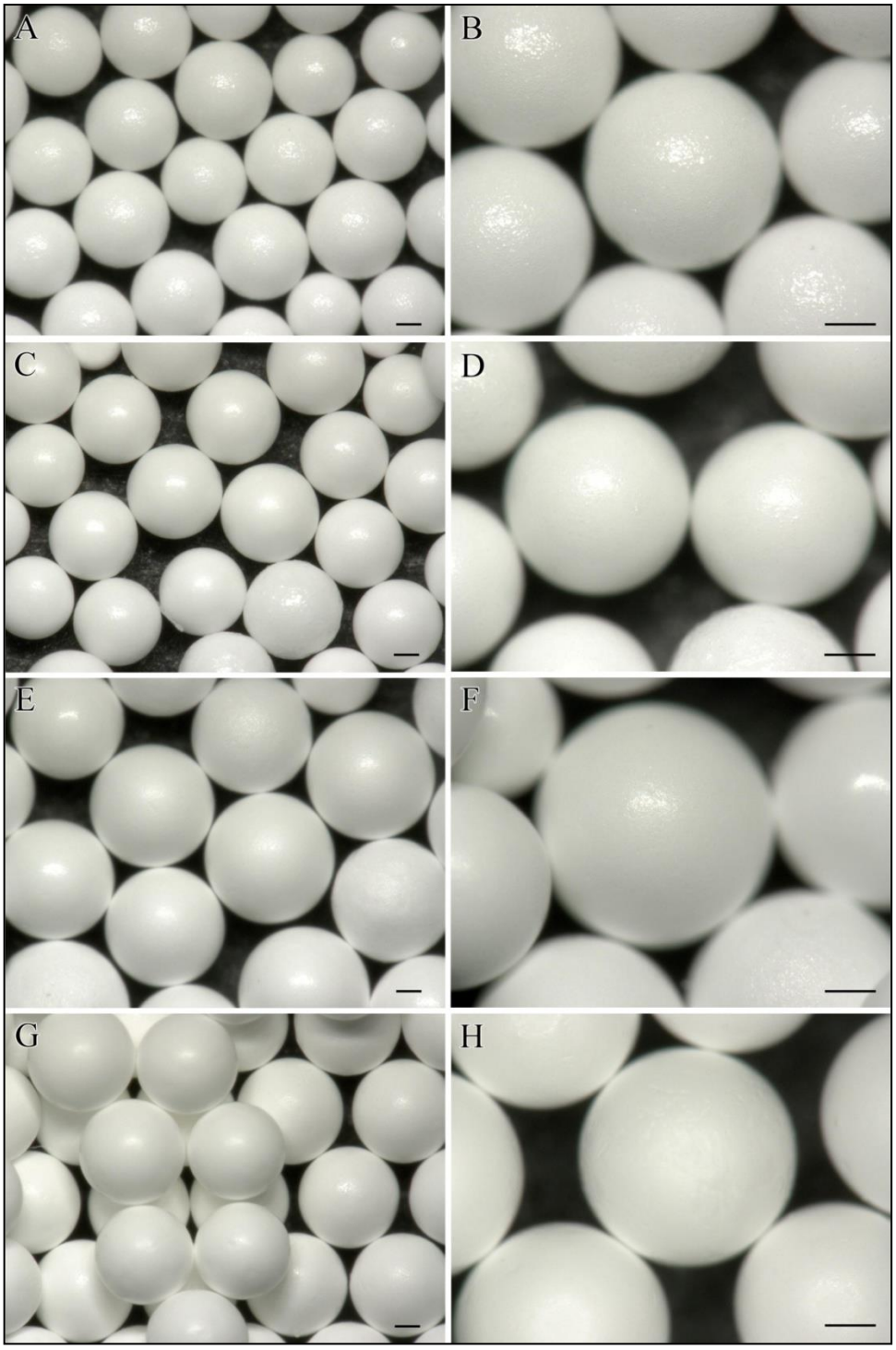

Fig. 3- 1. Morphology of the microspheres, visualized by a digital optical microscopy. (A and B for micro; C and D for ß-TCP-micro; E and F for ß-TCP/Silica-micro; G and F for ß-TCP/silicatein-micro). left panel: 10× magnification; right panel: 200× magnification, scale bar = 100 µm.

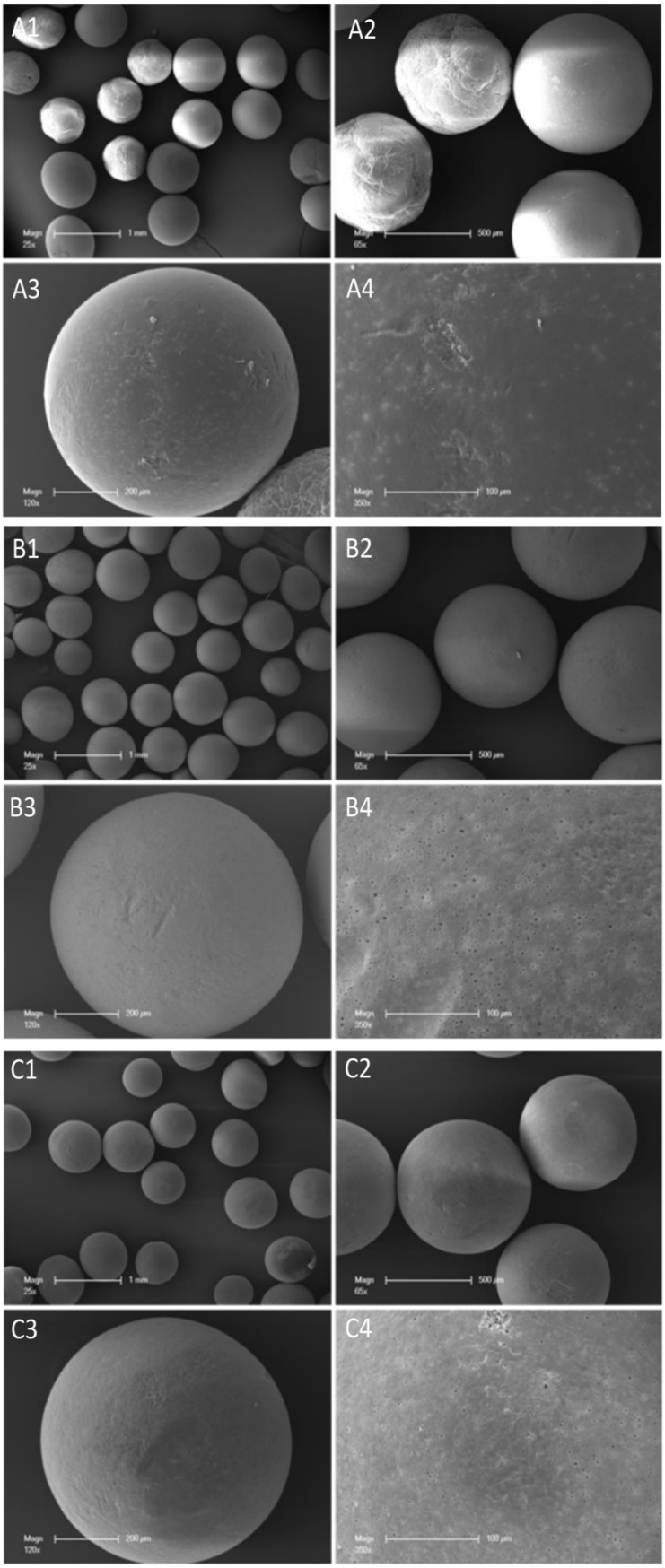

Fig. 3- 2. SEM images of various PLGA microspheres at different magnifications. (A: ß-TCP-micro; B: ß-TCP/Silica-micro; C: ß-TCP/Silicatein-micro)

For detailed morphology inspection of the microspheres, SEM analysis was performed. In addition, EDX was applied for element determination. The SEM images of the microspheres at various magnifications (25×, 65× 120× and 350×) are shown in Fig. 3-2. In optical digital microscopy, all the microspheres showed a similar spherical morphology (Fig. 3-1). However, by using SEM, the morphological differences of each group have been highlighted. At low magnifications, all three types of microspheres have a spherical morphology, similar results as shown in Fig. 3-1. With higher magnification, it is clear to observe that some of the ß-TCP-micro microspheres (Fig. 3-2A1 and A2) show no perfect spherical morphology, more like twisted spheres with a rough surface. The ß-TCP/Silica-micro (Fig. 3-2B1 and B2) and ß-TCP/Silicatein-micro (Fig. 3-2C1 and C2) show perfect spherical morphology with a smooth surface and micron or sub-micron porous structure (Fig. 3-2B4 and C4), while a micron porous structure is missing on ß-TCP-micro surface (Fig. 3-2A4). The pore size of the ß-TCP/Silica-micro is slightly larger than that of the ß-TCP/silicatein-micro. Instead of the porous structure on the surface of ß-TCP-micro, white micro-particles are found, indicating the presence of ß-TCP particles on the surface of this group of microspheres. With higher magnification, the nano-porous surface of ß-TCP/Silicate-micro was clearly observed (Fig. 3-3A) and the pore size was determined to be around 10 nm.

To verify the presence of the silicate substrate in ß-TCP/Silica-micro, the element composition of ß-TCP/silica-micro was analyzed by electron dispersive X-rays (EDX) analyzer. The EDX spectrum of ß-TCP/Silica-micro is presented in Fig 3-3B. The spectrum shows strong peaks of carbon, oxygen and silicon and week peaks of calcium and phosphorus. The peaks of carbon and oxygen are mainly derived from the PLGA polymer; the silicon peak confirms that silicate was successfully encapsulated into the microspheres and the peeks of calcium and phosphorus originate from ß-TCP entrapped in the PLGA microspheres. The weak peaks of calcium and phosphorus indicate that ß-TCP particles are mainly entrapped inside the PLGA microspheres. This result is confirmed by the SEM images (Fig 3-2); only a few ß-TCP particles were found on the microsphere surface.

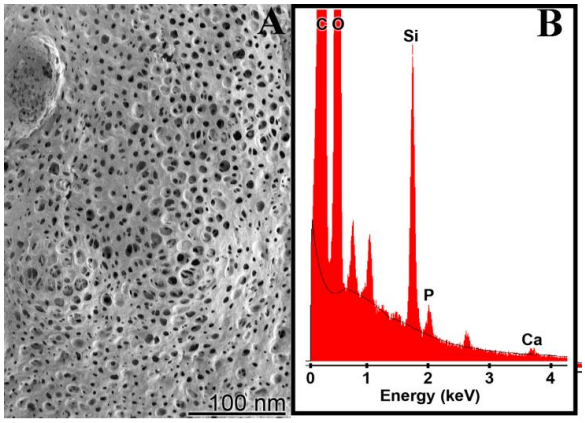

Fig. 3- 3. Nano-porous structure and elemental spectrum of ß-TCP/Silica-micro microspheres. A: SEM images; B: EDX spectrum.

3.2.2 Determination of active components in the microspheres

3.2.2.1 Concentrations of active components (ß-TCP, silica and silicatein) in the microspheres

In order to quantify the active components (ß-TCP, silica and silicatein) in the microspheres, the PLGA microspheres were dissolved in DCM to release the active components from the microspheres. The remaining ingredients were treated with 1 M HCl (to dissolve ß-TCP), 1M NaOH (to dissolve silica) or PBS with 3 % SDS (to extract silicatein). Calcium in the HCl solution was quantitatively determined by ICP-AES. Silica was analyzed by the molybdenum blue colorimetric method using the Silica-Test kit. Afterwards, silicatein in the supernatant was quantified by the bicinchoninic acid (BCA) microassay and the absorbance was obtained at 562 nm. The results are shown in Table 5. The silicatein encapsulation efficiency was calculated to be 45.07 ± 4.53 %.

Table 5: Concentration of active components in the microspheres

Components	ß-TCP-micro	ß-TCP/Silica-micro	ß-TCP/Silicatein-micro
ß-TCP (%)	7.92 ± 0.20	4.97 ± 0.24	6.49 ± 0.075
Silica (%)		9.38 ± 0.53	
Silicatein (µg/mg)			0.32 ± 0.11

3.2.2.2 Stability and integrity of silicatein in the ß-TCP/Silicatein-micro microspheres

During the preparation of ß-TCP/Silicatein-micro microspheres, hazardous conditions, such as organic solvents and intensive mixing, may destroy or degrade the proteins. In order to confirm the stability and integrity of the encapsulated silicatein in the microspheres, SDS-polyacrylamide gel electrophoresis (SDS-PAGE) and immunochemistry assay were carried out. The images of Coomassie blue staining and immunostaining were shown in Fig. 3-4. Fig. 3-4A shows a single clear band (in the middle lane) that occurred at around 25 kDa, associated with the positive control-recombinant silicatein. However, the concentration of extracted silicatein is not strong enough to give us a clear band as the positive control.

Parallel gels were used for immunodetection of extracted silicatein. The extracted silicatein was transferred to a PVDF membrane and the recombinant silicatein was taken as the positive control. Then the membrane was further blocked and treated with the first antibody, primary anti-silicatein (produced in rabbit), for 1.5 h at room temperature. After that, the second antibody was followed and finally visualized with NBT/BCIP color development substrate (alkaline phosphates substrate) (Fig. 3-4B). The extracted silicatein (middle lane of Fig. 3-4B) shows a clear signal, indicating the presence of the silicatein. The protein marker (25 kDa) is on the left (pink) and the positive control (on the right) shows a stronger signal than that of the extracted silicatein, indicating a higher protein concentration.

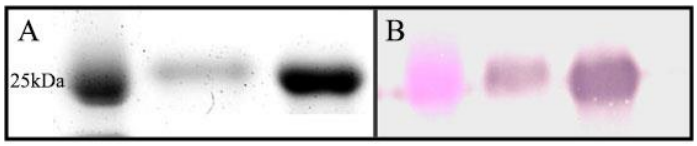

Fig. 3- 4. Stability of silicatein in microspheres, identified by SDS-PAGE and Western blotting. A: Stained with Coomassie Brilliant Blue; B: Western blot test. Samples from left to right (A and B): Protein marker, silicatein extracted from ß-TCP/silicatein-micro and positive control-recombinant silicatein.

3.2.3 *In vitro* silicate and silicatein release study

In vitro silicate release was carried out at 37 °C for one month in triplicate with 0.9 % saline as the release medium. The release medium was refreshed every two days and stored at -20 °C. The silicate concentration was determined by Silica-Kit. The

releasing curve was expressed as the accumulative percentage of release time, and the mean values and standard deviations were calculated, as shown in Fig. 3-5. As seen in Fig. 3-5, the release profile of silicate can be divided into three phases: the initial burst (first day), the diffusional release (from 5 to 17 day) and the final slower release phase (from 17 to 24 day). After 1 day incubation, only 2 % silicate was released from microsphere. This shows no obvious initial burst, which is defined as cumulative drug release one day after incubation. During the first 5 days, it showed a slow diffusional release of 7 %. In the second phase, the release was faster than the previous 5 days. The cumulative release percentage reached 35 % after 17 days. In the third phase, it showed a very slow release rate. Only 2 % was released in the last week (from 17 to 24 day). In order to evaluate the drug release rate in the release profile, a zero-order model was used to fit the three phases as reflected by the acceptable regression coefficients. The regression equations were presented as follows:

Phase 1 (1 to 5 day): $y=1.37x+0.94$; $R^2=0.92$

Phase 2 (5 to 17 day): $y=2.45x-4.57$; $R^2=0.97$

Phase 3 (17 to 24 day): $y=0.32x+30.78$; $R^2=0.83$

For ß-TCP/Silica-micro, totally approximately 37 % of silicate was released during the whole experimental period.

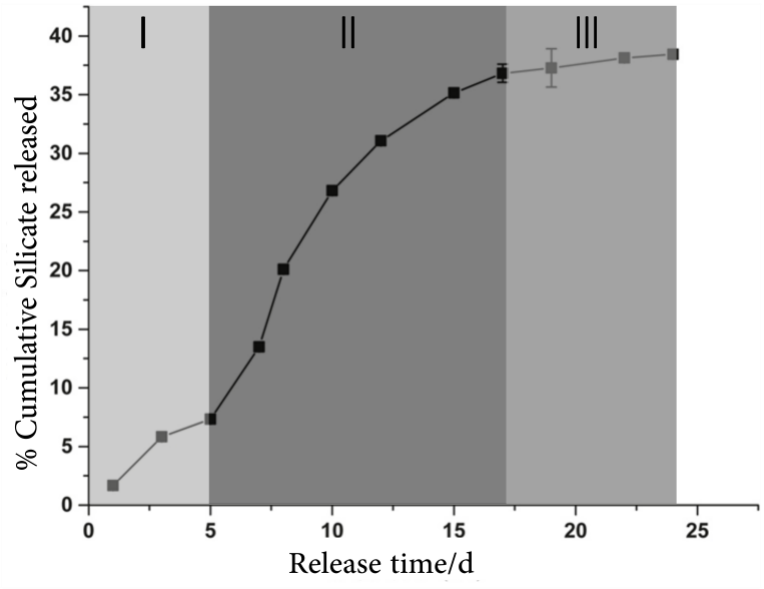

Fig. 3- 5. *In vitro* silicate release profile of ß-TCP/Silica-micro

The release characterization of silicatein from ß-TCP/silicatein-micro was also performed at 37 ^{o}C with sterilized PBS as the release medium. At defined time intervals, the total release medium was collected and refreshed. The silicatein concentration in the release medium was directly determined by micro-BCA assay. The silicatein released during the first day was defined as the initial burst. The release profile of silicatein was expressed as the cumulative percentage of release during the release time period (Fig. 3-6). The data shows a slow continuous silicatein release over one month. Theoretically, the release profile and the initial burst are correlated with the amount of protein in the microspheres. A high silicatein load is associated with a higher initial burst. As shown in Fig. 3-6, the release profile of silicatein can be divided into three phases: initial burst (first day), second phase (from 2nd to 17th day) and third phase (from 19th to 24th day). In the first days, the initial burst reached 15 %, which is consistent with the previous result. After the initial burst, a slow and constant released profile follows until day 17. After day 17, silicatein was released slightly faster than during the second phase, while 10 % of silicatein was released from ß-TCP/Silicatein-micro in the last phase. In summary, the percentage of cumulative release of silicatein reached 50 % in the whole period.

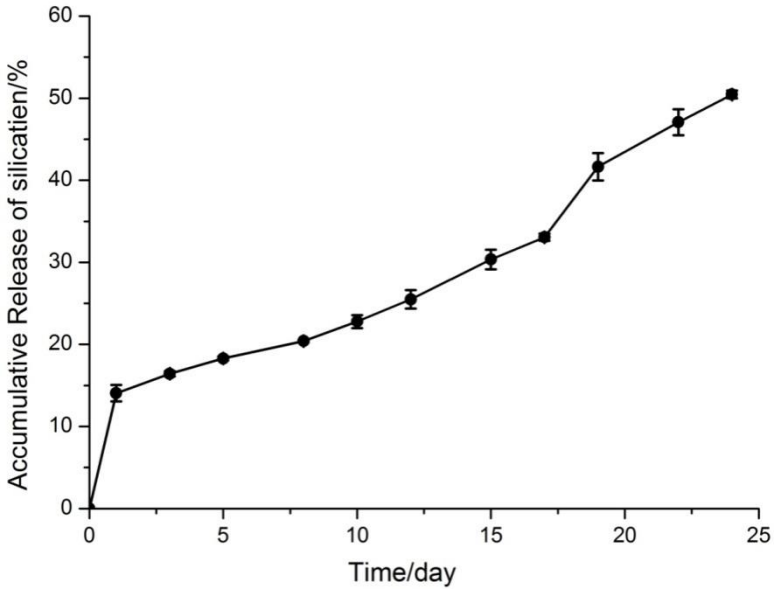

Fig. 3- 6. *In vitro* cumulative release curve of silicatein from ß-TCP/Silicatein-micro in sterilized PBS as the release medium.

3.2.4 Water uptake and swelling assay for microsphere-based scaffolds

The water uptake and swelling capabilities are important properties of biomaterials for tissue engineering. They are related to the hydrophilicity and porous structure of the scaffold. Therefore, the water uptake and swelling properties of the microsphere-based scaffold (ß-TCP/Silica-micro) were carried out by immersion the scaffold in phosphate buffer saline for 24 h. Their behavior in this study were presented in Fig. 3-7. It was founs that after 1h immersing in water, the water uptake reached a maximum value, while the volume of the scaffold reamained almost unchanged. The water uptake increased dramatically, reaching over 120 % (dashed line). In contrast, the scaffold volume remained constant and only increased by 2 % (solid line). From 1 h to 12 h, the scaffold started to shrink dramatically (solid line), 15 % smaller than the initial volume. Meanwhile, water uptake showed a similar trend. The water was pushed out of scaffold during shrinkage. The percentage of water uptake went down to 85 % after 12 h incubation, matching to the scaffold shrinkage (15 %). At the last 12 h (from 12 h to 24 h), the volume of the scaffold and the water uptake remained almost constant, as shown in the two curves.

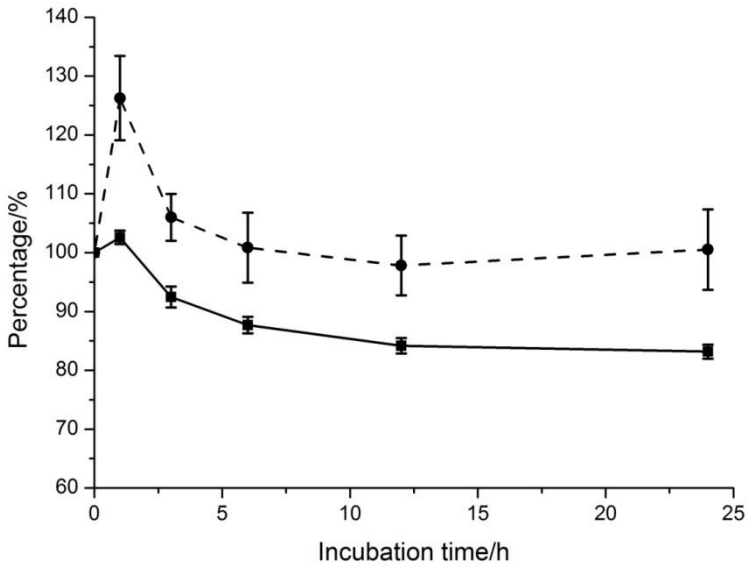

Fig. 3- 7. Water uptake and swelling curves of the ß-TCP/Silica microsphere-based scaffold. ■: swelling; ●: water uptake.

3.2.5 Mechanical properties of microspheres during enzymatically degradation *in vitro*

The mechanical properties of the PLGA microspheres (ß-TCP-micro, ß-TCP/silica-micro and ß-TCP/silicatein-micro) during a degradation period of 100 days in serum were determined using a newly developed ferrule top glass nanoindenter.

At selected time points, several microspheres were taken out from the medium and washed three times with distilled water to remove the absorbed protein and polymer fragments. The microspheres were mounted on a sample stage for stiffness measurements. Different factors, such as molecular weight, copolymer composition, morphology and porosity, significantly affect the stiffness of the PLGA microspheres. PLGA polymers are degraded by random hydrolytic or enzymatic cleavage of their backbone ester linkages. The microspheres were incubated with serum at 37 ^{o}C for 0, 21 and 100 days. The stiffness data of the degraded microspheres are shown in Fig. 3-8. Initially, ß-TCP/Silica-micro microspheres have a relatively higher stiffness (31 MPa) compared to those of the other two microspheres (21 MPa for ß-TCP-micro and 15 MPa for ß-TCP/Silica-micro). With the degradation, all the microspheres started to partially lose their mechanical properties. For ß-TCP-micro microspheres, the stiffness values decease from 22 MPa to 16 MPa, and to 3 MPa during the incubation of 0, 21 and 100 d. Similar trends were observed for ß-TCP/silica-micro microspheres and ß-TCP/Silicatein-micro microspheres. After 100 day incubation, all microspheres became very soft. Part of the microspheres even lost their spherical morphology and became polymer fragments (data not shown).

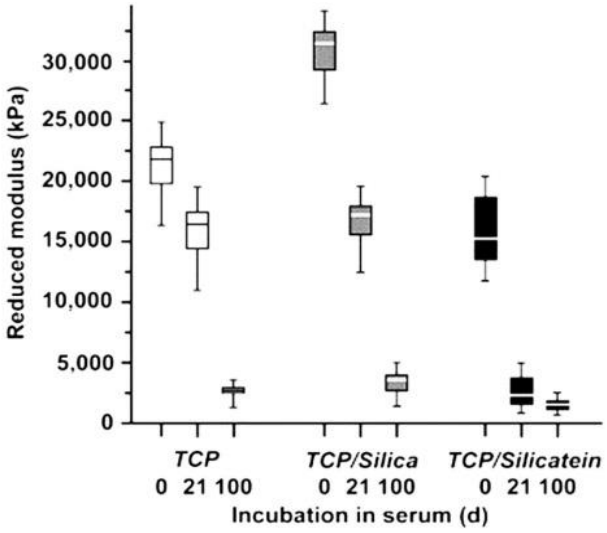

Fig. 3- 8. Stiffness value of the microspheres during *in vitro* degradation (TCP: ß-TCP-micro microspheres; TCP/Silica: ß-TCP/silica-micro microspheres; TCP/Silicatein: ß-TCP/silicatein-micro microspheres) [81].

3.3 Discussion

3.3.1 Morphology of microspheres with different ingredients

Under an optical microscopy, all microspheres have a similar spherical morphology. They are solid, whitish and show smooth surfaces devoid of irregularities. The diameter of the microspheres is around 700 - 800 µm without significant difference in all groups. The size of microspheres is primarily determined by the polymer concentration, stirring rate and needle diameter in our work. It is positively correlated with polymer concentration and needle size, and is negatively related with stirring rate. High polymer concentration increases the viscosity in the polymer solution; it makes the polymer solution more difficult to be broken into smaller polymer droplets. The microsphere size decreases as the stirring rate increases, due to the higher shear force. The parameters for all the microsphere groups are similar, as described detailly in section 2.4.1. Therefore, the microsphere morphology shows no significant difference.

Under an SEM, a nano-porous structure was clearly observed on the microspheres surface with a pore size of ～10 nm (Fig. 3-3A). It can be seen that the nano-porous structure on the surface of the microspheres from two groups (ß-TCP/silica-micro and ß-TCP/silicatein-micro) is much more obvious than of the ß-TCP-micro group (Fig. 3-2). In contrast, the ß-TCP-micro shows dense, nonporous polymer shell layers (Fig. 3-2A4). The nanoporous surface structure was mainly generated by the rapid evaporation of DCM and the diffusion of additives caused by concentration gradient [158,160]. The nanoporous surface structure can increase the release of silicate and silicatein from PLGA microsphere.

The ß-TCP and silicate encapsulated in the microspheres can be indirectly determined, when the relevant e*lements in the m*icrospheres are determined by EDX. The EDX spectrum of ß-TCP/Silica-micro microspheres shows strong peaks of C, O, Si and weak signals of Ca and P (Fig. 3-3B). So it is clear that ß-TCP and silicate are successfully encapsulated in the PLGA microspheres, since C and O are derived from PLGA polymer, Si represents silicate, and Ca and P come from ß-TCP. The week signals of Ca and P indicate that most of ß-TCP particles are blocked by the polymer. The strong signal of Si is due to a large amount of encapsulated silicate in the PLGA

microspheres. For the identification of silicatein, the biochemical techniques (SDS-PAGE and Western-blot) are used. Silicatein was extracted from PLGA microspheres with PBS buffer containing 3 % SDS and determined by SDS-PAGE and Western-blot (Fig.3-4). The results show that no significant change in the molecular weight of the encapsulated silicatein was observed during the encapsulation process. The bioactivity of released silicatein was proved in previous work, and the formation of biosilica was induced by incubation of PLGA/silicatein microspheres with silicate substance [140].

Instability and deactivity of protein are still major problems in the incorporation of proteins into polymer microspheres by the use of microencapsulation methods. Possible causes of protein denaturation can be the interface, organic solvent, contact with polymer, mechanical agitation, sonication, etc., presenting in three key steps: protein loading, microsphere formation and drying [177]. In the w/o/w double emulsion method, the emulsification procedure is the main cause of loss of activity [178]. Approaches for minimizing protein degradation are developed by adding stabilization (sugar, PRG, PVA and BSA), increasing protein loading, avoiding sonication and reducing homogenization time [177]. If PEG 400 and nerve growth factor (NGF) ere co-encapsulated into PLGA microspheres, PEG 400 can improve the stability of NGF and allow for a sustained release [179].

3.3.2 Active ingredients release from PLGA microspheres

Controlled drug release is an attainable and desirable characteristic of drug delivery systems [180]. Many factors influence the release characteristics of the drug in the polymer microspheres. The drug carrier degradation rate and the drug diffusion rate are the main factors controlling the drug release from the matrix. Drug release can be composed of up to three steps: initial burst, internal diffusion and polymer degradation. All these three steps can be found in the silicate and silicatein release profiles. A typical protein release profile exhibits an initial burst quick release in the first 24 h, then an increase in the release rate due to internal diffusion and polymer degradation, and ends with an incomplete release, although the microspheres are degraded significantly [181]. The typical initial burst was found in

the silicatein release profile, but not in the silicate release profile (Fig. 3-5). Silicatein has a typical initial burst of 15 %, but only 2 % for silicate release. The two key factors driving drug release from polymer microspheres are the drug diffusion rate and the polymer degradation rate [182]. The drug diffusion rate is related to the physicochemical properties of the drug, such as molecular size and hydrophilicity. The release profile of silicatein, as a water-soluble protein, also consists of an initial burst (24 h), a controlled slow diffusion release period (2 to 18 days) and an increased release period (from 20th day to the end). The initial burst release of drug from microsphere is also defined as the amount of drug that escapes from the microsphere before the beginning of polymer erosion, the contribution of drug dissolution and diffusion [183]. Burst release is often harmful and may cause an overdose toxicity to the body, even it normally happens at the beginning [184]. The strategy to control the burst release is to improve the miscibility of the drug and the polymer, increase the resistance to diffusion and reduce the porosity of the microspheres [183]. Another difference in the release of silicate and silicatein is that from 17 days to 24 days, almost no silicate (only 2 %) was released from the microspheres. That is to say, the internal diffusion of silicate release continues to the end of the release. With the PLGA further corrosion, the internal silicate can be released again from PLGA microsphere.

3.3.3 Water uptake and swelling behavior of scaffold

The water uptake and swelling behaviors of the microsphere-based scaffolds are critical for their applications in tissue engineering. When the scaffolds are implanted into the tissue, they absorb body fluid from the surrounding tissue and start to swell. In tissue engineering, swelling behavior can influence the physical characteristics of scaffolds after and prior to implantation. It depends on the hydrophobicity, hydrophilicity and porosity of the implantation scaffold. With increasing the pore size, the scaffolds show an increasing swelling ability due to the easy diffusion of fluids and nutrients [185]. However, the mechanical properties of the scaffolds are opposite to the pore size and porosity. In general, hydrophilic materials interact easily with water and change their dimensions [186]. Microsphere-based scaffolds are

characterized by interconnected porous structures. With an open porous structure, the fluid can easily enter the scaffolds and simultaneously makes the scaffolds swelling. Besides entering the micropores, aqueous medium is able to penetrate into the PLGA microspheres to hydrate the PLGA microspheres. Subsequently, PLGA scaffolds start to shrink slightly after 1 h of incubation and remain around 90 % of the volume after 24 h of incubation. The water uptake capacity of the scaffolds was simultaneously measured by a swelling test. Regardless of the hydrophilicity of PLGA, the capacity of water uptake depends mainly on pore size and porosity [187].

3.3.4 PLGA microsphere degradation behavior in serum

PLGA is degraded by hydrolysis of its ester linkages in the presence of water to produce the original monomers: lactic acid and glycolic acid. These two monomers are excreted from the body by urine under normal physiological conditions. There are many factors that affect the degradation of PLGA, such as polymer composition, molecular weight and medium. PLGA degradation can be divided into four steps: hydration, initial degradation, further degradation, and solubilization [188]. The higher the ratio of glycolide units, the shorter the degradation time, except for the ratio of PLGA of 50:50 [189]. The degradation time is directly related to the molecular weight of the polymer [149]. The pH of the medium has a significant effect on the PLGA degradation, which is rapidly hydrolytically degraded in alkaline and acid solutions [190]. The mechanism of PLGA degradation changes from "inside-out" under neutral conditions to "outside-in" under acid conditions [191]. This "inside-out" degradation theory was discovered by Vey et al. [192], who studied PLGA degradation in phosphate buffered saline at 37 ^{o}C. In the presence of enzymes (trypsin or lysozyme), the accumulated weight loss rate of PLGA is significant by the dispersion of the degradation products. However, these enzymes do not contribute to chain cleavage [193,194]. Therefore, the enzymatic degradation of PLGA is still primarily a hydrolysis process [193]. Large size PLGA devices have a heterogeneous degradation and are characterized by a degradation rate in the core that is greater than the degradation rate at the surface. It is unlikely that PLGA microspheres of less than 300 μm show a homogeneous degradation [195]. During the degradation

process, the PLGA microspheres release water-soluble monomers that are promoted from the interior and surface of the microspheres. In the end, it results in the formation of an alveolar and porous structure that loses mechanical stiffness. The varying stiffness can be measured by Piuma nanoindentation to indicate the degradation degree of the PLGA microspheres.

Chapter IV:

Biological evaluation of PLGA/Biosilica microspheres

4 Biological evaluation of PLGA/Biosilica microspheres

4.1 Materials and equipments

4.1.1 Cell line and cell culture materials

Cell line Human primary osteogenic sarcoma (SaOS-2)	ATCC®HTB-85™
McCoy's 5A Medium Modified	Gibco™*16600082
Fetal Bovine Serum (FBS)	Gibco™*A3840001
Gentamicin solution	SIGMA*G1397
Cell culture CO_2 incubator	ThermoFisher
Phosphate Buffered Saline (PBS), pH=7.4, w/o Ca^{2+}/Mg^{2+}	ThermoFisher* 10010001
Trypsin-EDTA (0.25 %), phenol red	ThermoFisher* 25200056
Dimethyl sulfoxide (DMSO), cell culture grade	SIGMA
3 - (4,5-Dimethylthiazol-2-yl)-2,5-diphenyltetrazolium bromide (MTT)	SIGMA
Dimethylformamide (DMF)	SIGMA*D4551
Sodium dodecyl sulfate solution (SDS), 20 % in water	SIGMA*D05030
Alarm Blue	AbDserotec*BUF012B
eBioscience™ DRAQ5™	ThermalFisher*65088092
Rhodamine Phalloidin	Cytoskeleton*PHDR1
Paraformaldehyde (PFA)	Sigma*P6148
Triton X-100	Sigma*T8787
Bovine serum albumin, Albumin Fraktion V (BSA)	Roth*8076
OsteoImage™ bone mineralization Assay	Lonza*PA-1503
Alizarin Red s	SIGMA*A5533
Cetylpyridinium chloride	SIGMA*C0732

4.1.2 Equipments

Cell culture CO_2 incubator	ThermoFisher
Cell Counter Scepter™ 2.0	Millipore
Spectrophotometer Varioskan Flash Ⅱ	Thermo Fisher
Fluorescence microscopy, AMG, EVOS®Microscopy,	Thermo Fisher

Fluorescence microscope, AMG, EVOS®Microscopy	ThermoFisher
Confocal laser scanning microscopy (CLSM)	Carl Zeiss GmbH

4.2 Sample sterilization and cell culture

4.2.1 Sample sterilization for biological assay

All microspheres and microsphere-based scaffolds used in the biological assay, were sterilized under UV light for 1h (for scaffolds, 1h per side) in a laminar hood. To ensure complete sterilization, the sterilized samples were incubated with the culture medium overnight before the further assay. Treatment with 70 % ethanol for more than 30 minutes may be an alternative sterilization method. But it should be noted that the hydrophilicity and topography of PLGA microsphere can be changed by ethanol wetting [196].

4.2.2 SaOS-2 cell line and its incubation conditions

The osteoblast SaOS-2 cell line (human osteogenic sarcoma cells) was chosen for the following *in vitro* biological assay. This cell line was derived from the primary sarcoma, and firstly isolated and characterized by Fogh et al in 1973 [197]. The SaOS-2 cells were cultured in a humidified incubator containing 5 % CO_2, using 10 ml McCoy's medium supplemented with 15 % heated-inactivated FCS (fetal calf serum), 2 mM L-glutamine and 50 mg/ml of gentamicin in a 25 ml culture flask or in a multi-well culture plate. When SaOS-2 cells grow up to 90% confluence, the culture medium was discarded and the cell monolayer was gently washed three times with 10 ml pre-warmed PBS without Ca^{2+}/Mg^{2+}. The washed cell monolayer can then be isolated by treatment with pre-warmed trypsin-EDTA solution (2.5 mg/ml trypsin and 0.38 mg/ml EDTA), which takes 3-5 min at 37 ^{o}C. This progress should be monitored by examining the culture flask under an inverted phase-contrast microscope. After cell isolation, the cells are ready for further experimentation or subculture.

4.2.3 Counting of cell number with Scepter^{TM} 2.0 cell counter

Each cell line has an optimal concentration to maintain growth and viability. In tissue engineering, the cells are usually seeded on a scaffold. Therefore, the cell

density on the scaffold should be controllable. Traditionally, hemocytometers are widely used for the cell counting. They consist of a thick glass microscope slide with a vertical line grid etched in the middle. However, this method is quite time-consuming. In our laboratory, we use Millipore's cell counter Scepter™ 2.0 to count the cell. This counter is based on advanced electronic sensor technique. The scepter™ 2.0 cell counter is compatible with two micro-fabricated and precision-engineered sensors. The 60 µm sensor is for particles between 6 and 36 µm and 40 µm sensor is for particles between 3 and 17 µm. With these two sensors, the Scepter™ 2.0 cell counter can automatically analyze a loaded cell suspension within 30 seconds and provide an accurate and reliable cell number (Scepter™ 2.0 cell counter Product brochure, Merck Millipore).

The counting process is as follows:

- Prepare a cell suspension in PBS (500 µl) with 1×10^4 to 5×10^5 cells/ml;
- Insert a 60 µm sensor (depending on the cell size) and switch on the cell counter;
- Submerge the sensor tip in the cell suspension, release the plunger to allow 50 µl cell suspension drawn into the Scepter™ sensor;
- As cells flow through the aperture in the sensor, resistance increases. This increase in resistance causes a subsequent increase in voltage. Voltage changes are recorded as spikes with each passing cell. Spikes of the same size are bucketed into a histogram and counted. This histogram gives you quantitative data on cell morphology that can be used to examine the quality and health of your cell culture.

4.3 Biological evaluation of PLGA microspheres

4.3.1 Cytotoxicity assay for PLGA microspheres

4.3.1.1 Indirect method—extraction/dilution method

As described in the International Standard ISO 10993-5: Biological evaluation of medical devices -- Part 5: Tests for *in vitro* cytotoxicity, MTT assays have been widely used to assess cell viability. MTT [3-(4,5-Dimethylthiazol-2-yl)-2,5-diphenyltetrazolium bromide], a yellow tetrazole, can be reduced to purple formazan

(water-insoluble) in living cells, and the amount of formazan is directly proportional to the number of viable cells. The absorbance of the purple solution, dissolved in DMSO, can be quantified with a spectrophotometer at 570 nm. The extract was prepared by shaking the medium (freshly prepared McCoy's medium containing 15 % FCS) with 30 mg/ml microspheres at 90 rpm and 37 ^{o}C for 24 h. Latex Rubber (~6 cm^2/ml) was extracted in the same medium as positive control (carrying the maximum cytotoxic effect). McCoy's medium containing 15 % FCS was selected as the negative control.

Briefly, SaOS-2 (1×10^4 cell/well) were seeded in triplicate into 24-well plate and incubated at 37 ^{o}C for 48 h in order to obtain confluent cell monolayer prior to assay. After 48h incubation, the culture medium was replaced with extraction medium. Subsequently, the cells were continually incubated for 24 h. On the next day, the extraction medium was replaced by 450 µl pre-warmed culture medium and 50 µl MTT solution (5 mg/ml, dissolved in sterilized PBS). During the 3 hours' incubation, the yellow MTT was reduced to purple formazan by living cells. Subsequently, the medium and unreduced MTT were aspirated, and the remained formazan was dissolved in 600 µl of dilution medium (40 % DMF and 10 % SDS) at 37 ^{o}C for 1h, pretected from light. Finally, 150 µl of purple solution (in triplicate) was transferred to a 96-well plate, and the absorbance was measured at 570 nm using the spectrophotometer (Varioskan, Thermo Fisher), taking the dilution buffer as the blank. The percentage of the viable cell was determined, which correlates with the optical density of each sample by deduction of negative control (100 % viability).

4.3.1.2 Direct method — directly seeding cells on scaffold

To value the biocompatibility of the microspheres, the direct contact method was performed as previously described [198]. SaOS-2 cells were directly seeded on the microsphere-based scaffolds and cultured in a humidified incubator for 3 days. The Alarm Blue cell viability assay was performed according to the manufacturer's protocol. Briefly, SaOS-2 cells were carefully seeded on the top of the microsphere-based scaffolds (micro, ß-TCP-micro, ß-TCP/Silica-micro, ß-TCP/Silicatein-micro, and Biosilica-micro, n = 4) in a 24-well plate at a density of 1×10^5 cells per well and cultured in a humidified incubator containing 5 % CO_2 at 37 ^{o}C for 3d. In order to

prevent the scaffolds from floating in the medium, the scaffolds were fixed on the bottom by tetrafluoroethylene (TFE) ring. After 3d's incubation, the culture medium was carefully aspirated without contacting the scaffolds and cell layers. Subsequently, the remaining cells were incubated with 500 µl of pre-warmed medium (without FCS) containing 10 % Alarm Blue (BUF012B, AbDserotec) at 37 ^{o}C for 4h with light-protection. Then, 150 µl of pink medium was transferred in triplicate to a 96-well plate. The blue indicator (resazurin, blue and nonfluorescent) was reduced to resorufin (pink and highly fluorescent) by living cells [199]. The fluorescence intensity was monitored by using a fluorescence spectrophotometer (Varioskan, Thermo Fisher) at an excitation wavelength of 570 nm and an emission wavelength of 590 nm. The culture medium containing 10 % Alarm Blue was taken as the blank. The percentage of viable cells was calculated by comparing the fluorescence intensity of each sample to the control microspheres (micro), which is considered to have 100 % viability.

4.3.2 Cell attachment and proliferation assay

To evaluate cell attachment and proliferation on the microspheres, the fluorescence microscope (AMG, EVOS®Microscopy, ThermoFisher, Germany) and the confocal laser scanning microscopy (CLSM; Carl Zeiss GmbH, Göttingen, Germany) were used to inspect the morphology of cells on scaffolds. The SaOS-2 cells, at a density of 1×10^5 cells per well, were carefully seeded on Biosilica-micro based scaffold which was prepared by mixing ß-TCP/Silica-micro and ß-TCP/Silicatein-micro at a ratio of 1:1. After 3 days and one week incubation, the cells were stained with DRAQ5^{TM} (DRAQ5^{TM}, eBioscience, Biostatus, Ltd) to stain the nuclei and with Rhodamine Phalloidin (Cytoskeleton Inc. Cat.PHDR1) to stain the filamentous actin (F-actin), as described in Hung 2009 and Sisson 2010 [200,201] separately. Then cell attachment, spreading and morphology on the microspheres were visualized by a microscope.

Briefly, the scaffolds were sterilized on each side by UV light irradiation for 1h and fixed in a 24 well plate with a TFE loop prior to seeding the cells. 200 µl of cell suspension (1×10^5 cells) was seeded on the scaffolds. After 2h of attachment, an

additional 1 ml of fresh culture medium was slowly added into each well without disturbing the cell layer on the scaffold. The medium (1 ml) was refreshed twice a week to avoid agitation of the cell layer. At selected time points, the culture medium was discarded and the cell layer was washed twice with pre-warmed PBS buffer. Then, the scaffold with the cells was moved into a new well containing 500 µl of 4 % PFA, Sigma, dissolved in PBS, pH = 7.4) for fixation. After 30 min fixation, the cells were washed three times with PBS buffer (1 ml) to wash away the PFA. The fixed cells were permeabilized with 0.2 % Triton X-100 (in PBS) for 5 min at room temperature and then washed three times with PBS. The blocking step, 1 % Bovine serum albumin, Albumin Fraktion V (BSA) in PBS was used as the blocking solution. The fixed cells were incubated with 1 ml of blocking solution on a shaker for 30 min. Subsequently, the blocked cells were washed again three times with PBS for ten minutes each time.

Finally, the fixed cells were ready for staining with Rhodamine Phalloidin (for F-actin) and DRAQ5™ (for nuclei). First, a working solution of 100 nM Rhodamine Phalloidin was prepared by diluting 7 µl of a 14 µM stock solution with 1 ml of PBS. Then, 300 µl of working solution was used for staining cell fibrin in the dark for 30 min at room temperature. After F-actin staining, the cells were washed once with PBS buffer. Then, the cell nuclei was stained with 10 µM DRAQ5™ (diluted 1:500 with PBS) for 10 min at room temperature (light protection). Subsequently, the cells were washed twice again with PBS. Ultimately, the scaffolds were glued onto the slides with a drop of anti-fade mounting medium. The excessive medium was gently removed with the tissue and the scaffolds were sealed each side with nail polish. The slides were stored at 4 ^{o}C in the dark for microscopic analysis.

4.3.3 Biomineralization assay

Biomineralization of SaOS-2 cells on different microspheres was determined by the Osteoimage mineralization assay [144,202] and the Alizarin Red S/cetylpyridium chloride method [203,204]. With the Osteoimage staining, the mineralized nodules were shown as yellow particles under a fluorescence microscopy. For Alizarin Red S/cetylpyridium chloride method, the mineralized nodules were first stained with Alizarin red, and then Alizarin staining was extracted with 10 % cetylpyridium

chloride. The optical density was measured at 562 nm using a spectrophotometer (Varioskan Flash, Thermo Scientific, Germany) and the amount of biomineralization was given as absorbance units at 562 nm.

4.3.3.1 OsteoImage mineralization assay

The SaOS-2 cells (1×10^5) were seeded on the microsphere-based scaffolds in a 24-well plate. After 3 days incubation, the culture medium was refreshed with 1 ml osteogenic medium (complete culture medium plus 100 nM dexamethasone, 50 µM ascorbic acid and 10 mM ß-glycerol phosphate) to induce HA formation. The osteogenic medium was refreshed every two days.

The osteoimage mineralization assay was performed according to the manufacturer's recommendation (OsteoImage™ Mineralization Assay PA-1503, LONZA). Briefly, after 5 days incubation with osteogenic medium, the samples were ready for osteoimage staining. Upon discarding the culture medium, the cells were washed twice with pre-warmed PBS buffer. Then, the washed cells were fixed with 0.5 ml of 4 % paraformaldehyde (in PBS) at room temperature for 30 min with shaking. After fixation, the fixed cells were rinsed twice with 500 µl diluted wash buffer supplied with the assay Kit. Subsequently, the cells were incubated with 0.5 ml (for a 24-well plate, enough to cover the cell layer) diluted staining reagent at room temperature for 30 min on the shaker, prevented from light. After staining, the samples were washed three times, each time for 5 min, with diluted wash buffer. Finally, the stained samples were adhered to the slides with antifade mounting medium and stored at 4 °C in the dark. For visualization, the stained mineralization nodules were inspected with a fluorescence microscopy (AMG, EVOS®Microscopy, ThermoFisher, Germany), using a laser with an excitation wavelength of 492 nm and an emission wavelength of 520 nm.

4.3.3.2 Alizarin Red S/cetylpyridium chloride assay

In this approach, the mineralized samples were prepared in the same way which is described in section 4.3.3.1. The SaOS-2 cells were seeded on the scaffold and co-cultured for 3 days. Then, the cells were activated with osteogenic medium for mineralization. After 5 days activation, the samples are ready for Alizarin red staining.

This staining was performed as follows:

- Wash the cells gently three times with pre-warmed PBS
- Fix the cells for 20 min at room temperature with 300 µl of 4 % PFA
- After fixation, wash the cells again three times with pre-warmed PBS
- Stain with 500 µl 1 % Alizarin red (pH = 4.1) for 30 min while shaking
- Wash three times with 1 ml distilled water for 10 min per wash
- Dissolve the Alizarin staining with 500 µl of 10 % cetylpyridinium chloride for 30 min at room temperature with shaking
- Measure the absorbance at 562 nm with a spectrophotometer

4.4 Results

4.4.1 Cytotoxicity of microspheres

The toxicity assay of the microspheres was carried out by indirect and direct methods using the classical MTT assay. The extraction dilution method (indirect assay) follows the International Standard ISO-10993-5 for testing biomaterials and medical devices. The SaOS-2 cells were cultured in extraction medium (five groups: ß-TCP-micro, ß-TCP/silica-micro, ß-TCP/silicatein-micro, as well as positive and negative control) for 24h, then cell viability was determined by MTT, as shown in Fig. 4-1A. For the direct assay, SaOS-2 cells were directly seeded on the microspheres (five groups: micro, ß-TCP-micro, ß-TCP/Silica-micro, ß-TCP/Silicatein-micro and Biosilica-micro), allowing cell attachment and proliferation on the microspheres for 3 days, then MTT determination was followed. The viability was calculated according to the absorbance of the sample to control, considered to be 100 % viability, as shown in Fig. 4-1B.

In Fig. 4-1, it is shown that all the microsphere groups do not cause any significant difference in cell viability, compared to the control group. In Fig. 4-1A, the cell viability of TCP-micro group is slightly increased. In contrast, the cell viability of TCP/Silica-micro and TCP/Silicatein-micro groups has a slight decrease of 1-2 %. Obviously, the cells cannot survive in Latex extraction medium, with a cell viability of 2-3 %. A severe cytotoxic reaction to the extraction medium of natural latex rubber was verified. This result indicates that all microsphere groups do not release toxic

substance in the extraction medium. Before MTT addition, the cell morphology was clearly visualized under the microscope. Fig. 4-2A, B, C and D show that the cells show a similar spindle-shape morphology, are oriented and attach closely to the bottom of the culture plate. As one exception, latex rubber (Fig. 4-2E) had a few living cells on the bottom. This observation correlates with the cell viability assay (Fig. 4-1A). In the direct contact assay (Fig. 4-1B), the results show that all microspheres do not cause any significant change in viability compared to control (PLGA-micro). Cell proliferation is slightly faster in the group of ß-TCP-micro and Biosilica-micro than in the group of ß-TCP/Silica-micro and ß-TCP/Silicatein-micro. Apparently, there is no difference in cell viability between them.

In conclusion, all microspheres *in vitro* show no potential cytotoxicity for SaOS-2 cells. Taken together, they can be considered as candidates for biomedical applications.

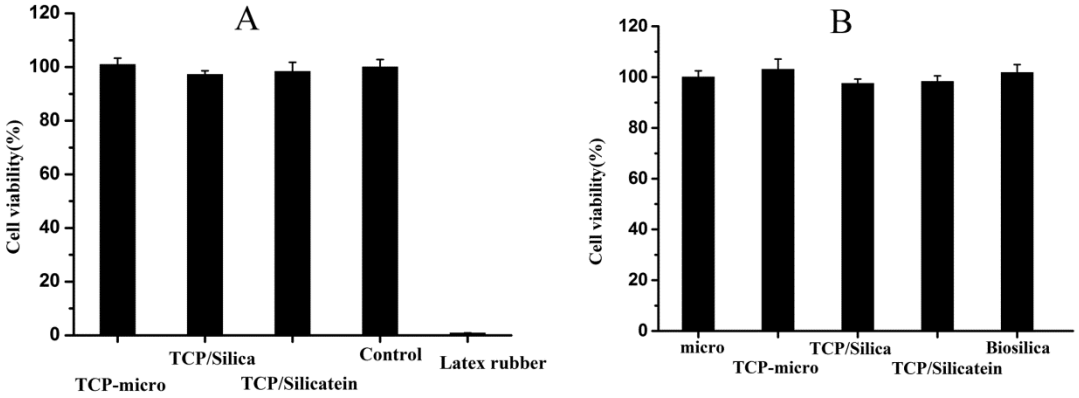

Fig. 4- 1. Cell viability of SaOS-2 cells from indirect assay (A) and direct assay (B). A: Cells cultured with extraction medium; B: Cells seeded directly on the microspheres. (micro: PLGA microsphere; TCP-micro: ß-TCP-micro; TCP/Silica: ß-TCP/Silica-micro; TCP/Silicatein: ß-TCP/Silicatein-micro; Control: culture medium + 15% FBS; Silica/Silicatein: mixture of ß-TCP/Silica-micro and ß-TCP/Silicatein-micro (1:1). Control group (A) and micro group (B) were considered to have 100% cell viability.

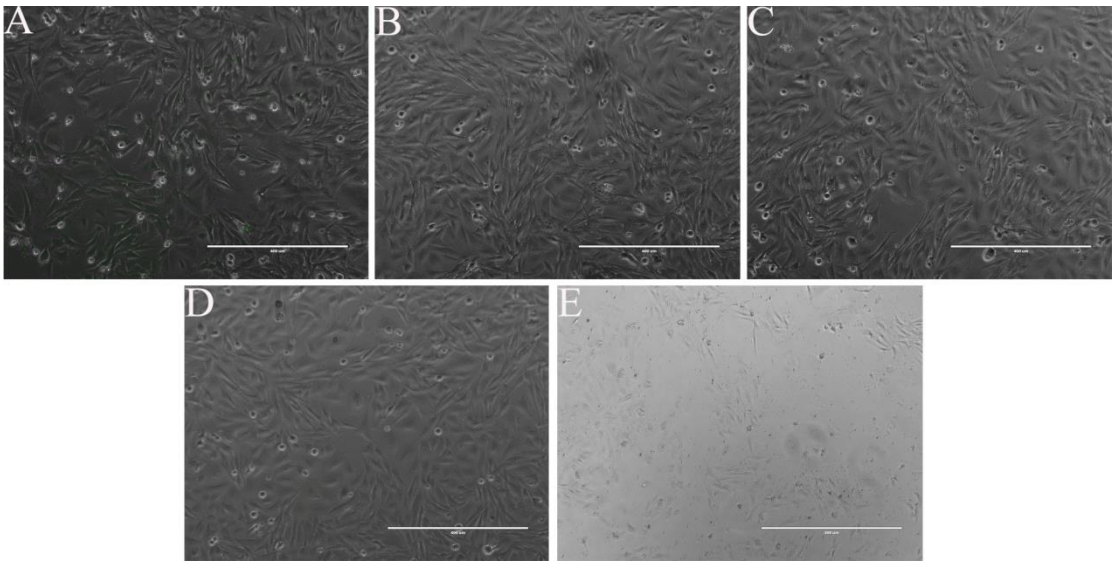

Fig. 4- 2. Cell morphology after incubation with extraction medium for 24 h. (A: ß-TCP-micro; B: ß-TCP/silica-micro; C: ß-TCP/silicatein-micro; D: Negative control: culture medium + 15% FBS; E: Positive control: latex rubber). Culture medium with 15% FBS as the extraction medium, the extraction ratio is 30 mg/ml for all microspheres group and 6 cm^2/ml for latex rubber; Scale bar: 400 µm.

4.4.2 Cell attachment and proliferation on Biosilica-micro based scaffold

Cell attachment and growth on the scaffold were assessed by cell nuclei and F-actin staining, which were determined using fluorescence and confocal microscopy. SaOS-2 cells were seeded on the biosilica microsphere-based scaffolds (1:1 mixture of ß-TCP/silica-micro and ß-TCP/Silicatein-micro). At defined time points, the cells were washed with PBS, and then cell nuclei and F-actin were co-stained with DRAQ5 and Phalloidin-rhodamine conjugate, respectively. Fig. 4-3 shows the cell morphology and cell spreading at different culture times. Bundles of F-actin, so-called stress fibers, and counterstained cell nuclei were observed. On day 3 (Fig. 4-3A and B), a limited number of cells was found on the microsphere (Fig. 4-3A), but most of the cells settled down at the gap between the microspheres (Fig. 4-3B). The cells had a flat, spindle-shaped and polarized morphology with well-developed stress fibers. The cells spreading on the surface show that the biosilica microspheres have a positive effect on cell adhesion, demonstrating good biocompatibility. As shown in Fig. 4-3A, the microspheres were surrounded by intensive blue and red color, indicating numerous cells around the microspheres. For close inspection, confocal microscopy was used to visualize the cells in the valley. Fig. 4-3B clearly shows the well organized filamentous

actin surrounding the oval nuclei, some cells even start to migrate along the surface of microspheres. The cells with elongated morphology on the microspheres show a healthy condition. On day 7 (Fig. 4-3C, D, E and F), a confluent monolayer of cells was observed on microspheres (Fig. 4-3C and D), and some areas even show very high cell density (Fig. 4-3E and F). Cells seem to aggregate to form branched and interconnected multicellular networks that cover the entire surface of the microspheres. Overall, the extent of F-actin formation increases with culture time. Taken together, these observations indicate that the biosilica microspheres allow the cells to adhere, proliferate and even migrate along the microspheres with time.

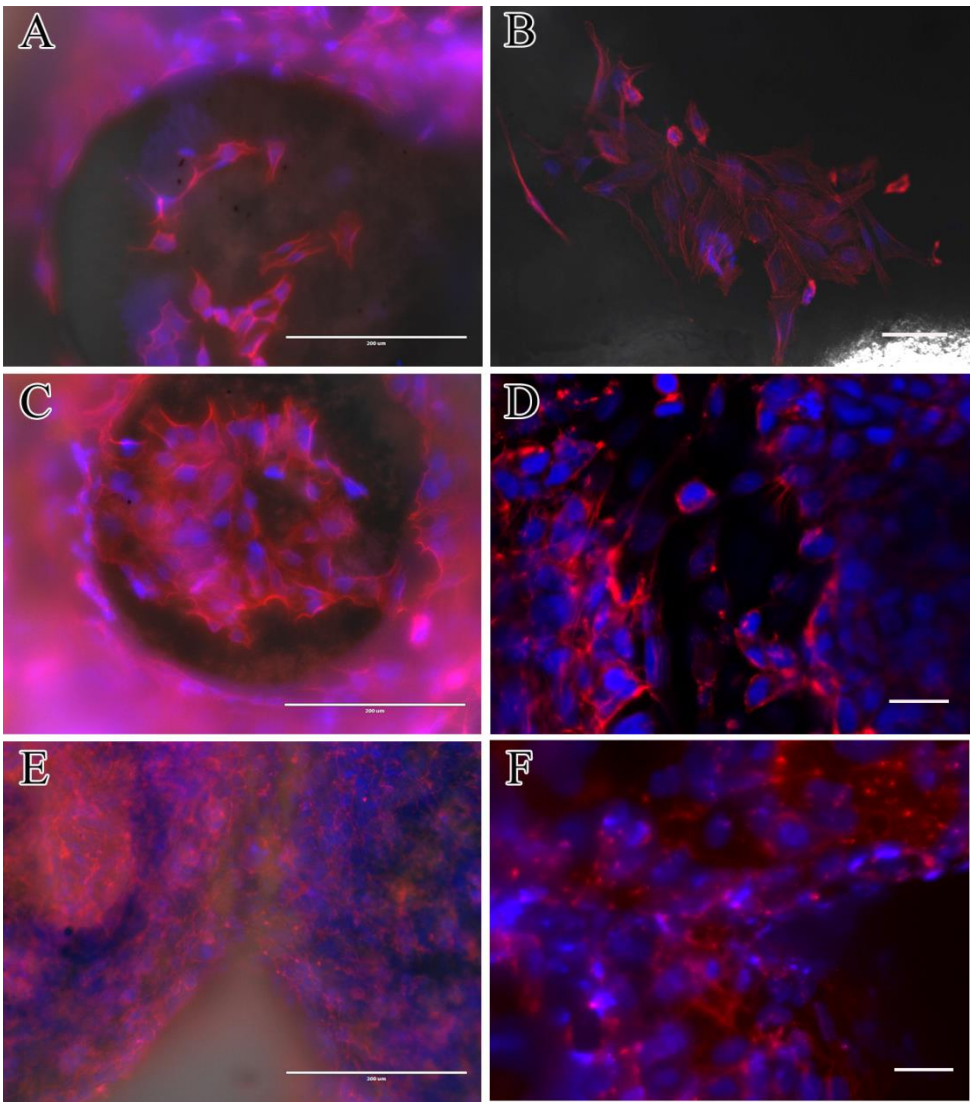

Fig. 4- 3. Characterization of cell attachment and proliferation on biosilica microsphere. F-actin was stained red with Phalloidin conjugated with Rhodamine, and cell nuclei were stained with DRAQ5 (blue), which were inspected by fluorescence and laser microscopy. Three days of incubation: A and B; Seven days of incubation: C, D, E and F. (left panel: fluorescence microscopic images, scale bar: 200 µm; right panel: Layer microscopic images, scale bar: 50 µm).

4.4.3 Microspheres mineralization assay

The mineralized matrix was collectively evaluated quantitatively by OsteoImage staining and Alizarin Red S/cetylpyridinium chloride assay. The SaOS-2 cells were carefully seeded on the various microspheres and incubated in osteogenic medium for 5 days to induce the formation of hydroxyapatite (HA). After 5 days of biomineralization, mineral deposits were quantified using the OsteoImage mineralization assay to visualize the Ca-deposits. The OsteoImage assay is based on binding of the staining reagent to Ca, giving a green fluorescence at the appropriate extraction wavelength (492 nm). The OsteoImage stained mineral deposits on the microspheres were clearly observed under the fluorescence microscope, as shown in Fig. 4-4. In Fig. 4-4, the brightly green dots on the microspheres indicate the stained mineral particles. For ß-TCP-micro (Fig. 4-4A) and ß-TCP/Silicatein-micro (Fig. 4-4C), which contain no silica, only a few green shining dots were found on the microspheres. It revealed that both groups have a low potential on inducing SaOS-2 mineralization. Conversely, a strongly increased fluorescence intensity was visualized in ß-TCP/Silica-micro group (Fig. 4-4B), covering all microspheres. With close inspection, we found that the green dots are mainly surrounding the microspheres, but a few were on the top. A similar intensity of green fluorescence was obtained in the Biosilica-micro group (Fig. 4-4D), but with larger green pitches, compared to ß-TCP/Silica-micro. The intensive fluorescence indicates a higher mineralization capability in silica containing groups (ß-TCP/Silica-micro and Biosilica-micro).

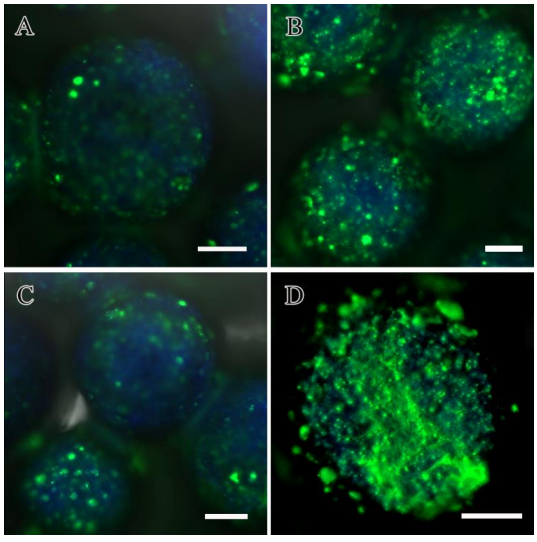

Fig. 4- 4. OsteoImage stained mineral nodules on the microspheres surface, induced by the incubation of SaOS-2 cells in osteogentic medium for 5 days. A: ß-TCP-micro; B: ß-TCP/silica-micro; C: ß-TCP/silicatein-micro; D: 1:1 mixture of ß-TCP/silica-micro and ß-TCP/silicatein-micro. Scale bar: 200 µm

Using of the Alizarin Red S/cetylpyridinium chloride assay, the mineralization of SaOS-2 on the different microspheres was quantitatively determined. The mineralized deposits were stained for 10 min with 1 % Alizarin Red S (pH = 4.2), then gently washed several times with distilled water to remove the non-specific bound Alizarin Red. The remaining calcium-bound Alizarin Red was released with an addition of 0.5 ml of 10 % cetylpyridinium chloride (CPC). Afterward, the solution was collected and the absorbance at 562 nm was measured by a spectrophotometer. The results are shown in Fig. 4-5. According to the absorbance of extraction, the four microsphere groups can be divided into two groups. Group without silica (ß-TCP-micro and ß-TCP/Silicatein-micro) has a lower value. That means the mineralization is also lower. A mean value of 0.29 ± 0.06 (ß-TCP-micro) and 0.32 ± 0.08 (ß-TCP/Silicatein-micro) were achieved, showing no significant difference between them. Interestingly, the group containing silica (ß-TCP/silica-micro as well as the 1:1 mixture of ß-TCP/Silica-micro and Biosilica-micro) shows a significant increase in mineralization. Values of 0.51 ± 0.09 (for ß-TCP/Silica-micro) and 0.71 ± 0.12 (Biosilica-micro) were achieved. With respect to ß-TCP-micro, there was a significant difference to ß-TCP/Silica-micro and Biosilica-micro.

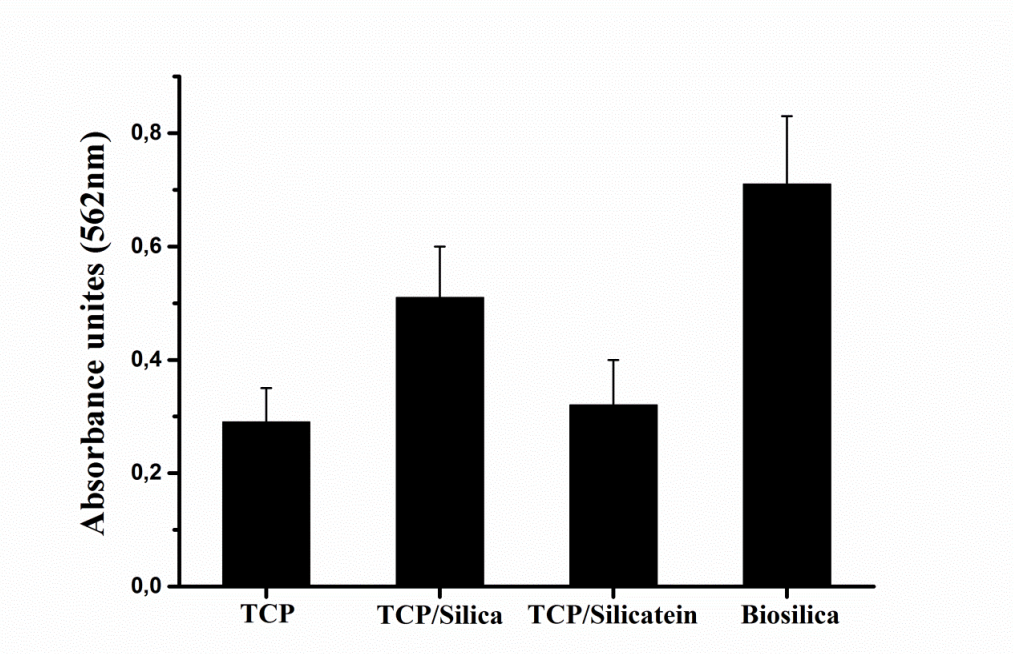

Fig. 4- 5. Absorbance of Alizarin Red S staining for the mineralization of SaOS-2 cells on the microspheres. (TCP: ß-TCP-micro; TCP/Silica: ß-TCP/silica-micro; TCP/Silicatein: ß-TCP/silicatein-micro; Biosilica: Biosilica-micro). The data represent the mean ± SD of five independent

4.5 Discussion

4.5.1 Biocompatibility of microspheres

The biocompatibility of the microspheres was evaluated with cytotoxicity as well as cell attachment and proliferation assay. In 2011, B. Ratner suggested the following definition of biocompatibility: Biocompatibility is the ability of materials to locally trigger and guide normal wound healing, reconstruction and tissue engineering [205]. The cytotoxicity test is the first step in ensuring the biocompatibility of medical materials and is characterized by being rapid, standardized, sensitive and inexpensive. The standard method is described in ISO 10993-5 [206]. In this study, the cytotoxicity of various PLGA microspheres was evaluated by the extraction method and the direct contact method. In general, extraction methods are more commonly used for the *in vitro* evaluation of medical materials and devices, which may release toxins from the exposed surfaces. The extraction conditions vary with the physicochemical properties of the test materials. The extraction medium may consist of 0.9 % saline, cell culture medium (with or without serum) and physiological buffer (PBS). The extraction time is recommended to be 24 h or 72 h, even 1 h at high extraction temperature [207]. The direct contact method is highly sensitive for detecting weak cytotoxicity. It involves the direct incubation of cells on the surface of the test materials. Bone implants materials should not contain components that are toxic for the cells and surrounding tissue, and should additionally support cell migration and growth on the implants. Based on the cytotoxicity test, all PLGA microsphere groups *in vitro* are harmless to the SaOS-2 cells. The main component of the microspheres is PLGA, which amounts to about 80-90 % in the microspheres. It is one of the most attractive biomaterials (approved by FDA) which is characterized by high biocompatibility and biodegradable properties. It has been extensively investigated as a biodegradable drug delivery system (PLGA microspheres) [208] and implant in tissue engineering [209]. ß-TCP, around 5-9 % in the microspheres, is the second major component of the microspheres. ß-tricalcium phosphate (ß-TCP) belongs to the bioceramics family which have been proposed to be a suitable biomaterial for bone tissue engineering [210]. It has a Ca/P ratio of 1.5, and is much more soluble in aqueous environment than hydroxyapatite. Due to its low interfacial energy with apatite, it is considered to

be osteoconductive and osteoinductive and induces apatite formation on the surface. Incorporation of HA into a PLGA scaffold can enhance the proliferation and differentiation of osteoblasts, compared to pure PLGA scaffolds. Biosilica, a natural inorganic biopolymer, formed enzymatically from orthosilicate, is a promising biomaterial for the treatment of bone diseases and dysfunctions [118].

To further evaluate the biocompatibility of PLGA microspheres, cell attachment and proliferation were quantified. Visualization of cell attachment and actin cytoskeleton was performed by immunostaining with DRAQ5 and Phalloidin. The interaction between cells and implant surface is referred to as cells sensing their physicochemical environment, resulting in focal adhesion. Three steps are involved in cell adhesion on scaffold: cell sedimentation, cell flatting and spreading, and focal adhesion formation [211]. PLGA as a biomedical material has been intensively investigated in tissue engineering. In the first 3 days of incubation, linear F-actin and a few microfilaments are observed on the PLGA microsphere matrix. With a longer incubation period, more F-actin microfilaments are distributed around the cell membrane, and only a few fibers cross the cell center. The cells migrated into the porous structure after one week of incubation, and the PLGA microspheres became completely covered with the cells.

4.5.2 Biomineralization of SaOS-2 cells on microspheres

Biomineralization of microspheres *in vitro* was evaluated after one week of incubation with osteoblasts in osteogentic medium containing dexamethasone, ß-glycerophosphate and ascorbic acid. It has been reported that dexamethasone stimulates significantly MSC proliferation and osteogenic differentiation [212] by inducing the expression of Runx2 and regulating its activity. However, it inhibits cell proliferation and is critical for the differentiation process [213]. The role of ascorbic acid in the osteogenic medium is primarily attributed to the facilitation of collagen type 1 secretion. ß-glycerophosphate serves as a phosphate resource for bone mineral and induces osteogenic gene expression [214]. The newly formed HA nodules were labeled with OsteoImage staining (green fluorescence) and visualized under the fluorescence microscope. The ß-TCP/Silica-micro and Biosilica-micro

groups show intensive fluorescence on PLGA microspheres, compared to the control group and the silicatein group, indicating that silicate and biosilica accelerate the differentiation of osteoblasts and induce biomineralization. Orthosilicic acid can stimulate the synthesis of collagen type I and the differentiation of osteoblasts and induce the gene expression of alkaline phosphatase (ALP) and osteocalcin [105]. Biosilica has been found to induce an increased mineralization of osteogenic cells, and also displays a morphogenetic potential. After exposure to biosilica, osteoblasts increase strongly and significantly the expression of bone morphogenetic protein 2 (BMP-2) and alkaline phosphatase (ALP) [215]. The expression of bone markers (such as ALP, Col-I and osteocalcin) can promote an abundant mineralization [216]. As an early bone marker for cell osteogenic differentiation, the role of ALP in mineralization has been consistently solidified. Its function has been postulated to be as follows: 1) Increase of the local concentration of inorganic phosphate (a mineralization promoter); 2) Decrease of the extracellular pyrophosphate concentration (inhibitor of mineral formation) [217]. The potential mechanism for pyrophosphate as a mineralization inhibitor is to antagonize the ability of calcium to crystallize with phosphate to form hydroxyapatite as well as to bind strongly to the surface of hydroxyapatite crystals and to block further crystal growth [218]. Quantitative determination of the extent of mineralized calcium phosphate nodules was performed using the Alizarin Red S/Cetylpyridium chloride assay. It came out with a similar tendency of biomineralization, as shown in osteoimage staining assay. Taking ß-TCP microspheres and silicatein microspheres as references, ß-TCP/Silica-micro and Biosilica-micro groups significantly increase biomineralization.

Chapter V:
In vivo — Animal studies

5 *In vivo* – Animal studies

5.1 Operation and histological examination

5.1.1 Animal model and experimental groups

Animals used in the following experiment were housed in separate cages and provided with water and food *ad libitum*. The animal experiments were performed with female adult New Zealand White rabbits (weight 1.5 to 2.5 kg) according to the required guidelines. An artificially cylindrical bone defect of 5 mm in diameter and 5-7 mm in depth was created in the iliac crest of the two knees to achieve a bilateral comparison. The study involved three implantation materials: ß-TCP-micro (control), ß-TCP/Silica-micro and Biosilica-micro group, as described before. The detailed implantation plan is shown in Table 6. The left leg is filled with control group (ß-TCP-micro) and the right leg is filled with ß-TCP/Silica-micro or Biosilica-micro.

Table 6: Implantation plan with PLGA microspheres in rabbits

	Left leg	Right leg
Rabbit 1	ß-TCP-micro	ß-TCP/Silica-micro
Rabbit 2	ß-TCP-micro	ß-TCP/Silica-micro
Rabbit 3	ß-TCP-micro	ß-TCP/Silica-micro
Rabbit 4	ß-TCP-micro	Biosilica-micro
Rabbit 5	ß-TCP-micro	Biosilica-micro
Rabbit 6	ß-TCP-micro	Biosilica-micro

5.1.2 Surgery

All animal surgery procedures in this study follow the principles of laboratory animal care and use guidelines. Prior to operation, the animals were anesthetized with a 2:1 mixture of ketamine (ketavet) and zolazepam at the dose of 0.8-1.7 ml, initially intramuscularly, followed by intraperitioneal injection. The surgical area (both knees) was then shaved and sterilized, ready for surgery. Under strict aseptic conditions, cut the skin along the medial side of the knee (Fig. 5-1B). The tibia was slightly dislocated laterally and the femoral groove was exposed. A defect with a critical size of 5 mm × 5 mm was mechanically created in the sulcular groove using a surgical drill (Implatmed; W&H Dentalwerk, Bürmoos; Austria) with a

trephine (Diamond-Trephine Transfer Control Set; Meisinger, Neuss; Germany) supplemented with a room temperature physiological saline for irrigation to prevent thermal damage to surrounding bone and cartilage. According to the experimental plan, the microspheres were filled into the defect area by a press fit technique with the aid of a 1 ml syringe (Fig. 5-1B3). After insertion, the implants were gently pressed with a finger to force the microspheres to rigidly fit into the bone defect. The soft tissues were layered and closed with Vicryl 3-0 (Medelo, Kenn; Germany) reabsorbable sutures. Finally, antibiotic treatments were performed immediately after surgery. Each rabbit was kept in a cage, fed regularly, allowing unrestricted activities. After duration of 100 days, the animals were sacrificed by an excess of ketamine (200 mg per animal), the healing knees were harvested and fixed in 10 % buffered formalin for further analysis.

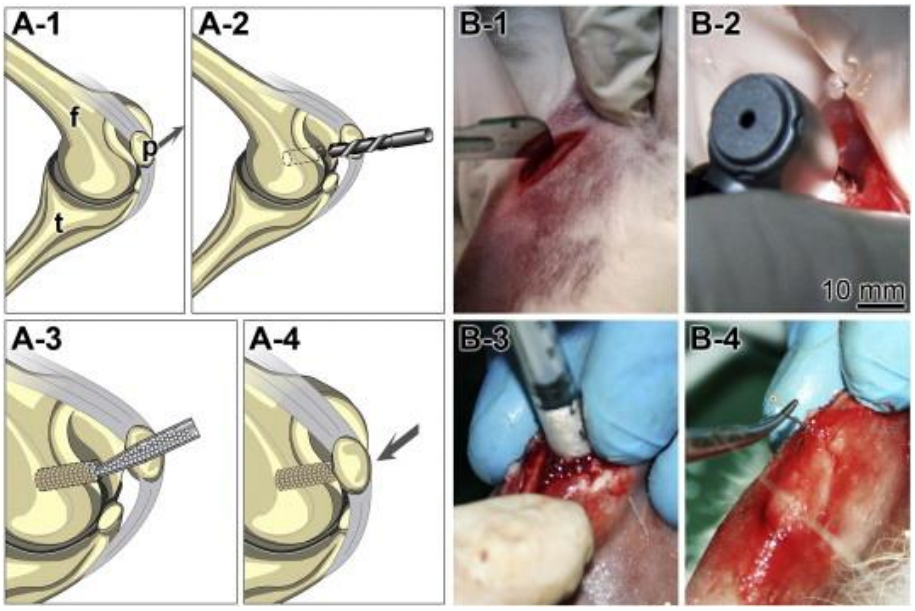

Fig. 5- 1. Surgery procedures in the anterior groove of the tibia: Creation of artificial bone defects and implantation of microspheres into the defects. (A) Schematic sketch; (B) Digital photos. (A-1, B-1) Remove the hair, sterilize the skin by iodophor and then cut the skin to get a median incision about 2 cm long; f: femur, t: tibia, P: patella. (A-2, B-2) Drill a defect of 5 mm in diameter and 5 mm in depth. (A-3, B-3) Fill the microspheres into the artificial defect. (A-4, B-4) Suture the periosteum and skin successively to close the incision. [81]

5.1.3 Microscopic evaluation of regenerated bone

The regenerated bone areas were labeled by administration of fluorochrome oxytetracycline (Alamycin LA 300; Norbrook Laboratories/Carnbane Industrial Estate, Newry, Down; UK) at a dose of 12 mg/kg once a week for the first four weeks and the last week prior to sacrification. This treatment was repeated again 48 h before euthanasia. Each specimen

was sliced into 300 µm thick sections by using a diamond saw microtone SP 1600 (Leica, Wetzlar; Germany). Meanwhile, all the sections were lightly wet-polished on a rotary polisher with 1 µm diamond particle abrasive (polishing system: LogitechWG2; MD-Dur, Struers, Willich; Germany). The visualization of regenerated bone was performed with a microscope Stemi 2000 (Zeiss, Oberkochen; Germany) under UV light with a black light filter (Dr. Hönle, Gräfelfing; Germany).

5.1.4 Mechanical property of the regenerated bone

The mechanical properties of the regenerated bone were measured by a newly developed ferrule-top nano-indenter which was described in section 1.2.2.2. The regenerated bone slice was fixed in a glass Petri dish with super glue and filled with PBS buffer to prevent dehydration during measurements. The probe was calibrated with polished metal in PBS. The mechanical properties of the regenerated bone were obtained with the following parameters. For each indentation, ten single indents were performed. The indentation process was depth controlled (maximum 10 µm depth). The loading time and unloading time were separately set at 2 s and 1 s. The holding time was kept to reach the maximum depth.

The glued bone slice was carefully place on the sample stage without touching the probe, and the sample stage was then moved to adjust the measurement area. The probe was brought close to the indent area with a distance of a few hundred micrometers by slowly rotating the coarse positioner knob in the clockwise direction. Then, the probe was finally moved and controlled by the z-piezoelectric translator at the rate of 1 µm/s until it contacts slightly with the measurement sample [49]. At the end of the process, indentation was performed according to the setting parameters previously by click the "Indent" button. The loading and unloading data were automatically recorded as the loading-displacement curve. Then, the reduced Young's modulus was calculated by Oliver-Pharr method [39].

5.1.5 Statistical analysis

The results were statistically evaluated using the data from triplicate samples in three independent experiments. They are presented as the means ± SD values. A comparison between the two samples was performed using Student's t-test. At $P \leq 0.05$, the difference was considered to be statistically significant.

5.2 Results

5.2.1 Fluorochrome labeled regenerated bone area

The newly formed bone was labeled with fluorochrome oxytetracyline (12 mg/Kg) once a week in the first month and at the last week prior to the sacrification. Oxytetracyline can form complexes with calcium from the newly mineralized tissue. These complexes are stable for a very long period until the mineralized tissue is desorbed by the osteoclasts. The bone sections were fluorescently photographed by a stereomicroscope Stemi 2000 (Zeiss, Oberkochen; Germany) under ultraviolet (UV) light and also under the normal light for comparison in order to identify the fluorescently labeled bone growth zones (Fig. 5-2). It was found that, after 100 days of regeneration, the artificial bone defect area was fully filled with newly formed bone-like tissue. There were no distinct boundaries between the original bone and newly formed bone. For the control group and the ß-TCP/Silica-micro group, most of the microspheres were still reserved and kept the original spherical morphology (Fig. 5-2A and C). For the biosilica group (ß-TCP/silica-silicatein-micro), most of the microspheres had lost their original spherical morphology (Fig. 5-2E). Clearly, over 50 % of the biosilica microspheres were degraded over 100 days. However, there was no obvious degradation in the ß-TCP-micro and the ß-TCP/Silica-micro group.

In the bright blue fluorescent images (Fig. 5- 2B, D and F), the trabecular bone structure, presenting a honeycomb morphology, in the newly formed tissue was observed (Fig. 5-2F). In contrast, in Fig. 5-2D, only the area along the original bone exhibits bright blue fluorescence. The core area of the defect is probably composed of extracellular matrix, missing the mineralization phase. In Fig. 5-2B, the defect area was not lighted up under ultraviolet light and shows few bluish fragments. Compared to the control (ß-TCP-micro, Fig. 5-2A and B) and the ß-TCP/Silica-micro group (Fig.5-2C and D), the biosilica group has new bone tissue formed and shows the re-mineralization process. The regenerated bone was grown into the centre of the defect and replaced the degraded microspheres. The images demonstrate that the Biosilica-micro group has much better regenerative potential for bone repair than the gold standard (control group) which is used in the hospital for patients. It is worth mentioning that in the present of biosilica/silicatein, the microspheres/implant materials are easier degraded and absorbed to promote new bone formation.

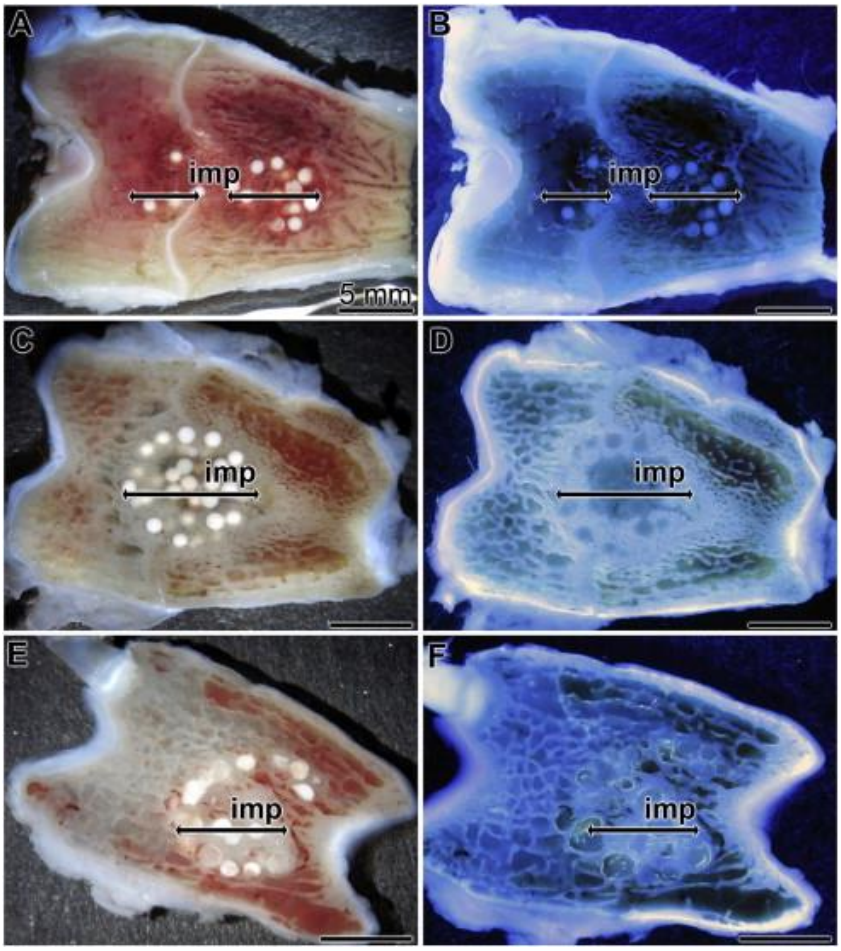

Fig. 5- 2. Fluorescent and normal images of labeled bone sections; left panel: images under normal light; right panel: fluorescent images under UV light. (A and B) Control group: ß-TCP-micro; (C and D) ß-TCP/silica-micro group; (E and F) Biosilica group: 1:1 mixture of ß-TCP/silica-micro and ß-TCP/silicatein-micro. imp means implanted region. Scale bar: 5 mm [81].

5.2.2 Mechanical property of regenerated bone

In order to evaluate the regenerative capacity of the test microspheres, the mechanical property of the regeneration area was determined with a newly developed indenter equipped with a glass probe, which is specially designed for determination of biological samples. Bone sections (300 µm thick) were glued in the glass Petri dish containing PBS buffer to prevent dehydration of the sections during the measurements. The measurement area can be visualized through the microscope conjugated to the probe (Fig. 5-3B). The mechanical properties of the trabecular bone tissue (tr-b), the regenerative bone area (re-b) and the adjacent area between microspheres were measured (Fig. 5-3A). Indentation area for the regenerated bone, which is located between the microspheres, was selected by a space of 30 µm. Then ten single indents were performed in one indentation area and at least ten indentation areas were selected for each section. Between the two indented areas, there was a minimum distance of 100 µm to minimize the interference effect. According to the rule

of nano-indentation, the distance between the two indents was at least 30 times the depth of the indentation (10 µm indent depth selected in our measurements). With reference to our bone slices, we have only limited indentation area between the microspheres, so we chose a distance of 100 µm between the two indent areas for our measurements. The reduced Young's modulus of the regenerated bone areas is presented as box plots in Fig. 5-3C. For healthy trabecular bone, the average value was 2.28 MPa as measured by the same nano-indenter. For the different test groups, the values of repaired areas change significantly. The lowest value was found in control group (ß-TCP-micro) with an average value of about 430 kPa. However, much higher values (over 1 MPa) were found in both ß-TCP/Silica-micro and Biosilica-micro. The biosilica group has the highest value, more close to the value of the natural bone.

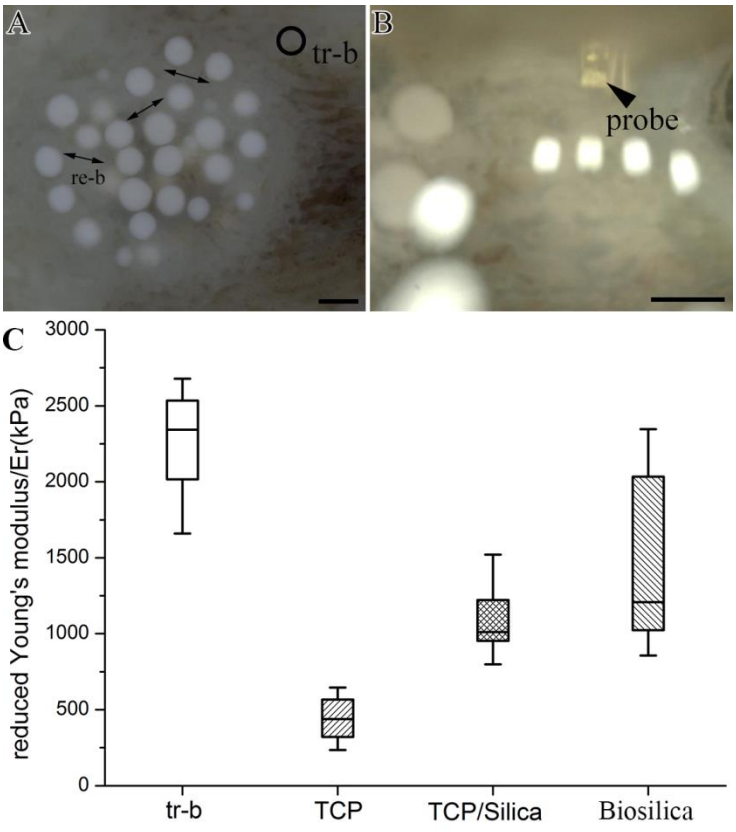

Fig. 5- 3. Reduced Young's modulus of bone defects repaired (re-b) and natural tribecular bone (tr-b) measured by nanoindenter with glass probes. (A) Digital photo of bone slices marked with indented areas (tr-b and re-b); (B) Photo taken by the microscope conjugated with the nanoindenter; (C) Box plot comparing the stiffness of natural trabecular bone and regenerated bone tissue.

5.3 Discussion

The ultimate goal of bone tissue engineering is to develop functional bone grafts that meet clinical needs and enhance bone regeneration, thereby improving the life quality of the

patients. In the last chapter, the *in vitro* biocompatibility of biosilica microspheres has been evaluated. PLGA-biosilica microspheres developed by us show no toxicity to the cells under cell culture conditions, while they induce proliferation and biomineralitation of osteoblasts. In order to further demonstrate the potential of microspheres to promote bone regeneration, *in vivo* studies were performed to understand the interaction between the microspheres and the natural bone tissue, since preclinical testing of animal models is an important part of the regulatory process. It is the keystep of preclinical development of transformational technologies [219]. For animal test, choosing a suitable animal model similar to human bone biology and repair is critical, and certain rules must be considered, as summarized in some reviews [220–222]. Animals are generaly available as dog, sheep, goat, pig, rabbit and rats. They are often used as animal models for evaluating the regeneration and repair potential of bone implants [220,222]. Among them, small animals (mouse, rats and rabbits) are easier to handle and house, and have much lower maintenance cost than large animals [223]. Therefore, small animals are often used to evaluate the biocompatibility, biodegradability, osteointegration, osteoconductivity, as well as osteoinductive and osteogenic potential of the bone implants engineered *in vivo*. It is reported that there is a similarity of bone density and fracture toughness between rabbit bone and human bone [224]. Large animals, such as dogs, sheep, goats and pigs, are better predictors of human response [225]. So, they are required for preclinical prevention and intervention studies [226].

Rabbits are one of the most commonly used animals for screening implant materials prior to testing in larger animal models [220]. This model is typically used to bridge the gap between small animal models (mice and rats) in the discovery phase of research and large animal models (dogs, pigs and sheep) for preclinical and translational research. Rabbits are phylogenetically closer to primates and provide a more diverse genetic background, which brings rabbits closer to human. To date, rabbits have been used as experimental animal models for atherosclerosis, Alzheimer's disease, ophthalmology, studies of osteoarthritis and tuberculosis [220,227,228]. Among the various strains, New Zealand white breed rabbits are commonly used because they are less invasive in nature and have fewer health problems [229]. The ideal implantation site for the rabbits should be the proximal femoral condyle, providing adequate space for implantation. The medial and lateral femoral condyles can also be implanted, but have a risk of injury to the nerves and tendons [229]. In this study, the implantation site was the anterior patellar groove, which is located between the medial and

laterial femoral condyles. The patellar groove is often taken as a standardized *in vivo* systems to investigate osseointegration of implants [230]. This model is also often used to study the repair and regeneration of focal cartilage defects [228]. The condyles of mature female New Zealand white rabbits is thick enough to create a full thickness cartilage defect for the study of chondral repair and regeneration [231].

The critical size of artificial cylindrical bone defects with a diameter of 5 mm and a length of 5-7 mm was drilled with a surgical drill on both legs. According to the definition, a critical size defect (CSD) is the smallest size tissue defect that does not completely heal during the natural life of the animal [219]. The bones have the self-healing property and can repair fractures and bruises during bone remodeling and resorption. However, for larger bone defects, if there is no bone grafts, the bones cannot be completely rebuilt. Only the bone graft is used as a filler and a scaffold to induce and promote bone formation. The size of the critical bone defect depends on the specific animal model and anatomic site. For the cavdel model, for rats, rabbits, dogs, goats and sheep, the critical sizes of defects should be 5-8 mm, 15 mm, 21-25 mm, 25-36 mm and 25-30 mm in diameter, respectively [232]. A critical size osteochondral defect was defined as 1.4 mm in diameter for rat model and 5 mm for rabbit model.

Assessing the regeneration area is a key step in estimation of the osteoconductive and osteoinductive capabilities of different PLGA microspheres. Common methods for the evaluation of newly formed bone are histological analysis, micro computed tomography (micro-CT), mechanical testing, radiography analysis, sequential fluorescence labeling and dynamic contrast-enhanced magnetic resonance imaging [224]. Dynamic bone labeling has become the gold standard technique for quantitative measurement of bone formation and bone remodeling *in vivo* [233]. In this study, fluorescence labeling and mechanical testing were selected to assess newly formed bone from different implants. Fluorochromes for bone labeling are calcium-seeking substances that are preferentially bound to the sites of newly mineralized tissue by chelation with calcium. However, this chelation effect is only applicable to the calcium site on the surface of newly formed apatite crystals. The reason could be that the apatite crystal size is smaller at the initial stage of mineralization. Another advantage of the fluorescence labeling technique is the stability of its fluorochrome-apatite complex, which is not released until the fluorochrome labeled bone matrix is resorbed. Commonly used fluorochromes are tetracycline (blue fluorescence), calcein (green fluorescence),

alizarins (red fluorescence) and xylenol orange (orange or red fluorescence). In our experiments, the fluorochrome oxytetracycline was used to continuously label the newly formed mineralized tissue to monitor the bone regeneration process. Typically, multiple labels are performed at different time points [234]. In addition, the mechanical properties of applied bone implants are important for the evaluation of cell micro-environments. Furthermore, the mechanical properties of regenerated bone are important for the evaluation of bone regeneration. During the regeneration process, the PLGA microspheres are degraded and provide space for the ingrowth of cells to generate organic matrix and further mineralization. Generally, the mechanical properties of bone are positively correlated with the content of mineral. The higher mineralization of organic matrix increases the stiffness of newly formed bone tissue [235]. The nanoindentation technique is widely applied in the field of biomedicine. The Young's modulus and hardness of small and thin specimens can be measured, even for the nano-scale tissue [236].

After 100 days of implantation, all groups showed incomplete osteointegration. The residual microspheres stayed in the newly formed tissue and show optimal reactivity with the surrounding tissue. This confirms that the PLGA microspheres are biocompatible and do not interfere with new bone formation. PLGA is one of the most fascinating biodegradable biomaterials in bone tissue engineering and has been proven by the U. S. Food and Drug Administration (FDA) for clinical use [237]. And a large number of studies have reported that ß-TCP has excellent biocompatibility and osteoconductivity, supporting cell attachment, proliferation and differentiation [238]. The use of additional ß-TCP increases the roughness of the PLGA microspheres and provides a favorable surface for cell attachment. As an alkaline substance, ß-TCP can also reduce inflammations by neutralizing acid molecules produced by PLGA degradation [238,239]. Both biosilica and silicatein are not cytotoxic to cells, and strongly induce osteoblasts to deposit biominerals *in vitro*.

For all groups, the PLGA microspheres were partially degraded and embedded in the organic matrix. However, the PLGA microspheres (Biosilica group; Fig. 5-2E) which is significantly degraded compared to the control group, lose their original spherical morphology [240]. This phenomenon can be facilitated by the rapid degradation of ß-TCP/Silicatein-micro and the improvement of cellular metabolic activity induced by biosilica formation. Due to the porous structure, the degradation of ß-TCP/Silicatein-micro is much faster than that of ß-TCP-micro and ß-TCP/Silica-micro. This was proved by the incubation of

all PLGA microspheres in serum for 100 days. It is assumed that the released silicatein from microspheres catalyze the polycondensation of silicate to biosilica *in vivo*. Biosilica, formed by released silicate and silicatein, would increase the metabolic activity of the surrounding cells and induce stem cells to differentiate into osteoblasts to build up new bone. Biosilica has an inducing effect on the expression of key regulators of osteogenesis, BMP-2 and osteoprotegerin [241]. Increased cellular metabolic activity will accelerate PLGA hydrolysis and rapidly transfer degradation products to the tricarboxylic acid cycle (TCA). Under UV light, the regeneration areas were lighted up in bluish, with a different morphological texture. The regenerated tissue showed lower values for the Young's modulus and hardness than the intact tissue since the biomineralization process of newly formed bone has not yet been completed and there are different contents of collagen fibers and hydroxyapatite crystals [236]. However, the regenerated area from biosilica group has a highest reduced Young's modulus of 1450 KPa, indicating that the regeneration potential of biosilica microspheres is much higher than the gold standard ß-TCP used in clinical applications. Therefore, it will be a promising biomaterial for bone regeneration.

CONCLUSION:

In this study, I modified the double emulsion method (solvent/non-solvent method) and prepared PLGA microspheres with a uniform particle size. Then, three-dimensional scaffolds were fabricated based on the PLGA microspheres. Afterwards, the physical and chemical properties as well as the biocompatibility of the PLGA microspheres and the porous scaffolds formed from them were investigated. The results can be summarized as follows:

1) The traditional double emulsion method for the preparation of the PLGA microspheres was modified. I used a syringe pump to control the dropping rate of the emulsion and an electronic stirrer to control the rate of formation of the PLGA microspheres. Under this dual control, large and uniform PLGA microspheres could be fabricated. The PLGA microspheres have a diameter of about 700 µm to 800 µm.

2) The active ingredients (ß-TCP, silicate substrate and silicatein) encapsulated in the PLGA microspheres were qualitatively and quantitatively determined by dissolving the PLGA polymer shell with DCM. Their concentrations in the various microsphere groups are listed in Table 5.

3) In order to maintain the original morphology of the microspheres and the mechanical properties of the sintered porous scaffolds, a bio-linker consisting of solvent (75 % NMP) and non-solvent (water) with a ratio of 3:1 turned out to be optimal as determined in a series of experiments.

4) The morphology and porous structure of microspheres were visualized by scanning electron microscopy (SEM). The chemical components of the PLGA microspheres were determined by EDX. The appearance of the Si Kα peak in the spectrum proved that the substrate silicate was indeed encapsulated into the microspheres.

5) *In vitro* release assays of silicate and silicatein were performed at 37 ^{o}C for one month. The cumulative release percentage of silicate and silicatein slowly reached 40 % and 55 %, respectively. There was no sudden release of silicate and silicatein. This suggests that if the scaffolds are implanted in human body, the release of silicate and silicatein will be slow

and occur continuously to form biosilica and induce bone formation during the regeneration process.

6) When the microsphere-based scaffolds were placed in PBS, the uptake of water and swelling were stabilized after 12h. It complies with the general standards for biological materials in tissue engineering.

7) Direct and indirect MTT assays showed that the biosilica microspheres and the scaffolds are not toxic. In contrast, biosilica microspheres induced the proliferation and differentiation of SaOS-2 cells, as well as mineralization on their surface, indicating that biosilica microspheres and their scaffolds have good biocompatibility. They can be used as bone regeneration materials.

8) *In vivo* animal studies were performed in female adult New Zealand rabbits for 100 days. Compared to the control group where most of the microspheres remained in the defects after 100 days, most of the microspheres of the biosilica group (ß-TCP/silica-silicatein-micro) was degraded and replaced by the newly formed bone. Furthermore, the mechanical properties of the newly formed bone tissue in the biosilica group are very close to the mechanical properties of natural bone.

In summary, chemical, physical and biochemical studies performed in this study have shown that biosilica-microsphere-based scaffolds have a good biocompatibility and can effectively control the release of silicate and silicatein, thereby inducing bone regeneration. Using this material, bone regeneration can be achieved without the addition of growth factors and stem cells. Therefore, this material is a promising implant material in bone tissue engineering and has a very broad range of applications.

FUTURE WORK:

Tissue-inducing biomaterials (without adding live cells and growth factors) will be the first choice of tissue engineering for applications due to their low cost, easy production, and because they are without ethical issues.

A new physiological polymer, polyphosphate (polyP; amorphous micro-particles), consisting of long chains (tens to hundreds) of phosphate units linked by high-energy phosphoanhydride bonds, recently discovered by our group which acts both as a structural/mechanical element in the implants and simultaneously as a morpho-active biomaterials, eliciting distinct signals to attract MSCs and stimulate them to proliferate, differentiate and migrate into the scaffolds because polyP provides an extracellular system for the production of metabolic energy and mono-phosphate needed for bone formation *via* the function of alkaline phosphatase (ALP). That is to say, polyP-based biomaterials have truly regenerative activities.

Therefore, in addition to biosilica, the inducer of bone regeneration, polyP, as the provider of substrate and energy needed for bone formation, should also be encapsulated in PLGA microspheres to fabricate bone scaffolds. By adding mophorgenetically active bio-polymers, biosilica and polyP, novel tissue-inducing and regenerative active scaffolds can be prepared to accelerate bone regeneration, benefiting an aging society by reducing of pain and suffering – increasing mobility of patients. This will definitely improve the quality of life of patients in society.

REFERENCES:

[1] D.G. Steele, C.A. Bramblett, The anatomy and biology of the human skeleton, Texas A&M University Press, 1988.

[2] D.J. Hadjidakis, I.I. Androulakis, Bone remodeling, Ann. N. Y. Acad. Sci. 1092 (2006) 385–396.

[3] B. Clarke, Normal bone anatomy and physiology, Clin. J. Am. Soc. Nephrol. 3 (2008) S131–S139.

[4] I. Fogelman, G. Gnanasegaran, H. van der Wall, Radionuclide and hybrid bone imaging, Springer, 2012.

[5] E. Beniash, Biominerals-hierarchical nanocomposites: the example of bone, Wiley Interdiscip. Rev. Nanomed. Nanobiotechnol. 3 (2011) 47–69.

[6] A. Kohutová, P. Honcová, L. Svoboda, P. Bezdička, M. Maříková, Structural characterization and thermal behaviour of biological hydroxyapatite, J. Therm. Anal. Calorim. 108 (2012) 163–170.

[7] B. Wopenka, J.D. Pasteris, A mineralogical perspective on the apatite in bone, Mater. Sci. Eng. C 25 (2005) 131–143.

[8] A. Bigi, G. Cojazzi, S. Panzavolta, A. Ripamonti, N. Roveri, M. Romanello, K.N. Suarez, L. Moro, Chemical and structural characterization of the mineral phase from cortical and trabecular bone, J. Inorg. Biochem. 68 (1997) 45–51.

[9] H. Ivankovic, E. Tkalcec, S. Orlic, G. Gallego Ferrer, Z. Schauperl, Hydroxyapatite formation from cuttlefish bones: kinetics, J. Mater. Sci. Mater Med. 21 (2010) 2711–2722.

[10] W.E.G. Müller, H.C. Schröder, U. Schlossmacher, V.A. Grebenjuk, H. Ushijima, X.H. Wang, Induction of carbonic anhydrase in SaOS-2 cells, exposed to bicarbonate and consequences for calcium phosphate crystal formation, Biomaterials 34 (2013) 8671–8680.

[11] X.H. Wang, H.C. Schröder, W.E.G. Müller, Biocalcite, a multifunctional inorganic polymer: building block for calcareous sponge spicules and bioseed for the synthesis of calcium phosphate-based bone, Beilstein J. Nanotechnol. 5 (2014) 610–621.

[12] H. Ding, H. Pan, X. Xu, R. Tang, Toward a detailed understanding of magnesium ions on hydroxyapatite crystallization inhibition, Cryst. Growth Des. 14 (2014) 763–769.

[13] Y. Tang, H.F. Chappell, M.T. Dove, R.J. Reeder, Y.J. Lee, Zinc incorporation into hydroxylapatite, Biomaterials 30 (2009) 2864–2872.

[14] J. Kolmas, A. Jaklewicz, A. Zima, M. Bućko, Z. Paszkiewicz, J. Lis, A. Ślósarczyk, W. Kolodziejski, Incorporation of carbonate and magnesium ions into synthetic hydroxyapatite: the effect on physicochemical properties, J. Mol. Struct. 987 (2011) 40–50.

[15] V. Aina, G. Lusvardi, B. Annaz, I.R. Gibson, F.E. Imrie, G. Malavasi, L. Menabue, G. Cerrato, G. Martra, Magnesium- and strontium-co-substituted hydroxyapatite: the effects of doped-ions on the structure and chemico-physical properties, J. Mater. Sci.-Mater. Med. 23 (2012) 2867–2879.

[16] W.T. Dempster, The anthropometry of body action, Ann. N.Y. Acad. Sci. 63 (1955) 559–585.

[17] T.A. Linkhart, S. Mohan, D.J. Baylink, Growth factors for bone growth and repair: IGF, TGFβ and BMP, Bone 19 (1996) S1–S12.

[18] J.A. Buckwalter, M.J. Glimcher, R.R. Cooper, R. Recker, Bone biology I: structure, blood supply, cells, matrix, and mineralization, Instr. Course Lect. 45 (1996) 371–386.

[19] J.Y. Rho, L. Kuhn-Spearing, P. Zioupos, Mechanical properties and the hierarchical structure of bone, Med. Eng. Phys. 20 (1998) 92–102.
[20] A.K. Nair, A. Gautieri, S.-W. Chang, M.J. Buehler, Molecular mechanics of mineralized collagen fibrils in bone, Nat. Commun. 4 (2013) 1724.
[21] M.J. Olszta, X. Cheng, S.S. Jee, R. Kumar, Y.Y. Kim, M.J. Kaufman, E.P. Douglas, L.B. Gower, Bone structure and formation: a new perspective, Mater. Sci. Eng. R Rep. 58 (2007) 77–116.
[22] R. Florencio-Silva, G.R. da S. Sasso, E. Sasso-Cerri, M.J. Simões, P.S. Cerri, Biology of bone tissue: structure, function, and factors that influence bone cells, BioMed Res. Int. 2015 (2015) 1–17.
[23] Y. Imai, M.-Y. Youn, K. Inoue, I. Takada, A. Kouzmenko, S. Kato, Nuclear receptors in bone physiology and diseases, Physio. Rev. 93 (2013) 481–523.
[24] H.C. Blair, Q.C. Larrouture, Y. Li, H. Lin, D. Beer-Stoltz, L. Liu, R.S. Tuan, L.J. Robinson, P.H. Schlesinger, D.J. Nelson, Osteoblast differentiation and bone matrix formation *in vivo* and *in vitro*, Tissue Eng. Part B Rev. 23 (2017) 268–280.
[25] M. Tavafoghi, M. Cerruti, The role of amino acids in hydroxyapatite mineralization, J. R. Soc. Interface 13 (2016) 20160462.
[26] M. Pereira, E. Petretto, S. Gordon, J.H.D. Bassett, G.R. Williams, J. Behmoaras, Common signalling pathways in macrophage and osteoclast multinucleation, J. Cell. Sci. 131 (2018) jcs216267.
[27] H.K. Väänänen, Y. Liu, P. Lehenkari, T. Uemara, How do osteoclasts resorb bone?, Mater. Sci. Eng. C 6 (1998) 205–209.
[28] M.B. Schaffler, W.-Y. Cheung, R. Majeska, O. Kennedy, Osteocytes: master orchestrators of bone, Calcif. Tissue Int. 94 (2014) 5–24.
[29] S.C. Miller, W.S. Jee, The bone lining cell: a distinct phenotype?, Calcif. Tissue Int. 41 (1987) 1–5.
[30] S. Weiner, H.D. Wagner, The material bone: structure-mechanical function relations, Annu. Rev. Mater. Sci. 28 (1998) 271–298.
[31] R.O. Ritchie, The conflicts between strength and toughness, Nat. Mater. 10 (2011) 817–822.
[32] G.M. Pharr, W.C. Oliver, Measurement of thin film mechanical properties using nanoindentation, MRS Bull. 17 (1992) 28–33.
[33] D.M. Ebenstein, L.A. Pruitt, Nanoindentation of biological materials, Nano Today 1 (2006) 26–33.
[34] U. Ramamurty, J. Jang, Nanoindentation for probing the mechanical behavior of molecular crystals–a review of the technique and how to use it, CrystEngComm 16 (2014) 12–23.
[35] D. Newey, M.A. Wilkins, H.M. Pollock, An ultra-low-load penetration hardness tester, J. Phys. E Sci. Instrum. 15 (1982) 119.
[36] B. Poon, D. Rittel, G. Ravichandran, An analysis of nanoindentation in linearly elastic solids, Int. J. Solids Struc. 45 (2008) 6018–6033.
[37] D.A. Lucca, K. Herrmann, M.J. Klopfstein, Nanoindentation: measuring methods and applications, CIRP Ann. Manuf. Technol. 59 (2010) 803–819.
[38] L. Qian, H. Zhao, Nanoindentation of soft biological materials, Micromachines 9 (2018) 654.
[39] W.C. Oliver, G.M. Pharr, An improved technique for determining hardness and elastic modulus using load and displacement sensing indentation experiments, J. Mater. Res. 7 (1992) 1564–1583.

[40] W.C. Oliver, G.M. Pharr, Measurement of hardness and elastic modulus by instrumented indentation: advances in understanding and refinements to methodology, J. Mater. Res. 19 (2004) 3–20.
[41] A.C. Fischer-Cripps, Nanoindentation, Springer New York, NY, 2011.
[42] J.A. Last, P. Russell, P.F. Nealey, C.J. Murphy, The applications of atomic force microscopy to vision science, Investig. Ophthalmol. Vis. Sci. 51 (2010) 6083–6094.
[43] V. Králík, J. Němeček, Comparison of nanoindentation techniques for local mechanical quantification of aluminium alloy, Mater. Sci. Eng. A 618 (2014) 118–128.
[44] R.C. Paietta, S.E. Campbell, V.L. Ferguson, Influences of spherical tip radius, contact depth, and contact area on nanoindentation properties of bone, J. Biomech. 44 (2011) 285–290.
[45] J. Mencík, Mechanics of components with treated or coated surfaces, Springer Science & Business Media, 2013.
[46] N. (Mohan) Ranganathan, Materials characterization: modern methods and applications, CRC Press, 2016.
[47] K.L. Johnson, Contact mechanics, Cambridge University Press, Cambridge, New York, 1985.
[48] L. Zheng, A.W. Schmid, J.C. Lambropoulos, Surface effects on Young's modulus and hardness of fused silica by nanoindentation study, J. Mater. Sci. 42 (2007) 191–198.
[49] D. Chavan, T.C. van de Watering, G. Gruca, J.H. Rector, K. Heeck, M. Slaman, D. Iannuzzi, Ferrule-top nanoindenter: an optomechanical fiber sensor for nanoindentation, Rev. Sci. Instrum. 83 (2012)
[50] S.S. Meysami, P. Dallas, J. Britton, J.G. Lozano, A.T. Murdock, C. Ferraro, E.S. Gutierrez, N. Rijnveld, P. Holdway, K. Porfyrakis, N. Grobert, Ultra-stiff large-area carpets of carbon nanotubes, Nanoscale 8 (2016) 11993–12001.
[51] P.R. Moshtagh, B. Pouran, N.M. Korthagen, A.A. Zadpoor, H. Weinans, Guidelines for an optimized indentation protocol for measurement of cartilage stiffness: the effects of spatial variation and indentation parameters, J. Biomech. 49 (2016) 3602–3607.
[52] M.L. Oyen, Handbook of nanoindentation with biological applications, Pan Stanford Publ, Singapore, 2011.
[53] E.D. Hintsala, U. Hangen, D.D. Stauffer, High-throughput nanoindentation for statistical and spatial property determination, JOM 70 (2018) 494–503.
[54] J.D. Currey, Bones: structure and mechanics, Princeton university press, 2002.
[55] S. Hengsberger, A. Kulik, P. Zysset, Nanoindentation discriminates the elastic properties of individual human bone lamellae under dry and physiological conditions, Bone 30 (2002) 178–184.
[56] J.L. Cuy, A.B. Mann, K.J. Livi, M.F. Teaford, T.P. Weihs, Nanoindentation mapping of the mechanical properties of human molar tooth enamel, Arch. Oral Biol. 47 (2002) 281–291.
[57] T. Sumitomo, H. Kakisawa, Y. Kagawa, Nanoscale structure and mechanical behavior of growth lines in shell of abalone Haliotis gigantea, J. Struct. Biol. 174 (2011) 31–36.
[58] R. Akhtar, N. Schwarzer, M.J. Sherratt, R.E.B. Watson, H.K. Graham, A.W. Trafford, P.M. Mummery, B. Derby, Nanoindentation of histological specimens, J. Mater. Res. 24 (2009) 638–646.
[59] W.E.G Müller, H.C. Schröder, X.H. Wang, The understanding of the metazoan skeletal system, based on the initial discoveries with siliceous and calcareous sponges, Mar. Drugs. 15 (2017) 172.
[60] N. Poulsen, M. Sumper, N. Kröger, Biosilica formation in diatoms: characterization of

native silaffin-2 and its role in silica morphogenesis, Proc. Natl. Acad. Sci. USA 100 (2003) 12075–12080.

[61] S.F. Wang, X.H. Wang, L. Gan, M. Wiens, H.C. Schröder, W.E.G. Müller, Biosilica-glass formation using enzymes from sponges [silicatein]: basic aspects and application in biomedicine [bone reconstitution material and osteoporosis], Front. Mater. Sci. 5 (2011) 266–281.

[62] A. Miserez, J.C. Weaver, P.J. Thurner, J. Aizenberg, Y. Dauphin, P. Fratzl, D.E. Morse, F.W. Zok, Effects of laminate architecture on fracture resistance of sponge biosilica: Lessons from nature: effects of laminate architecture on fracture resistance of biosilica, Adv. Funct. Mater. 18 (2008) 1241–1248.

[63] W.E.G. Müller, X.H. Wang, M. Wiens, U. Schloßmacher, K.P. Jochum, H.C. Schröder, Hardening of bio-silica in sponge spicules involves an aging process after its enzymatic polycondensation: evidence for an aquaporin-mediated water absorption, Biochim. Biophys. Acta Gen. Subj. 1810 (2011) 713–726.

[64] H.C. Schröder, X.H. Wang, A. Manfrin, S.H. Yu, V.A. Grebenjuk, M. Korzhev, M. Wiens, U. Schlossmacher, W.E.G. Müller, Acquisition of structure-guiding and structure-forming properties during maturation from the pro-silicatein to the silicatein form, J. Biol. Chem. 287 (2012) 22196–22205.

[65] I. Zlotnikov, D. Shilo, Y. Dauphin, H. Blumtritt, P. Werner, E. Zolotoyabko, P. Fratzl, *In situ* elastic modulus measurements of ultrathin protein-rich organic layers in biosilica: towards deeper understanding of superior resistance to fracture of biocomposites, RSC Adv. 3 (2013) 5798.

[66] W.E.G. Müller, X.H Wang, K.P. Jochum, H.C. Schröder, Self-healing, an intrinsic property of biomineralization processes, IUBMB Life 65 (2013) 382–396.

[67] D. Losic, K. Short, J.G. Mitchell, R. Lal, N.H. Voelcker, AFM nanoindentations of diatom biosilica surfaces, Langmuir 23 (2007) 5014–5021.

[68] J. Lu, C. Sun, Q.J. Wang, Mechanical simulation of a diatom frustule structure, J. Bionic Eng. 12 (2015) 98–108.

[69] M.D. Moreno, K. Ma, J. Schoenung, L.P. Dávila, An integrated approach for probing the structure and mechanical properties of diatoms: toward engineered nanotemplates, Acta Biomater. 25 (2015) 313–324.

[70] Z.H. Aitken, S. Luo, S.N. Reynolds, C. Thaulow, J.R. Greer, Microstructure provides insights into evolutionary design and resilience of Coscinodiscus sp. frustule, Proc. Natl. Acad. Sci. USA 113 (2016) 2017–2022.

[71] Joanna Aizenberg, James C. Weaver, Monica S. Thanawala, Vikram C. Sundar, Daniel E. Morse, Peter Fratzl, Skeleton of euplectella sp: structural hierarchy from the nanoscale to the macroscale, Science 309 (2005) 272–275.

[72] J D.Currey, Hierarchies in biomineral structures, Science 309 (2005) 252–253.

[73] P.K. Zysset, X. Edward Guo, C. Edward Hoffler, K.E. Moore, S.A. Goldstein, Elastic modulus and hardness of cortical and trabecular bone lamellae measured by nanoindentation in the human femur, J. Biomech. 32 (1999) 1005–1012.

[74] S. Habelitz, G.W. Marshall, M. Balooch, S.J. Marshall, Nanoindentation and storage of teeth, J. Biomech. 35 (2002) 995–998.

[75] A.J. Bushby, V.L. Ferguson, A. Boyde, Nanoindentation of bone: comparison of specimens tested in liquid and embedded in polymethylmethacrylate, J. Mater. Res. 19 (2004) 249–259.

[76] G. Balooch, G.W. Marshall, S.J. Marshall, O.L. Warren, S.A.S. Asif, M. Balooch, Evaluation of a new modulus mapping technique to investigate microstructural

features of human teeth, J. Biomech. 37 (2004) 1223–1232.
[77] N. Rodriguez-Florez, M.L. Oyen, S.J. Shefelbine, Insight into differences in nanoindentation properties of bone, J. Mech. Behav. Biomed. Mater. 18 (2013) 90–99.
[78] K.J. Chun, H.H. Choi, J.Y. Lee, Comparison of mechanical property and role between enamel and dentin in the human teeth, J. Dent. Biomech. 5 (2014) 1758736014520809.
[79] J.Y. Rho, R.B. Ashman, C.H. Turner, Young's modulus of trabecular and cortical bone material: Ultrasonic and microtensile measurements, J. Biomech. 26 (1993) 111–119.
[80] D.M. Ebenstein, A. Kuo, J.J. Rodrigo, A.H. Reddi, M. Ries, L. Pruitt, A nanoindentation technique for functional evaluation of cartilage repair tissue, J. Mater. Res. 19 (2004) 273–281.
[81] O. Franke, K. Durst, V. Maier, M. Göken, T. Birkholz, H. Schneider, F. Hennig, K. Gelse, Mechanical properties of hyaline and repair cartilage studied by nanoindentation, Acta Biomater. 3 (2007) 873–881.
[82] R. Vayron, E. Barthel, V. Mathieu, E. Soffer, F. Anagnostou, G. Haiat, Variation of biomechanical properties of newly formed bone tissue determined by nanoindentation as a function of healing time, Comput. Methods Biomech. Biomed. Engin. 14 (2011) 139–140.
[83] R. Vayron, E. Barthel, V. Mathieu, E. Soffer, F. Anagnostou, G. Haiat, Nanoindentation measurements of biomechanical properties in mature and newly formed bone tissue surrounding an implant, J. Biomech. Eng. 134 (2012) 021007-021007–6.
[84] S.F. Wang, X.H. Wang, F.G. Draenert, O. Albert, H.C. Schröder, V. Mailänder, G. Mitov, W.E.G. Müller, Bioactive and biodegradable silica biomaterial for bone regeneration, Bone 67 (2014) 292–304.
[85] W.E.G. Müller, E. Tolba, M. Ackermann, M. Neufurth, S.F. Wang, Q. Feng, H.C. Schröder, X.H. Wang, Fabrication of amorphous strontium polyphosphate microparticles that induce mineralization of bone cells *in vitro* and *in vivo*, Acta Biomater. (2016).
[86] D.M. Ebenstein, L.A. Pruitt, Nanoindentation of soft hydrated materials for application to vascular tissues, J. Biomed. Mater. Res A. 69A (2004) 222–232.
[87] R. Akhtar, N. Schwarzer, M.J. Sherratt, R.E.B. Watson, H.K. Graham, A.W. Trafford, P.M. Mummery, B. Derby, Nanoindentation of histological specimens: mapping the elastic properties of soft tissues, J. Mater. Res. 24 (2009) 638–646.
[88] M. Unal, A. Creecy, J.S. Nyman, The role of matrix composition in the mechanical behavior of bone, Curr. Osteoporos. Rep. 16 (2018) 205–215.
[89] D.M. Ebenstein, L.A. Pruitt, Nanoindentation of biological materials, Nano Today 1 (2006) 26–33.
[90] R.R. Crichton, Biological inorganic chemistry: a new introduction to molecular structure and function, Academic Press, 2018.
[91] Z.Q. Jia, Z.X. Guo, F. Chen, J.J. Li, L. Zhao, L. Zhang, Microstructure, phase compositions and *in vitro* evaluation of freeze casting hydroxyapatite-silica scaffolds, Ceram. Int. 44 (2018) 3636–3643.
[92] E. Epstein, The anomaly of silicon in plant biology, Proc. Natl. Acad. Sci. USA 91 (1994) 11–17.
[93] J.P. Bellia, J.D. Birchall, N.B. Roberts, Beer: a dietary source of silicon, The Lancet 343 (1994) 235.
[94] S. Sripanyakorn, R. Jugdaohsingh, H. Elliott, C. Walker, P. Mehta, S. Shoukru, R.P.H.

Thompson, J.J. Powell, The silicon content of beer and its bioavailability in healthy volunteers, Br. J. Nutr. 91 (2004) 403.

[95] K. Szurkowska, J. Kolmas, Hydroxyapatites enriched in silicon – Bioceramic materials for biomedical and pharmaceutical applications, Prog. Nat. Sci-Mater. 27 (2017) 401–409.

[96] W. Mertz, Trace elements in human and animal nutrition (Fifth Edition), Academic Press, San Diego, 1986: pp. 373–390.

[97] K. Van Dyck, H. Robberecht, R. Van Cauwenbergh, V. Van Vlaslaer, H. Deelstra, Indication of silicon essentiality in humans, Biol. Trace Elem. Res. 77 (2000) 25–32.

[98] R. Jugdaohsingh, S.H. Anderson, K.L. Tucker, H. Elliott, D.P. Kiel, R.P. Thompson, J.J. Powell, Dietary silicon intake and absorption, Am. J. Clin. Nutr. 75 (2002) 887–893.

[99] R. Jugdaohsingh, Silicon and bone health, J. Nutr Health. Aging. 11 (2007) 99.

[100] R. Jugdaohsingh, S. Sripanyakorn, J.J. Powell, Silicon absorption and excretion is independent of age and sex in adults, Br. J. Nutr. 110 (2013) 1024–1030.

[101] G.E. Abraham, The importance of bioactive silicates in human health, Origin. Internist. Spring. (2005) 13–19.

[102] P. Aggett, R. Crebelli, B. Dusemund, M. Filipič, M.J. Frutos, P. Galtier, D. Gott, U. Gundert-Remy, G.G. Kuhnle, J. Leblanc, I.T. Lillegaard, P. Moldeus, A. Mortensen, A. Oskarsson, I. Stankovic, I. Waalkens-Berendsen, R.A. Woutersen, M. Wright, P. Boon, D. Chrysafidis, R. Gürtler, P. Mosesso, D. Parent-Massin, P. Tobback, N. Kovalkovicova, A.M. Rincon, A. Tard, C. Lambré, Re-evaluation of silicon dioxide (E 551) as a food additive, EFSA Journal 16 (2018): 5008, 70pp

[103] E.M. Carlisle, Silicon: an essential element for the chick, Science 178 (1972) 619–621.

[104] K. Schwarz, D.B. Milne, Growth-promoting effects of silicon in rats, Nature 239 (1972) 333–334.

[105] D. Reffitt, N. Ogston, R. Jugdaohsingh, H.F. Cheung, B.A. Evans, R.P. Thompson, J. Powell, G. Hampson, Orthosilicic acid stimulates collagen type 1 synthesis and osteoblastic differentiation in human osteoblast-like cells *in vitro*, Bone 32 (2003) 127–135.

[106] S. Zou, D. Ireland, R.A. Brooks, N. Rushton, S. Best, The effects of silicate ions on human osteoblast adhesion, proliferation, and differentiation, J. Biomed. Mater. Res. B Appl. Biomater. 90B (2008) 123–130.

[107] Ž. Mladenović, A. Johansson, B. Willman, K. Shahabi, E. Björn, M. Ransjö, Soluble silica inhibits osteoclast formation and bone resorption *in vitro*, Acta Biomater. 10 (2014) 406–418.

[108] H.C. Schröder, X.H. Wang, M. Wiens, B. Diehl-Seifert, K. Kropf, U. Schloßmacher, W.E.G. Müller, Silicate modulates the cross-talk between osteoblasts (SaOS-2) and osteoclasts (RAW 264.7 cells): inhibition of osteoclast growth and differentiation, J. Cell. Biochem. 113 (2012) 3197–3206.

[109] F. Jafary, P. Hanachi, K. Gorjipour, Osteoblast differentiation on collagen scaffold with immobilized alkaline phosphatase, Int. J. Organ. Transplant. Med. 8(2017) 195-202

[110] A. Boguszewska-Czubara, K. Pasternak, Silicon in medicine and therapy, J. Elem. s. (2011) 489-497

[111] J. Roh, J.Y. Kim, Y.M. Choi, S.M. Ha, K.N. Kim, K.M. Kim, Bone regeneration using a mixture of silicon-substituted coral HA and β-TCP in a rat calvarial bone defect model, Materials 9 (2016) 97.

[112] K. Schwarz, A bound form of silicon in glycosaminoglycans and polyuronides, Proc. Natl. Acad. Sci. USA. 70 (1973) 1608–1612.

[113] E.M. Carlisle, Silicon: a possible factor in bone calcification, Science 167 (1970) 279–280.
[114] W.J. Landis, D.D. Lee, J.T. Brenna, S. Chandra, G.H. Morrison, Detection and localization of silicon and associated elements in vertebrate bone tissue by imaging ion microscopy, Calcif. Tissue Int. 38 (1986) 52–59.
[115] A. Policard, A. Collet, H. Daniel-Moussard, S. Pregermain, Deposition of silica in mitochondria: an electron microscopic study, J. Biophys. Biochem. Cytol. 9 (1961) 236-238
[116] H. Robberecht, R. Van Cauwenbergh, V. Van Vlaslaer, N. Hermans, Dietary silicon intake in Belgium: sources, availability from foods, and human serum levels, Sci. Total Environ. 407 (2009) 4777–4782.
[117] L.L. Hench, The story of Bioglass®, J. Mater. Sci. Mater. Med. 17 (2006) 967–978.
[118] X.H. Wang, H.C. Schröder, M. Wiens, H. Ushijima, W.E.G. Müller, Bio-silica and bio-polyphosphate: applications in biomedicine (bone formation), Curr. Opin. Biotechnol. 23 (2012) 570–578.
[119] K.A. Hing, P.A. Revell, N. Smith, T. Buckland, Effect of silicon level on rate, quality and progression of bone healing within silicate-substituted porous hydroxyapatite scaffolds, Biomaterials 27 (2006) 5014–5026.
[120] F.H. Liu, Y.K. Shen, J.L. Lee, Selective laser sintering of a hydroxyapatite-silica scaffold on cultured MG63 osteoblasts *in vitro*, Int. J. Precis. Eng. Manuf. 13 (2012) 439–444.
[121] J.R. Henstock, L.T. Canham, S.I. Anderson, Silicon: the evolution of its use in biomaterials, Acta Biomater. 11 (2015) 17–26.
[122] F.H. Nielsen, Update on the possible nutritional importance of silicon, J. Trace Elem. Med. Bio. 28 (2014) 379–382.
[123] R.W.M. Van Soest, N. Boury-Esnault, J. Vacelet, M. Dohrmann, D. Erpenbeck, N.J. De Voogd, N. Santodomingo, B. Vanhoorne, M. Kelly, J.N.A. Hooper, Global diversity of sponges (*Porifera*), PLoS ONE 7 (2012) e35105.
[124] H.C. Schröder, S. Perovic-Ottstadt, V.A. Grebenjuk, S. Engel, I.M. Müller, W.E.G. Müller, Biosilica formation in spicules of the sponge *Suberites domuncula*: Synchronous expression of a gene cluster, Genomics 85 (2005) 666–678.
[125] W.E.G. Müller, S.I. Belikov, W. Tremel, C.C. Perry, W.W.C. Gieskes, A. Boreiko, H.C. Schröder, Siliceous spicules in marine demosponges (example *Suberites domuncula*), Micron 37 (2006) 107–120.
[126] W.E.G. Müller, J. Li, H.C. Schröder, L. Qiao, X.H. Wang, The unique skeleton of siliceous sponges (*Porifera; Hexactinellida and Demospongiae*) that evolved first from the Urmetazoa during the Proterozoic: a review, Biogeoscience 4 (2007) 385–416.
[127] W.E.G. Müller, M. Rothenberger, A. Boreiko, W. Tremel, A. Reiber, H.C. Schröder, Formation of siliceous spicules in the marine demosponge *Suberites domuncula*, Cell Tissue Res. 321 (2005) 285–297.
[128] X.H. Wang, U. Schloßmacher, K.P. Jochum, L. Gan, B. Stoll, I. Uriz, W.E.G. Müller, Silica-protein composite layers of the giant basal spicules from *Monorhaphis*: basis for their mechanical stability, Pure Appl. Chem. 82 (2010) 175-192.
[129] J.N. Cha, K. Shimizu, Y. Zhou, S.C. Christiansen, B.F. Chmelka, G.D. Stucky, D.E. Morse, Silicatein filaments and subunits from a marine sponge direct the polymerization of silica and silicones *in vitro*, Proc. Natl. Acad Sci. USA 96 (1999) 361–365.
[130] K. Shimizu, J. Cha, G.D. Stucky, D.E. Morse, Silicatein α: cathepsin L-like protein in sponge biosilica, Proc. Natl. Acad Sci. USA 95 (1998) 6234–6238.
[131] X.H. Wang, M. Wiens, H.C. Schröder, S. Hu, E. Mugnaioli, U. Kolb, W. Tremel, D.

Pisignano, W.E.G. Müller, Morphology of sponge spicules: silicatein a structural protein for bio-Silica formation, Adv. Eng. Mater. 12 (2010) B422–B437.

[132] H.C. Schröder, M. Wiens, U. Schloßmacher, D. Brandt, W.E.G. Müller, Silicatein-mediated polycondensation of orthosilicic acid: modeling of a catalytic mechanism involving ring formation, Silicon 4 (2012) 33–38.

[133] R.D. Roer, R.M. Dillaman, The initiation and early stages of postmolt mineralization in the blue crab, *Callinectes sapidus*, Front. Mar. Sci. 5 (2018) 151.

[134] H.C. Schröder, M. Wiens, X.H. Wang, U. Schloßmacher, W.E.G. Müller, Biosilica-based strategies for treatment of osteoporosis and other bone diseases, Prog. Mol. Subcell. Biol. 52 (2011) 283–312.

[135] B.H. Jo, C.S. Kim, Y.K. Jo, H. Cheong, H.J. Cha, Recent developments and applications of bioinspired silicification, Korean J. Chem. Eng. 33 (2016) 1125–1133.

[136] H.C. Schröder, D. Brandt, U. Schloßmacher, X.H. Wang, M.N. Tahir, W. Tremel, S.I. Belikov, W.E.G. Müller, Enzymatic production of biosilica glass using enzymes from sponges: basic aspects and application in nanobiotechnology (material sciences and medicine), Naturwissenschaften 94 (2007) 339–359.

[137] S.R. Cicco, D. Vona, E. De Giglio, S. Cometa, M. Mattioli-Belmonte, F. Palumbo, R. Ragni, G.M. Farinola, Chemically modified diatoms biosilica for bone cell growth with combined drug-delivery and antioxidant properties, ChemPlusChem 80 (2015) 1104–1112.

[138] W.E.G. Müller, H.C. Schröder, M. Wiens, S. Perovic-Ottstadt, R. Batel, I.M. Müller, Traditional and modern biomedical prospecting: Part II—the benefits, Evid. Based Complement. Alternat. Med. 1 (2004) 133–144.

[139] H.C. Schröder, O. Boreiko, A. Krasko, A. Reiber, H. Schwertner, W.E.G. Müller, Mineralization of SaOS-2 cells on enzymatically (silicatein) modified bioactive osteoblast-stimulating surfaces, J. Biomed. Mater. Res. B Appl. Biomater. 75B (2005) 387–392.

[140] M. Wiens, X.H. Wang, F. Natalio, H.C. Schröder, U. Schloßmacher, S.F. Wang, M. Korzhev, W. Geurtsen, W.E.G. Müller, Bioinspired fabrication of bio-silica-based bone-substitution materials, Adv. Eng. Mater. 12 (2010) B438–B450.

[141] M. Wiens, X.H. Wang, U. Schloßmacher, I. Lieberwirth, G. Glasser, H. Ushijima, H.C. Schröder, W.E.G. Müller, Osteogenic potential of biosilica on human osteoblast-Like (SaOS-2) cells, Calcif. Tissue Int. 87 (2010) 513–524.

[142] F. Natalio, T. Link, W.E.G. Müller, H.C. Schröder, F.Z. Cui, X.H. Wang, M. Wiens, Bioengineering of the silica-polymerizing enzyme silicatein-α for a targeted application to hydroxyapatite, Acta Biomater. 6 (2010) 3720–3728.

[143] M. Wiens, X.H. Wang, H.C. Schröder, U. Kolb, U. Schloßmacher, H. Ushijima, W.E.G. Müller, The role of biosilica in the osteoprotegerin/RANKL ratio in human osteoblast-like cells, Biomaterials 31 (2010) 7716–7725.

[144] W.E.G. Müller, X.H. Wang, V. Grebenjuk, B. Diehl-Seifert, R. Steffen, U. Schloßmacher, A. Trautwein, S. Neumann, H.C. Schröder, Silica as a morphogenetically active inorganic polymer, Biomateri. Sci. 1 (2013) 669.

[145] X.H. Wang, E. Tolba, H.C. Schröder, M. Neufurth, Q. Feng, B. Diehl-Seifert, W.E.G. Müller, Effect of bioglass on growth and biomineralization of SaOS-2 cells in hydrogel after 3D cell bioprinting, PLoS ONE 9 (2014) e112497.

[146] W.E.G. Müller, E. Tolba, H.C. Schröder, B. Diehl-Seifert, T. Link, X.H. Wang, Biosilica-loaded poly(ϵ-caprolactone) nanofibers mats provide a morphogenetically active surface scaffold for the growth and mineralization of the osteoclast-related SaOS-2

cells, Biotechnol. J. 9 (2014) 1312–1321.
[147] M. Wiens, T.A. Elkhooly, H.C. Schröder, T.H.A. Mohamed, W.E.G. Müller, Characterization and osteogenic activity of a silicatein/biosilica-coated chitosan-graft-polycaprolactone, Acta Biomater. 10 (2014) 4456–4464.
[148] X.H. Wang, H.C. Schröder, W.E.G. Müller, Enzyme-based biosilica and biocalcite: biomaterials for the future in regenerative medicine, Trends Biotechnol. 32 (2014) 441–447.
[149] H.K. Makadia, S.J. Siegel, Poly lactic-co-glycolic acid (PLGA) as biodegradable controlled drug delivery carrier, Polymers (Basel) 3 (2011) 1377–1397.
[150] Z. Pan, J. Ding, Poly(lactide-co-glycolide) porous scaffolds for tissue engineering and regenerative medicine, Interface Focus 2 (2012) 366–377.
[151] C.E. Holy, M.S. Shoichet, J.E. Davies, Bone marrow cell colonization of, and extracellular matrix expression on, biodegradable polymers, Cell Mater. 7 (1997) 7.
[152] S. Freitas, H.P. Merkle, B. Gander, Microencapsulation by solvent extraction/evaporation: reviewing the state of the art of microsphere preparation process technology, J. Control. Release 102 (2005) 313–332.
[153] Y. Ogawa, M. Yamamoto, H. Okada, T. Yashiki, T. Shimamoto, A new technique to efficiently entrap leuprolide acetate into microcapsules of polylactic acid or copoly(lactic/glycolic) acid, Chem. Pharm. Bull. 36 (1988) 1095–1103.
[154] K. Shiga, N. Muramatsu, T. Kondo, Preparation of poly(D,L-lactide) and copoly(lactide-glycolide) microspheres of uniform size, J. Pharm. Pharmacol. 48 (1996) 891–895.
[155] M. Singh, B. Sandhu, A. Scurto, C. Berkland, M.S. Detamore, Microsphere-based scaffolds for cartilage tissue engineering: using subcritical CO_2 as a sintering agent, Acta Biomater. 6 (2010) 137–143.
[156] G.H. Ma, J. Yang, P.P. Lv, L.Y. Wang, W. Wei, R. Tian, J. Wu, Z.G. Su, Preparation of uniform microspheres and microcapsules by modified emulsification process, Macromol. Symp. 288 (2010) 41–48.
[157] C.E. Petrie Aronin, K.W. Sadik, A.L. Lay, D.B. Rion, S.S. Tholpady, R.C. Ogle, E.A. Botchwey, Comparative effects of scaffold pore size, pore volume, and total void volume on cranial bone healing patterns using microsphere-based scaffolds, J. Biomed. Mater. Res. A 89A (2009) 632–641.
[158] Q. Lv, L. Nair, C.T. Laurencin, Fabrication, characterization, and *in vitro* evaluation of poly(lactic acid glycolic acid)/nano-hydroxyapatite composite microsphere-based scaffolds for bone tissue engineering in rotating bioreactors, J. Biomed. Mater. Res. A 91A (2009) 679–691.
[159] C. Berkland, K. (Kevin) Kim, D.W. Pack, Fabrication of PLG microspheres with precisely controlled and monodisperse size distributions, J. Control. Release 73 (2001) 59–74.
[160] Y.Y. Yang, T.S. Chung, N. Ping Ng, Morphology, drug distribution, and *in vitro* release profiles of biodegradable polymeric microspheres containing protein fabricated by double-emulsion solvent extraction/evaporation method, Biomaterials 22 (2001) 231–241.
[161] P. Sansdrap, A.J. Moës, Influence of manufacturing parameters on the size characteristics and the release profiles of nifedipine from poly(DL-lactide-co-glycolide) microspheres, Int. J. Pharm. 98 (1993) 157–164.
[162] E. Sah, H. Sah, Recent trends in preparation of poly(lactide- co -glycolide) nanoparticles by mixing polymeric organic solution with antisolvent, J. Nanomater. 2015 (2015) 1–22.
[163] S.V. Dorozhkin, Bioceramics of calcium orthophosphates, Biomaterials 31 (2010)

1465–1485.
[164] S. Samavedi, A.R. Whittington, A.S. Goldstein, Calcium phosphate ceramics in bone tissue engineering: a review of properties and their influence on cell behavior, Acta Biomater. 9 (2013) 8037–8045.
[165] S.H. Chen, M. Lei, X.H. Xie, L.Z. Zheng, D. Yao, X.L. Wang, W. Li, Z. Zhao, A. Kong, D.M. Xiao, D.P. Wang, X.H. Pan, Y.X. Wang, L. Qin, PLGA/TCP composite scaffold incorporating bioactive phytomolecule icaritin for enhancement of bone defect repair in rabbits, Acta Biomater. 9 (2013) 6711–6722.
[166] H. Li, J. Chang, pH-compensation effect of bioactive inorganic fillers on the degradation of PLGA, Compos. Sci. Technol. 65 (2005) 2226–2232.
[167] M. Borden, M. Attawia, C.T. Laurencin, The sintered microsphere matrix for bone tissue engineering: *in vitro* osteoconductivity studies, J. Biomed. Mater. Res. 61 (2002) 421–429.
[168] J.L. Brown, L.S. Nair, C.T. Laurencin, Solvent/non-solvent sintering: a novel route to create porous microsphere scaffolds for tissue regeneration, J. Biomed. Mater. Res. B Appl. Biomater. 86B (2008) 396–406.
[169] A. Luciani, V. Guarino, L. Ambrosio, P.A. Netti, Solvent and melting induced microspheres sintering techniques: a comparative study of morphology and mechanical properties, J. Mater. Sci. Mater. Med. 22 (2011) 2019–2028.
[170] E. Swider, O. Koshkina, J. Tel, L.J. Cruz, I.J.M. de Vries, M. Srinivas, Customizing poly(lactic-co-glycolic acid) particles for biomedical applications, Acta Biomater. 73 (2018) 38–51.
[171] W.Y. Dong, M. Körber, V. López Esguerra, R. Bodmeier, Stability of poly(lactide-co-glycolide) and leuprolide acetate in *in-situ* forming drug delivery systems, J. Control. Release. 115 (2006) 158–167.
[172] F. Mottu, P. Gailloud, D. Massuelle, D.A. Rüfenacht, E. Doelker, *In vitro* assessment of new embolic liquids prepared from preformed polymers and water-miscible solvents for aneurysm treatment, Biomaterials 21 (2000) 803–811.
[173] B.S. Miguel, C. Ghayor, M. Ehrbar, R.E. Jung, R.A. Zwahlen, P. Hortschansky, H.G. Schmoekel, F.E. Weber, N-methyl pyrrolidone as a potent bone morphogenetic protein enhancer for bone tissue regeneration, Tissue Eng. Part A 15 (2009) 2955–2963.
[174] C. Ghayor, R.M. Correro, K. Lange, L.S. Karfeld-Sulzer, K.W. Grätz, F.E. Weber, Inhibition of osteoclast differentiation and bone resorption by *N*-methylpyrrolidone, J. Biol. Chem. 286 (2011) 24458–24466.
[175] C. Ghayor, B. Gjoksi, B. Siegenthaler, F.E. Weber, N-methyl pyrrolidone (NMP) inhibits lipopolysaccharide-induced inflammation by suppressing NF-κB signaling, Inflamm. Res. 64 (2015) 527–536.
[176] R. Ramachandran, P.K. Gupta, An improved spectrophotometric determination of silicate in water based on molybdenum blue, Anal. Chim. Acta. 172 (1985) 307–311.
[177] M. van de Weert, W.E. Hennink, W. Jiskoot, Protein instability in poly(lactic-co-glycolic acid) microparticles, Pharm. Res. 17 (2000) 1159–1167.
[178] X. Li, Y. Zhang, R. Yan, W. Jia, M. Yuan, X. Deng, Z. Huang, Influence of process parameters on the protein stability encapsulated in poly-D,L-lactide–poly(ethylene glycol) microspheres, J. Control. Release 68 (2000) 41–52.
[179] J.M. Péan, F. Boury, M.C. Venier-Julienne, P. Menei, J.E. Proust, J.P. Benoit, Why does PEG 400 co-encapsulation improve NGF stability and release from PLGA biodegradable microspheres?, Pharm. Res. 16 (1999) 1294–1299.

[180] S. Rezvantalab, M.K. Moraveji, Microfluidic assisted synthesis of PLGA drug delivery systems, RSC Adv. 9 (2019) 2055–2072.
[181] W. Lu, T.G. Park, Protein release from poly(lactic-co-glycolic acid) microspheres: protein stability problems, PDA J. Pharm. Sci. Technol. 49 (1995) 13–19.
[182] F.Y. Han, K.J. Thurecht, A.K. Whittaker, M.T. Smith, Bioerodable PLGA-based microparticles for producing sustained-release drug formulations and strategies for improving drug loading, Front. Pharmacol. 7 (2016).
[183] S.D. Allison, Analysis of initial burst in PLGA microparticles, Expert. Opin. Drug Deliv. 5 (2008) 615–628.
[184] X. Huang, B.L. Chestang, C.S. Brazel, Minimization of initial burst in poly(vinyl alcohol) hydrogels by surface extraction and surface-preferential crosslinking, Int. J. Pharm. 248 (2002) 183–192.
[185] S.K. Kim, Marine biomaterials: characterization, isolation and applications, CRC Press, 2013.
[186] E.M. Ahmed, Hydrogel: preparation, characterization, and applications: a review, J. Adv. Res. 6 (2015) 105–121.
[187] E.H. Gang, C.S. Ki, J.W. Kim, J. Lee, B.G. Cha, K.H. Lee, Y.H. Park, Highly porous three-dimensional poly(lactide-co-glycolide) (PLGA) microfibrous scaffold prepared by electrospinning method: a comparison study with other PLGA type scaffolds on its biological evaluation, Fiber Polym. 13 (2012) 685–691.
[188] X.S. Wu, N. Wang, Synthesis, characterization, biodegradation, and drug delivery application of biodegradable lactic/glycolic acid polymers. Part II: biodegradation, J. Biomat. Sci. Polym Ed. 12 (2001) 21–34.
[189] S. Kalia, L. Avérous, Biopolymers: biomedical and environmental applications, John Wiley & Sons, 2011.
[190] K. Makino, H. Ohshima, T. Kondo, Mechanism of hydrolytic degradation of poly(L-lactide) microcapsules: effects of pH, ionic strength and buffer concentration, J. Microencapsul. 3 (1986) 203–212.
[191] B.S. Zolnik, D.J. Burgess, Effect of acidic pH on PLGA microsphere degradation and release, J. Control. Release 122 (2007) 338–344.
[192] E. Vey, A. F. Miller, M. Claybourn, A. Saiani, *In vitro* degradation of poly(lactic-co-glycolic) acid random copolymers, Macromol. Symp. 251 (2007) 81–87.
[193] Q. Cai, G. Shi, J. Bei, S. Wang, Enzymatic degradation behavior and mechanism of Poly(lactide-co-glycolide) foams by trypsin, Biomaterials 24 (2003) 629–638.
[194] X. Zhou, Q. Cai, N. Yan, X. Deng, X. Yang, *In vitro* hydrolytic and enzymatic degradation of nestlike-patterned electrospun poly(D,L-lactide-co-glycolide) scaffolds, J. Biomed. Mater. Res. 95A (2010) 755–765.
[195] G. Spenlehauer, M. Vert, J.P. Benoit, A. Boddaert, *In vitro* and *in vivo* degradation of poly(D,L lactide/glycolide) type microspheres made by solvent evaporation method, Biomaterials 10 (1989) 557–563.
[196] B. Wright, N. Parmar, L. Bozec, S.D. Aguayo, R.M. Day, A simple and robust method for pre-wetting poly (lactic-co-glycolic) acid microspheres, J. Biomater. Appl. 30 (2015) 147–159.
[197] J. Fogh, J.M. Fogh, T. Orfeo, One hundred and twenty-seven cultured human tumor cell lines producing tumors in nude mice, J. Natl. Cancer Ins. 59 (1977) 221–226.
[198] B.D. Ratner, Biomaterials science: an introduction to materials in medicine, Elsevier Academic Press, Amsterdam, 2004.
[199] J. O'brien, I. Wilson, T. Orton, F. Pognan, Investigation of the alamar blue (resazurin)

fluorescent dye for the assessment of mammalian cell cytotoxicity, Eu. J. Biochem. 267 (2000) 5421–5426.

[200] H.S. Hung, C.C. Wu, S. Chien, S. Hsu, The behavior of endothelial cells on polyurethane nanocomposites and the associated signaling pathways, Biomaterials 30 (2009) 1502–1511.

[201] K. Sisson, C. Zhang, M.C. Farach-Carson, D.B. Chase, J.F. Rabolt, Fiber diameters control osteoblastic cell migration and differentiation in electrospun gelatin, J. Biomed. Mater. Res. A 94A. (2010) 1313-1320

[202] F. Langenbach, K. Berr, C. Naujoks, A. Hassel, M. Hentschel, R. Depprich, N.R. Kubler, U. Meyer, H.-P. Wiesmann, G. Kögler, J. Handschel, Generation and differentiation of microtissues from multipotent precursor cells for use in tissue engineering, Nat. Protoc. 6 (2011) 1726–1735.

[203] L. Hessle, K.A. Johnson, H.C. Anderson, S. Narisawa, A. Sali, J.W. Goding, R. Terkeltaub, J.L. Millán, Tissue-nonspecific alkaline phosphatase and plasma cell membrane glycoprotein-1 are central antagonistic regulators of bone mineralization, Proc. Natl. Acad. Sci. USA 99 (2002) 9445–9449.

[204] C.A. Gregory, W. Grady Gunn, A. Peister, D.J. Prockop, An alizarin red-based assay of mineralization by adherent cells in culture: comparison with cetylpyridinium chloride extraction, Anal. Biochem. 329 (2004) 77–84.

[205] G. Perale, J. Hilborn, Bioresorbable polymers for biomedical applications: from fundamentals to translational medicine, Woodhead Publishing, 2016.

[206] W. Li, J. Zhou, Y. Xu, Study of the *in vitro* cytotoxicity testing of medical devices, Biomed. Rep. 3 (2015) 617–620.

[207] H.S. Baek, J.Y. Yoo, D.K. Rah, D.W. Han, D.H. Lee, O.H. Kwon, J.C. Park, Evaluation of the extraction method for the cytotoxicity testing of latex gloves, Yonsei Med. J. 46 (2005) 579–583.

[208] J.M. Anderson, M.S. Shive, Biodegradation and biocompatibility of PLA and PLGA microspheres, Adv. Drug Deliv. Rev. 64 (2012) 72–82.

[209] P. Gentile, V. Chiono, I. Carmagnola, P.V. Hatton, An overview of poly(lactic-co-glycolic) acid (PLGA)-based biomaterials for bone tissue engineering, Int. J. Mol. Sci. 15 (2014) 3640–3659.

[210] A.-M. Haaparanta, S. Haimi, V. Ellä, N. Hopper, S. Miettinen, R. Suuronen, M. Kellomäki, Porous polylactide/β-tricalcium phosphate composite scaffolds for tissue engineering applications, J. Tissue Eng. Regen. Med. 4 (2010) 366–373.

[211] A. Khalili, M. Ahmad, A review of cell adhesion studies for biomedical and biological applications, Int. J. Mol. Sci. 16 (2015) 18149–18184.

[212] N. Jaiswal, S.E. Haynesworth, A.I. Caplan, S.P. Bruder, Osteogenic differentiation of purified, culture-expanded human mesenchymal stem cells *in vitro*, J. Cell. Biochem. 64 (1997) 295–312.

[213] N. Schecroun, C. h Delloye, Bone-like nodules formed by human bone marrow stromal cells: comparative study and characterization, Bone 32 (2003) 252–260.

[214] F. Langenbach, J. Handschel, Effects of dexamethasone, ascorbic acid and β-glycerophosphate on the osteogenic differentiation of stem cells *in vitro*, Stem Cell Res. Ther. 4 (2013) 117.

[215] X.H. Wang, H. Schröder, V. Grebenjuk, B. Diehl-Seifert, V. Mailänder, R. Steffen, U. Schloßmacher, W.E.G. Müller, The marine sponge-derived inorganic polymers, biosilica and polyphosphate, as morphogenetically active matrices/scaffolds for the differentiation of human multipotent stromal cells: potential application in 3D

printing and distraction osteogenesis, Mar. Drugs. 12 (2014) 1131–1147.
[216] H.-S. Kim, M. Zheng, D.-K. Kim, W.-P. Lee, S.-J. Yu, B.-O. Kim, Effects of 1,25-dihydroxyvitamin D_3 on the differentiation of MC3T3-E1 osteoblast-like cells, J. Periodontal. Implant. Sci. 48 (2018) 34-46.
[217] E.E. Golub, K. Boesze-Battaglia, The role of alkaline phosphatase in mineralization, Curr. Opin. Orthop. 18 (2007) 444–448.
[218] I.R. Orriss, T.R. Arnett, R.G.G. Russell, Pyrophosphate: a key inhibitor of mineralisation, Curr. Opin. Pharm. 28 (2016) 57–68.
[219] P.P. Spicer, J.D. Kretlow, S. Young, J.A. Jansen, F.K. Kasper, A.G. Mikos, Evaluation of bone regeneration using the rat critical size calvarial defect, Nat. Protoc. 7 (2012) 1918–1929.
[220] A.I. Pearce, R.G. Richards, S. Milz, E. Schneider, S.G. Pearce, Animal models for implant biomaterial research in bone: a review, Eur. Cell Mater. 13 (2007) 1–10.
[221] P.M. Conn, ed., Source book of models for biomedical research, Humana Press, Totowa, N.J, 2008.
[222] B.D. Ratner, ed., Biomaterials science: an introduction to materials in medicine, 3rd Ed, Elsevier/Academic Press, Amsterdam ; Boston, 2013.
[223] N. Milani-Nejad, P.M.L. Janssen, Small and large animal models in cardiac contraction research: advantages and disadvantages, Pharmacol. Ther. 141 (2014) 235–249.
[224] Y. Li, S.K. Chen, L. Li, L. Qin, X.L. Wang, Y.X. Lai, Bone defect animal models for testing efficacy of bone substitute biomaterials, J. Orthop. Translat. 3 (2015) 95–104.
[225] J. Harding, R.M. Roberts, O. Mirochnitchenko, Large animal models for stem cell therapy, Stem Cell Res. Ther. 4 (2013) 23.
[226] S. Reinwald, D. Burr, Review of nonprimate, large animal models for osteoporosis research, J. Bone Miner. Res. 23 (2008) 1353–1368.
[227] M. Narayanaswamy, K.C. Wright, K. Kandarpa, Animal models for atherosclerosis, restenosis, and endovascular graft research, J. Vas. Interv. Radiol. 11 (2000) 5–17.
[228] C.R. Chu, M. Szczodry, S. Bruno, Animal models for cartilage regeneration and repair, Tissue Eng. Part B Rev. 16 (2010) 105–115.
[229] M. Mapara, B.S. Thomas, K.M. Bhat, Rabbit as an animal model for experimental research, Dent. Res. J. (Isfahan). 9 (2012) 111–118.
[230] C. von Wilmowsky, T. Moest, E. Nkenke, F. Stelzle, K.A. Schlegel, Implants in bone: Part II. research on implant osseointegration: material testing, mechanical testing, imaging and histoanalytical methods, J. Oral Maxillofac. Surg. 18 (2014) 355–372.
[231] T. Taniyama, T. Masaoka, T. Yamada, X. Wei, H. Yasuda, T. Yoshii, Y. Kozaka, T. Takayama, M. Hirano, A. Okawa, S. Sotome, Repair of osteochondral defects in a rabbit model ssing a porous hydroxyapatite collagen composite impregnated with bone morphogenetic protein-2, Artif. Organs. 39 (2015) 529–535.
[232] J.O. Hollinger, An introduction to biomaterials, Second Edition, CRC Press, 2011.
[233] Y.H. An, K.L. Martin, Handbook of histology methods for bone and cartilage, Humana Press, Totowa, NJ, 2003.
[234] S.M. van Gaalen, M.C. Kruyt, R.E. Geuze, J.D. de Bruijn, J. Alblas, W.J. Dhert, Use of fluorochrome labels in *in vivo* bone tissue engineering research, Tissue Eng. Part B Rev. 16 (2010) 209–217.
[235] P. Roschger, E.P. Paschalis, P. Fratzl, K. Klaushofer, Bone mineralization density distribution in health and disease, Bone 42 (2008) 456–466.
[236] T. Ishimoto, T. Nakano, Evaluation of mechanical properties of regenerated bone by nanoindentation technique, Mater. Sci. Forum 654–656 (2010) 2220–2224.

[237] P. Gentile, V. Chiono, I. Carmagnola, P. Hatton, An overview of poly(lactic-co-glycolic) acid (PLGA)-based biomaterials for bone tissue engineering, Int. J. Mol. Sci. 15 (2014) 3640–3659.

[238] H. Cao, N. Kuboyama, A biodegradable porous composite scaffold of PGA/β-TCP for bone tissue engineering, Bone 46 (2010) 386–395.

[239] Y. Yang, Y. Zhao, G. Tang, H. Li, X. Yuan, Y. Fan, *In vitro* degradation of porous poly(l-lactide-co-glycolide)/β-tricalcium phosphate (PLGA/β-TCP) scaffolds under dynamic and static conditions, Polym. Degrad. Stab. 93 (2008) 1838–1845.

[240] W.E.G. Müller, A. Boreiko, X.H. Wang, A. Krasko, W. Geurtsen, M.R. Custódio, T. Winkler, L. Lukić-Bilela, T. Link, H.C. Schröder, Morphogenetic activity of silica and bio-silica on the expression of genes controlling biomineralization using SaOS-2 cells, Calcif. Tissue Int. 81 (2007) 382–393.

[241] X.H. Wang, H.C. Schröder, Q. Feng, F. Draenert, W.E.G. Müller, The deep-sea natural products, biogenic polyphosphate (Bio-PolyP) and biogenic silica (Bio-Silica), as biomimetic scaffolds for bone tissue engineering: fabrication of a morphogenetically-active polymer, Mar. Drugs 11 (2013) 718–746.

ABBREVIATIONS:

°C	Grad Celsius
µg/l	Microgramm per liter
µg/ml	Microgram per milliliter
µm	Micrometer
µM	Micromole

A

ALP	Alkaline phosphatase

B

BCA	Bicinchoninic acid
BCIP	5-bromo-4-chloro-3'-indolyphosphate p-toluidine salt
BMP-2	bone morphogenetic protein-2
BSA	Bovine serum albumin
BSP	Bone sialoprotein

C

CA-II	Carbonic anhydrase II
COL-I	Collegen-I
CPC	Cetylpyridinium chloride

D

d	Day
DAF	Diamond area funtion
DCM	Dichloromethane
DMF	Dimethylformamide
DMSO	Dimethyl sulfoxide
DTT	Dithiothreitol

E

EDTA	Ethylenediaminetetraacetic acid
EDX	Electron dispersive X-rays
Er	Reduced Young's modulus

F

F-actin	Filamentous actin
FCS	Fetal calf serum

G

Glu	Glutamine

GPa	Gigapascal
H	
H	Hardness
h	Hour
HR-SEM	High resolution scanning electron microscopy
I	
ICP-AES	Inductively Coupled Plasma Atomic Emission Spectrometer
M	
mg/kg	
mg/ml	Milligram per milliliter
Mg	Magnesium
min	Minute
mm	Millimeter
ml	Milliliter
MSC	Mesenchymal stem cells
MTT	3 - (4,5-Dimethylthiazol-2-yl)-2,5-diphenyltetrazolium bromide
N	
N	Newton
N/m	Newton per meter
NBT	Nitro-blue tetrazolium chloride
NCPs	Noncollagen proteins
nm	Nanometer
NMP	N-Methyl-2-pyrrolidinone
nN	Nano mole
nN	Nanonewton
O	
OC	Osteocalcin
ON	Osteonectin
OPG	Osteoprotegrin
P	
PBS	Phosphate Buffered Saline
PFA	Paraformaldehyde
PLGA	Poly(lactic-co-glycolic acid)
PVA	Poly(vinyl alcohol)
PVDF	Poly(vinylidene fluoride)
Q	
qRT-PCR	quantitative Real-Time Polymerase Chain Reaction

R

RANKL	Receptor activator of nuclear factor kappa-B ligand
RUNX2	Runt-related transcription factor 2

S

Saos-2	Human primary osteogenic sarcoma
SDS	Sodium dodecyl sulfate
SDS	Sodium dodecyl sulfate solution
Si	Silicon
Si-HA	Silicon-substituted hydroxyapatite
SN_2	Nucleophilic attack

T

ß-TCP	ß-tricalcium phosphate
TBS	Tris-Buffered Saline
TBST	Tris-Buffered Saline and Tween 20
TEOS	Tetraethoxysilane
TRAP	Tartrate-resistant acid phosphatase

U

UV	Ultraviolet

W

W/O/W	Water-in-oil-in-water emulsions

FIGURES and TABLES:

1. Figures

2. Tables

ACKNOWLEDGEMENTS:

ERKLÄRUNG:

Hiermit erkläre ich, die vorliegende Arbeit selbständig und nur mit Hilfe der angegebenen Personen und Mittel (Literatur, Apparaturen, Material) angefertigt zu haben. Bei den von mir durchgeführten Untersuchungen habe ich die Grundsätze guter wissenschaftlicher Praxis, wie sie in der Satzung der Johannes Gutenberg-Universität Mainz niedergelegt sind, eingehalten.

_____ _____

Ort, Datum Shunfeng WANG

CURRICULUM VITAE: